THE ROLE THAT CONNECTED AND AUTOMATED VEHICLES CAN PLAY IN RE-ORGANIZING TRAFFIC FLOW: WORK ZONES AND EMERGENCY SERVICES

Yun Zou

Candidate of Doctor of Philosophy

Principle Supervisor: Prof. Jianchun Li

Co-supervisor: Prof. Xiaobo Qu

Co-supervisor: Dr. Kasun De Silva Wijayaratna

Submitted in fulfilment of the requirements for the degree of
Doctor of Philosophy

School of Civil & Environment Engineering
Faculty of Engineering and Information Technology
University of Technology Sydney

July 2020

Certificate of Original Authorship

I, Yun Zou declare that this thesis, is submitted in fulfilment of the requirements for the award of Doctor of Philosophy, in the School of Civil & Environment Engineering at the University of Technology Sydney.

This thesis is wholly my own work unless otherwise reference or acknowledged. In addition, I certify that all information sources and literature used are indicated in the thesis. This document has not been submitted for qualifications at any other academic institution.

This research is supported by the Australian Government Research Training Program.

Signature: Production Note: Signature removed prior to publication.

Date: 09/07/2020

Acknowledgements

First and foremost, I would like to express my sincere gratitude to my supervisory panel, Prof. Jianchun Li, Prof. Xiaobo Qu and Dr. Kasun Wijayaratna for their continuous support of my Ph.D study. It would not have been possible to accomplish my researches without their guidance and patience.

I gratefully acknowledge the University of Sydney Technology for the generous supports and the helpful academic environment during my candidature. Besides, I am really thankful to the AI Innovation of Sweden for offering me an internship.

My friends and colleagues have provided me encouragement and collaboration during my candidature, and my life would not be so enjoyable without them; therefore, I cannot express enough thanks to Jun Li, Weiwei Qi and Yuancheng Mao for inspiring me on my researches, and Yang Yu, Jian Zhang, Mengtian Li, Lufei Huang, Bentuo Xu, Jiawei Ren, Haodong Chang, TianmingWang, Zhongqin Wang, Caoyuan Li, Lingxiang Wu etc. for their ideas and collaborations.

Finally, I would like to thank my parents Fuxi Zou and Xiaoli Wang for their continuous support. I would like to thank my girlfriend, Zhexi Kuang, for accompanying me in Australia and Sweden.

List of Publications

Zou, Y., & Qu, X. (2018). On the impact of connected automated vehicles in freeway work zones: a cooperative cellular automata model based approach. Journal of Intelligent and Connected Vehicles.

Zou, Y., & Qu, X. (2019). On the Impact of Emergency Incidents on the Freeway: A Full Velocity Difference (FVD) Model Based Four-Lane Traffic Dynamics Simulation. In Smart Transportation Systems 2019 (pp. 165-174). Springer, Singapore.

Zou, Y., Kuang. Y., Zhi, Y., Qu, X. (2019). Investigation on linearization of data driven transport research: two representative case studies. IET Intelligent Transport Systems. (accepted) (as shown in Appendix A)

Table of Contents

List of Figures

List of Tables

List of Abbreviations

CAV	= Connected and Automated Vehicles;
HDV (or MV)	= Human-driven Vehicles (or Manual-driven Vehicles);
CA	= Cellular Automata;
FVD	= Full Velocity Difference;
ICAM	= Improved Cellular Automata Model;
CCAM	= Cooperative Cellular Automata Model;
AFV	= Anticipated (Adjacent) Following Vehicle;
APV	= Anticipated (Adjacent) Preceding Vehicle;
SVM	= Support Vector Machines
k-NN	= k Nearest Neighbor
NGSIM	= Next Generation Simulation
US-101	= U.S. Highway 101
I-80	= Interstate 80 Freeway
SITRAS	= Simulation of Intelligent Traffic System
sEMA	= symmetric Exponential Moving Average
VT-micro	= Virginia Tech microscopic
ILMCS	= Intelligent Lane Merge Control System
ITS	= Intelligent Transportation System
V2V	= Vehicle to Vehicle
V2I	= Vehicle to Infrastructure
USDOT	= U.S. Department of Transportation
CVRIA	= Connected Vehicle Reference Implementation Architecture
DSRC	= Dedicated short-range communication
CACC	= Cooperative Adaptive Cruise Control
OVM	= Optimal Velocity Model
GFM	= Generalized Forced Model
TTC	= Time to Collision
ANN	= Artificial Neural Network
LSM	= Least Squares Method
GA400	= Georgia State Route 400
WLSM	= Weighted Least Squares Method
RMSE	= Root-Mean-Square Error
WLSMT	= Weighted Least Squares Method with Data Transformation
OLSMT	= Ordinary Least Squares Method with Data Transformation
OLSM	= Ordinary Least Squares Method

Abstract

The extensive progresses in computer science and communication technology in recent decades facilitate the development of the connected and automated vehicles (CAV). Since the emergence of the concept, the commercialization of CAV has been looked forward to providing an effective tool to the regulation of the freeway re-organizing traffic flow who normally initiate the evolvement of the congestion. To analyse the benefits of the CAV on traffic dispersion, the re-organizing traffic in the work zone and the incident-affected zone (under emergency services) were adopted as two cases of non-recurrent congestion, and the microscopic simulations were conducted on the basis of various car-following models and lane-change models. Furthermore, collaborative instances were added to the traditional traffic dynamic models to emulate the motions of the CAV. Trajectories data extracted from NGSIM open-access database were applied to calibrate the Bayes-classifier-based lane-change prediction model in order to better emulate the human drivers' lane-change decision and to assist the CAV's collaborations. With the increasing percentage of the CAV, the traffic congestion on the aforementioned bottlenecks were significantly mitigated. While CAV are proved to be capable of facilitate the cooperative lane-changes, they were also trained to refuse the lane-change request if there would be great impact on the target lanes. Although the lane-changes would inevitably impact the target lanes owing to the increasing densities and the disturbances during the lane-change motions, the simulation results showed that CAV are capable of minimizing the negative effects for the entire traffic system's perspective.

Keywords

Connected and automated vehicle; Work zone; Emergency Service; incident-affected traffic; freeway; bottleneck; microscopic simulation; car-following model; lane-change model; cooperative lane-change.

Chapter 1: Introduction

1.1 BACKGROUND

Annually, the traffic accidents lead to about 1.2 million fatalities around the world, and this number will boost by 65% after two decades if we do not take any preventing action (Peden et al. 2004). Among all crashes, the rear-end crashes account for around a quarter of total populations. The lane-change maneuvers which account for 70% vehicle miles in highway driving (Federal Highway Administration 1998) are regarded to be closely related to the occurrence of rear-end crashes; furthermore, they bring great impacts on the traffic system, including congestions, oscillations. It is estimated that crashes caused by the lane-change account for around 10% of annual crashes in the United States (Kiefer et al. 1999; Lee, Olsen &Wierwille 2004) Apart from the fatality, the lane-change crashes also represent 10% of delay time (Ding et al. 2013).

The re-organizing traffic flow where lane-change maneuvers can happen frequently are usually induced by a work zone or an emergency service. In the re-organizing traffic flow, vehicles attempt to escape from the blocked lane to a target lane (through lane); therefore, a high frequency of lane-changes are witnessed until the platoon pass the obstacles. In that case, the vehicles may not comply with a consistent car-following rule because the lane-changes leads to a re-distribution of the density and sharp changes of the headways. Due to the heterogeneity of human drivers, there will appear conflicts among drivers. On the other hand, the misleading indications (lane-change indicators or excessive motion of vehicles) sent by lane-change vehicles will induce the wrong judgements of the surrounding vehicles. The lane change maneuvers may benefit the individual vehicle, but it could possibly result in traffic instability (Weng & Meng 2014). In that case, drivers may frequently apply the accelerator and the brake, which causes severe oscillations.

To mitigate the heterogeneity and enhance the collaboration among human drivers, the intelligent transport systems (ITS) are introduced as an efficient method of traffic regulation. ITS aims for assisting the human driver on typical driving tasks so as to creating a collision-free and congestion-free traffic environment (Ding et al. 2013; Mandalia & Salvucci 2005). Vehicle-to-vehicle (V2V) and vehicle-to-infrastructure

(V2I) are two prevailing architectures of ITS, which allow vehicles to share the dynamic information with its surrounding vehicles or infrastructures (Miller 2008). More specifically, V2I enable vehicles to upload their speed and location to the central server, and the vehicles will be provided with optimized routes via motion planning technologies. In our case, the significance of the V2I architecture is reporting the downstream events such as the occurrence of a traffic accident and the existence of a work zone. While V2I mainly focuses on the macroscopic level, V2V puts more efforts on the microscopic collaborations among vehicles. Vehicles are turned into nodes that communicate with their surrounding vehicles (Miller 2008; Bento, Parafita & Nunes 2012). To accurately control the collaborative process, those vehicles are expected to precisely and comprehensively detect the surrounding traffic conditions, rapidly communicate and propagate the information, and accurately execute the command; therefore, the connected and automated vehicles (CAV) are introduced to the ITS. The CAV are vehicles equipped with sensors like camera, microwave radar, ultrasonic sensors and lidar to precisely detect and rebuild the surrounding environment, and the embedded computers are able to take the control of the vehicles based on the collected 'point-cloud map' without any human driver's attention. Ideally, the CAV are expected to improve the traffic performance by avoiding excessive application of accelerator or brake, detecting the downstream event and optimizing the approaching speed, providing acceptable gaps to the lane-change vehicles without significant sacrifice of ego travel time, executing determined lane-change maneuvers without violating the safety criteria, etc. While the CAV is still an emerging concept that comprehensive trajectories with sensor data are scarcely available, we have to rely on microscopic simulations to evaluate the impact of CAV. The microscopic simulation, as an efficient tool for transport analysis and management, allows transport researchers to evaluate the traffic performance operatively (Hidas 2002). With such operative feature, new technologies are able to be tested in the simulated environment by adjusting the operational parameters according to the need of research (Hidas 2002) . The microscopic simulation needs to be as practical as possible so as to sufficiently demonstrate the effects of the collaborations. Hence, how to reproduce the trajectories of vehicles and the decision of drivers becomes the key point of the research.

Conventionally, researchers applied rule-based models to simulate car-following (Luo et al. 2016; Ntousakis, Nikolos & Papageorgiou 2016; Zohdy & Rakha 2016;

Nagel & Schreckenberg 1992; Lárraga, Del Rio & Alvarez-Lcaza 2005; Meng & Weng 2010, 2011; Jiang & Wu 2002; Bando et al. 1995) and lane-change maneuvers (Helbing & Tilch 1998; Jiang, Wu & Zhu 2001; Yu, Jiang & Qu 2019; Nagel et al. 1998; Gipps 1986; Zheng 2014). Others applied data-based methodologies to predict the decision of the drivers (Sledge & Marshek 1998; Gackstatter et al. 2010; Kasper et al. 2012; Hunt & Lyons 1994; Tomar, R., Verma & Tomar, G 2010; Toar & Verma 2012; Tang et al. 2018; Zheng, Suzuki & Fujita 2014; Yi et al. 2016; Hou, Edara & Sun 2013, 2015; Mandalia & Salvucci 2005; Dou, Yan & Feng 2016). Using a data-based methodology is more fault-tolerant when compared to applying either dynamic or static models yet require the support of a large quantity of accurate and comprehensive data. However, no matter which method is used there are some significant concepts and variables to be clarified:

- Ego lane (or origin lane): An ego lane refers to a lane being affected by a lane closure. In our research, a work zone or an emergency service is the reason of a lane closure. It worth noting that ego lane denotes the blocked lane for lane-change vehicles.
- Target lane: A target lane refers to the destination of a lane-change maneuver. Normally, it is a through lane in proximity to the lane closure.
- Ego vehicle: An ego vehicle (also known as the subject vehicle) refers to the vehicles on the ego lane. They are the starters of each respective lane-change collaboration.
- Preceding vehicle (or leading vehicle): A preceding vehicle refers to the vehicle directly ahead of the ego vehicle in the platoon.
- Following vehicle: A following vehicle refers to the vehicle who directly follows the ego vehicle in the platoon.
- Immediate preceding vehicle (or anticipated preceding vehicle or adjacent preceding vehicle): an immediate preceding vehicle refers to the ego vehicle’s preceding vehicle in the target lane after the lane change.
- Immediate following vehicle (or anticipated following vehicle or adjacent following vehicle): an immediate preceding vehicle refers to the ego vehicle’s following vehicle in the target lane after the lane change.

- x; $\dot{x}$; $\ddot{x}$: longitudinal position; longitudinal speed; longitudinal acceleration
- y; $\dot{y}$; $\ddot{y}$: lateral position; lateral speed; lateral acceleration
- Gap: The gap refers to the net distance of two successive vehicles, where the net distance indicates the distance from mid-end point of the preceding vehicle of these two vehicles to the mid-front point of the following vehicle of these two vehicles.
- Space headway: The distance between the mid-front point of two successive vehicles.
- (Time) Headway: The headway here refers to how long the following vehicle can travel through the space headway. It depicts the 'distance' with regards to the cruise speed.

The collaborative events involve two aspects that are the collaboration among the CAV and the collaboration among a mix traffic flow of the CAV and the human-driven vehicles (HDV). There is no doubt that the latter requires more considerations due to the heterogeneity of human drivers. The CAV will not dominate the traffic within a short time, and it may take decades for the customers to accept such emerging technology and for legislation to specify the responsibilities of all involved parties. Hence, the most important elaboration to incorporate the CAV into the traffic system is to teach CAV the rule (rule-based method) or the experience (data-based method) to cooperate with human drivers or assist the human drivers.

1.2 MAIN CHALLENGES

In some of the districts, short-term work zones will only be deployed during the night-time. As traffic density is not as high as the that during the daytime, the vehicles are able to make free (or discretionary) lane-changes which are not much different from a car-following maneuvers. Long-term work zones and intermediate-term work zones, on the other hand, require the transport engineers to deal with almost all kinds of traffic condition from low-density to high-density, even the unexpected accidents who obviously make the situation worse need to be taken into account. In the dense traffic flow, the vehicles on the origin lane will make forced (or mandatory) lane-change decisions to avoid approaching to the end of the lane. Otherwise, vehicles will

have to decelerate, what make the situation worse is that the growing speed difference between two platoons will bring even more difficulties to the drivers on making lane-change decisions.

Alternatively, drivers can expect cooperative lane-changes which strictly reply on the collaboration of surrounding vehicles. For human drivers, the willingness of aforementioned collaboration depends on many features, e.g. relative velocity and positions (both longitudinal and lateral), the lateral distance to the lane mark, the application of the lane-change indicators, the driving manner of the involved drivers; at the meanwhile, the willingness is rather unpredictable. For CAV, the transport researchers are expecting them to be competent enough to provide deterministic collaborations to the lane-change vehicles; however, there remains a huge gap on hardware and software technologies to the goal that the CAV are applied into real traffic flow and substantially help with the traffic. To sufficiently evaluate the impact of CAV, the microscopic simulation method is adopted because it is not only economical but also manageable. Most of the researchers focus either the car-following models or the lane-change models, but the truth is that no high-fidelity trajectory can be reproduced unless these two models are combined, especially when we are dealing with re-organizing traffic flow. Also, due to the frequent lane-change tasks, the preceding vehicle will not the only factor on a car-following motion. As a matter of fact, any vehicle who would potentially merge into the front gap of the ego vehicle will impact the cruise speed of the ego vehicle. Sometimes, even a lane-change indication or a lateral movement of adjacent preceding vehicle can terminate a car-following motion. One of the challenges is incorporating the impact from adjacent lanes into the car-following models, followed by another challenge that fusing the deterministic collaborative content and the human drivers' heterogeneities. A criterion that balancing the cost of both CAV passengers and HDV passengers also need to be fulfilled; therefore, a dynamic threshold is going to be required to control CAV passengers' sacrifices on travel time. Furthermore, different scenarios when the participation rate of CAV varies from 0 to 100% also bring the complexity to our researches.

It is expected that there will be more improvement on traffic performance when the CAV dominate the traffic flow; however, the performance will not necessarily be poor when the HDV dominate the traffic with the assistance of minority of CAV.

Hence, a feasible collaborative norm needs to be introduced to mitigate the conflict among vehicles and avoid the risk of crash at the meanwhile.

In summary, the main objectives of the following studies are to develop the car-following and lane-change models that compatible with the prevailing microscopic models for the CAV, and to evaluate the impacts brought by the emerging CAV to our current traffic systems by incorporating the CAV and HDV into a same highway section, especially in the re-organizing traffic flows.

1.3 CONTRIBUTIONS

The CAV were intuitively introduced into the microscopic simulations as a solution of the congestions from the re-organizing traffic flow, which complement the gaps of CAV-related researches to the best knowledge of the authors. In order to avoid the limitation of the developed microscopic traffic simulation software, we programmed original micro-simulation environments based on MATLAB and the Python (Spyder IDE) to deliver visible trajectories and related datasets. New microscopic models were proposed on the basis of the traditional car-following and lane-change models to simulate the collaborative instances of the CAV, while the traditional traffic dynamic models were also modified to practically emulate the human drivers' car-following motions and lane-change maneuvers. More specifically, original CAV-related micro-simulation car-following models were developed based on the frame of the CA model and the FVD model respectively, and the lane-change models were established based on some prevailing criteria. Realistic lane-change duration and trajectories were considered; therefore, the on-going variable effects on both the ego lane and the target lane were accessed during the lane-change motions. The impacts of the lane-change tasks were discussed based on the collaborations with the surrounding vehicles that were involved into the lane-change maneuvers, and it was found that the collaboration with the preceding vehicles and the following vehicles were equally important. An original data-based lane-change prediction model was established based on Bayes classifier. Datasets extracted from the NGSIM databased were processed for the purposed of lane-change prediction. A combination of k-nearest-neighbor and SVM were adopted for assigning weights to different features from the Bayes classifier. We intuitively employed trajectories on the basis of 10 Hz, which facilitate more logical and controllable cooperative lane-changes. The

prediction model was then applied to enhance the collaboration among the CAV and the human drivers.

1.4 OUTLINE

The following context can be outlined as: Chapter 2 lists and illustrates the related literatures; Chapter 3 demonstrates microscopic simulations in the work zone of a two-lane freeway based on the cooperative cellular automata model; Chapter 4 presents the microscopic simulations of a four-lane traffic under emergency service based on the full velocity difference model; Chapter 5 extracts trajectories data from NGSIM database and calibrates a Bayes classifier-based lane-change prediction model. Chapter 6 describes a microscopic simulation and analyses the traffic performance in the work zone of a three-lane freeway based on the proposed prediction model; Chapter 7 presents the microscopic simulation and analyses the traffic performance of a four-lane traffic under emergency service, and Chapter 8 concludes.

Chapter 2: Literature Review

This chapter is outlined with the following topics: the connected and automated vehicles (section 2.1) where some applications of CAV are illustrated; followed by the car-following and lane-change models (section 2.2 and section 2.3); the trajectory planning to improve the traffic flow dynamics (section 2.4). Section 2.5 highlights the contribution from the transport engineer to facilitate the traffic flow dynamics in work zone and incident-affected zone.

2.1 CONNECTED AND AUTOMATED VEHICLES

With the development of the communication technology and the computer science, the vehicle equipped with sensors are being capable of detecting the environment, communicating with surrounding vehicles or infrastructures, and automatically controlling the trajectories. The concept of CAV can be separated into two parts: the connected vehicle and the automated vehicle. Connected vehicles enables the ego vehicle to communicate with it surrounding vehicles which is called the Vehicle-to-Vehicle (referred as V2V hereafter) communication, and (or) the infrastructures which is called the Vehicle-to-Infrastructure (referred as V2I hereafter) communication. On the other hand, the automated vehicles using the collected data to control the vehicles' movement precisely for optimal trajectories.

During the past ten years, the U.S. Department of Transportation (USDOT) have developed a comprehensive Connected Vehicle Reference Implementation Architecture (CVRIA) to standardize the technologies (USDOT 2015, Dey et al. 2016). Dedicated short-range communication (DSRC), as outlined by CVRIA, has been regarded as an efficient communication technology for its low latency, high security and fast connectivity (Lee & Park 2012). Based on the rapid development of communication technology on the connected vehicles, the transport engineer has been seeking helps from the connected vehicle for traffic regulations, especially at the intersections and the bottlenecks. To improve the safety and the efficiency of the intersection, Lee and Park (2012) proposed a cooperative vehicle intersection control system based on the participation of the connected vehicles. The system aimed at eliminating the potential overlaps of the trajectories; on the other hand, it was also

capable of dealing with the scenarios when the overlaps could not be avoided. They conducted the microscopic simulations to access the performance of the proposed system within the VISSIM, and results showed that the travel time was dramatically decreased. Li et al. (2019) presented a study on the deployment of connected infrastructures with the limited budget to optimize the connectivity, and they found distance-dependent utility measure and the concentration of the users can improve the entire utilities.

As for automation, vehicles are classified into six levels by society of automotive engineer (SAE On-Road Automated Vehicle Standards Committee 2014). Level 0 represents the vehicles who are fully driven by human driver, while level 1 to level 5 demonstrates different levels of autonomy (Hecht 2018). Diels and Bos (2016) illustrates the different levels of autonomy: level 1 refers to driver assistance which solely takes control of either longitudinal or lateral movement, for instance, the adaptive cruise control and lane-keeping assist system; level 2 refers to partial automation who combines the longitudinal control functions and the lateral control functions, although drivers are still requires to take control of the vehicles; level 3 refers to conditional automation who takes overs the driving tasks in some specific scenarios, but the drivers are required to be ready for taking the control of the vehicles; level 4 and level 5 refer to high automation and full automation respectively, and the only difference is that the level 4 automation cannot be applied on specific road while the level 5 refers to the capability of controlling the vehicle during the entire trip. Sensors like camera, microwave radar, ultrasonic sensors and lidar are employed to collect the data and build the cloud of surroundings, and these data will then be processed by artificial intelligence (Hecht 2018). Similar with the connected vehicles, automated vehicles are also engaged by researchers to improve the safety and efficiency of the traffic networks, and one of the most significant reasons is that the automated vehicles are error-free and controllable. Milanés et al. (2012) developed a fuzzy-logic based controller aiming at automatically executing overtaking tasks. The vision system, global positioning system and inertial measurement unit were applied to collect the positioning data as the input, while the steer, throttle and brake were output to automatically control the ego vehicle. The field test of a commercial car which was embedded with the proposed system shows that the controller is capable of deliver safe and efficient overtaking trajectories. Despite of the cutting-edge

researches into the CAV's perception, connection and automation, few has developed microscopic models to emulate the behaviours of the CAV in the microscopic simulations and evaluate the impacts of mixed traffic flow who includes both the CAV and the HDV on our current traffic infrastructure.

2.2 CAR-FOLLOWING MODEL

In 1992, Nagel and Schreckenberg (1992) intuitively introduced the cellular automata (CA) model which was admired for being computational efficient to emulate the drivers' car-following motions. Lárraga et al. (2005) proposed a cellular automate model to microscopically simulate a one-lane traffic flow dynamics in the highway. The car following rules are simplified, and the single lane traffic followed a loop topology. It showed that the simulation result can comply with the fundamental diagram. Meng and Weng (2011) proposed an improved CA model to simulate the traffic dynamic in work zones, incorporating a randomization probability function (Meng & Weng 2010) to emulate the drivers' car-following behaviour, while the heterogeneity of the vehicles was also considered. The trajectories are calibrated and validated based on the trajectory data collected from a work zone in Singapore, and the results showed good accordance with the fundamental diagram. Jiang and Wu (2002) analysed the microscopic simulation results macroscopically, and they proved that the CA model was capable of simulating the synchronized traffic flow. Despite of the advantage of computational efficiency, the CA model exposed its shortcomings that the parameters in the car-following are not continuous with the change of the traffic events. The determination of acceleration rate and deceleration rate follows discrete steps, and the trajectories cannot be described by one single function. Full velocity difference (FVD) model, on the other hand, is able to combine the discrete rule into a continuous process where continuous acceleration can be delivered by one single model. In 1995, Bando et al. (1995) proposed optimal velocity model (OVM) to calculate the optimal acceleration rate from the gap with the preceding vehicle during the car-following motion. The OVM intuitively introduced the sensitive constant to emulate the drivers' sensitivity to the difference between the current speed and the target speed. The simulation based on the OVM showed the capability of reproducing the evolvement of the traffic congestion and many other features that normally happens in real traffic. In 1998, Helbing and Tilch (1998) calibrated the function of optimal speed generation in OVM based on empirical data and validated

the model with the field data, and it was found that the model had the problem of generating unrealistically high acceleration and deceleration. A generalized forced model (GFM) was proposed by Helbing and Tilch (1998) to avoid the unrealistically high acceleration and deceleration, and they added factor of speed difference of two successive vehicles to modify the generated acceleration. The GFM complemented to the scenario when the following vehicle is faster than the preceding vehicle, and it outperformed the OVM on reproducing the field data. Jiang et al (2001) recognized that another complementary research on the scenario when the following vehicle is slower than its preceding vehicle was necessary, and they proposed the full velocity difference (FVD) model on the basis of this idea. It was found by Yu et al. (2019) that FVD model can still generate overshooting acceleration and deceleration; therefore Yu et al. (2019) proposed the confined FVD model, to limit the acceleration and deceleration into a reasonable range without any collision. Machine learning algorithms have also been employed to calibrate the car-following models. Zhou et al. (2019) presented a reinforcement-learning-based car-following model for the CAV to regulate the driving behaviours at the signalized intersections, and results showed that the traffic efficiency, level of safety and fuel consumption were improved. Qu et al. (2019) employed reinforcement learning algorithm to train the car-following model for electrical CAV aiming at alleviating the oscillation and optimizing the energy consumption. The analysis of the traffic performance proved the positive effects of the proposed car-following model; furthermore, the average electric energy consumption was clearly reduced.

2.3 LANE-CHANGE MODEL

Apart from computational advantages on car-following model, CA model was also found to be suitable for multi-lane simulations, and Nagel et al. (1998) introduced the incentive criterion and safety criterion into the symmetric lane-change rule to reproduce a two-lane freeway traffic. The simulation results not only comply with the fundamental diagram but demonstrate reasonable traffic dynamics. Meng and Weng (2011) employed the previously proposed incentive criterion and safety criterion to regulate the lane-change decisions. A lateral movement rule was proposed to limit the lateral speed within 1 m/s, and the lane-change span was primarily considered owing to the finer cell. To avoid the conflicts when a cell become a target of two vehicles,

Meng and Weng (2011) randomly gave one of the two vehicle the right to enter the cell.

Since Gipps (1986) proposed a structure of drivers' lane-change decisions, a lot of similar research has been done on the basis of Gipps-type lane-change model (2014). The Gipps' lane-change model was established in the context of urban area to instruct the simulated vehicle to maintain desire speed and traverse on the right lane for the following turning maneuver (Gipps 1986) . Zheng (2014) believed that the Gipps's model was deterministic because the possibility, necessity and desirability were evaluated by deterministic rules, and therefore the drivers' heterogeneity and the change of drivers' factor over time (e.g. the patience-related factor) were ignored. Yang and Koutsopoulos (1996) developed a lane-change model on the basis of Gipps' model to simulate the lane-change maneuvers on the freeway in the MITSIM traffic simulator. Four sequential steps that are decision-making, lane-picking, gap-searching and lane-change were included in the model (1996). The time-variable factor was represented by the distance that the vehicle traversed, and this factor was incorporated into the lane-change rule, as a result, this change made the simulation more realistic. Hidas (2002) developed a lane-change model for SITRAS, a multi-agent simulation system, to illustrate the forced and cooperative lane-change in incident-affected area. Hidas (2005) also proposed a lane-change rule with regards to the incident-affected zone where the distance to the end of the lane become the vital incentive for the lane-change. Data collected from video were classified into three groups that are free lane-change, cooperative lane-change and forced lane-change, and the calibration and the validation of the proposed model were conducted on the basis of three groups of data. This model took the interaction among vehicles into account, and it was applied on microscopic simulations on two hypothetical road networks which were freeway and signalized urban arterial road within the ARTEMiS traffic simulator. Kesting et al. (2007) proposed an acceleration-based lane-change model called MOBIL which is the abbreviation of minimizing overall braking induced by lane-changes. Similar to the aforementioned models, it included the safety criterion and the incentive criterion. The politeness factor which illustrates the degree of aggressive of the drivers was intuitively introduced into the lane-change model; therefore, a more realistic interaction among heterogenous drivers was presented. As for combining the car-following model and the lane-change model, it worth noting that the lane-change

model should be executed ahead of the car-following model in the microscopic simulations as advised by Zheng (2014).

2.4 TRAJECTORY PLANNING TO IMPROVED THE TRAFFIC FLOW DYNAMICS

An early research by Shiller and Sundar (1998) applied the planar bicycle model to emulate the vehicles control. A clearance curve was determined during an emergency lane-change, and it was capable of guiding the autonomous vehicle to minimize the longitudinal distances of the emergency lane-change to avoiding irretrievable collision with the obstacles. During the lane-change tasks, drivers may sometime face high potential collision risks because they cannot acquire accuracy and comprehensive information of the surrounding environment; therefore, Luo et al. (2016) introduced the V2V communication for the trajectory planning and the trajectory tracking to eliminate the collision risk. A quintic polynomial was computed with the constrains of safety, comfort and efficiency to reproduce the lane-change trajectories due to its advantages of a closed form, a continuous third derivative and smooth curvature (Luo et al. 2016). , Luo et al. (2016) applied the Simulink and the CarSim to simulate the traffic dynamics, while a driving simulator was engaged to validate the simulated trajectories. Five scenarios were established based on the relative speed of the origin lane and the target lane, the road geometry, and the traversing speed of the ego vehicle. The model was proved to be effective on avoiding the potential collision, and the most significant contribution was that they proposed a trajectory-tracking control which kept the vehicle on a well-designed reference trajectory. Ntousakis et al. (2016) proposed a trajectory planning methodology to determine the optimal longitudinal merging trajectories in a highway acceleration lane. Traffic efficiency, safety and passenger's comfort were able to be guaranteed by minimizing the cost function of acceleration, jerk and the derivative of the jerk. A further application of the combination of Linear-Quadratic Regulator and the Model Predictive Control also showed good performance on determining the optimal trajectory. Zohdy and Rakha (2016) engaged the cooperative adaptive cruise control (CACC) to automatically control the vehicles in the intersection so as to increase the traffic efficiency and improve the safety as the same time. Simulations based on the CACC-equipped vehicle were conducted, and the comparison with the signalized intersection, all-way stop control and the roundabout showed advantages on reducing

the delay and fuel consumption. While the car-following model, lane-change model and the trajectories planning have been well developed, few studies incorporates them into a same micro-simulation to the most of the auther's knowledge, which motivate the author to establish a complete micro-simulation system to emulate the performance of mixed traffic flow on the highway bottlenecks, such as the work zones and the emergency areas.

2.5 WORK ZONES AND EMERGENCY SERVICES

Work zones and emergency services are induced by different events, but they both create bottlenecks on the freeway. While work zone are mostly scheduled, the emergency incidents can happen anytime and anywhere; furthermore, it normally took long time till the emergency service arrived to regulate the traffic, which may bring even more impacts on the traffic system.

2.5.1 Emergency Services

Chung et al. (2010) divided the traffic congestion into two groups: recurrent congestions which are induced the imbalance between the lower road capacity and the higher the traffic demand, and nonrecurrent congestions which are induced by random incidents, among which 72 % were contributed by traffic accidents (Skabardonis Varaiya & Petty 2003). Chung et al. (2010) applied an accelerated failure time metric model to analyse the critical factors that affects the duration of an accident on the basis of a total 2940 datasets collected from a Korean freeway on 2004, and then gave advices on mitigating the impact to the road network by adjusting the factors. For emergency vehicle dispatching, Haghani et al. (2004) developed a model to simulate the response of emergency service vehicles real-time traffic information, and then guided those vehicles into the non-congested road. Smith et al. (2003) researched the impacts of traffic accident on the traffic capacity by applying traffic flow and accident dataset, and it was found that the percentage of capacity drop were far more than the number of the lane blocked. Yoo et al. (2010) proposed a road reservation scheme on the basis of ubiquitous sensor network to guarantee the quick response and safety of emergency service vehicles, and results show a 1.09 to 1.20 times faster on the response.

2.5.2 Work Zones

Compared to emergency service, a lot more researchers have done valuable works on the traffic regulation for work zones. Pei and Dai (2007) proposed an intelligent lane merge control system (ILMCS) on the basis of intelligent transportation system techniques. The ILMCS were capable of instructing the merge control based on the collected real-time traffic data, and the scale of the impacts brought by the work zone can be derived from the collected data (Pei & Dai 2007]. By conducting simulation in VISSIM, the ILMCS showed a good performance on mitigating the impacts on a two-lane traffic flow. Yang et al. (2009) demonstrated a lane-based signal merge control system to regulate the traffic flow at the entry of the work zone. Simulations in VISSIM were conducted to prove the efficiency of the control system, and the results showed that this control system outperformed all other existing strategies at that time (Su et al. 2016). Xue and Kang and Chang (2009) illustrated a lane-based dynamic merge control model and conducted extensive simulations in CORSIM-RTE simulation program to evaluable the optimized control thresholds with regards to the traffic flow dynamics. The overall traffic performance was improved by the proposed model, yet the inconsistency of the merge strategies lead to the oscillation of the speed. Hence, a further speed control strategy was required to be employed. Meng and Weng (2011) analysed the effects of configuration, traffic flow and heavy vehicle percentage on work zone traffic delay by simulations based on heterogenous CA model. The length of the transition area was proved to be the significant factor to the delay. Weng (2011) evaluate the binary effects of transition taper length on the work zone traffic capacity based on a collision avoidance analysis, and a minimum length of the taper was determined by the traffic condition and the road geometry. Wei and Pavithran (2006) employed dynamic merge metering to facilitate the dynamic late merge control, and VISSIM-based simulations were conducted to evaluate the performance. Papageorgiou et al. (2008) also applied a merging operation called ALINEA to mitigate the traffic congestion in the work zone, and results from the microscopic simulation demonstrated that the congestion problem can be potentially addressed by this algorithm. While the aforementioned literatures mainly focused on the congestion of the work zone, many other researchers developed great researches on the safety of the work zone. Tarko et al. (1999) presented a novel traffic control system that sets dynamic no pass zone to mitigate the traffic congestion at the entry of two-lane work zone. With the decreasing number of the aggressive lane-

changes, the traffic performance with regards to the safety and the travel time are improved, yet the microscopic improvement is not clearly illustrated. Su et al. (2016) compared the time-to-collision-based rear-end crash risks of work zones in Beijing and Singapore on the basis of the trajectories data collected from both cities. Factors that contributed to the collision were analysed, and this research was able to assist the traffic engineers on fixing traffic control strategies. Xue and Weng (2014) established a lognormal distribution function which was calibrated by Bayesian approach to forecast the response time of a traffic accident in the work zone, A series of factors were accessed in a case study on field data, and the road type, crash time, weather and light condition were regarded to be the most significant factors that affected the response time.

Chapter 3: CAV-based Traffic Regulation in Work Zones

3.1 INTRODUCTION

A work zone is a partially closed road section due to periodic maintenance, rehabilitation and reconstruction, bringing negative impacts on traffic performance, such as, accident, congestion, long travel time and dissatisfaction among road users (Meng & Weng 2011). The number of the through lanes declines; as a result, the traffic capacity is significantly reduced because of not only lane closure but also lane-changing activities (Laval & Daganzo 2006; Qu, Wang & Zhang 2015). Vehicles on non-through lanes have to merge into through lanes; otherwise, vehicles need to decelerate or even stop due to the existence of the work zone; in other words, lane-changing maneuvers become compulsory for those vehicles on non- through lanes. It makes the situation even worse when a large number of vehicles merge into a same target lane without cooperation. Indeed, the presence of a work zone can increase not only the possibility of traffic accidents happening but also the travel time due to the boost of density (Wang et al. 1996; Rouphail, Yang & Fazio 1988; Khattak, Khattak & Council 2002; Garber & Zhao 2002; Meng & Weng 2011).

With the continuous increase of the travel demand, traffic flow becomes more unstable and vulnerable. During peak hours, even a slight disturbance imposes high possibility of causing severe traffic interruptions, as human drivers are more likely to make heterogeneous responses under these conditions (Qu, Zhang & Wang 2017). It has been well recognized that these human driver's limit and heterogeneity are essentially non-controllable in traffic operations. Macadam (2003) proposed that human drivers show obvious reaction delay in reacting to different indications, such as merge indications and brake indications; moreover, the intensity of an indication has to reach a threshold to be sensed by human drivers. In this regard, transportation researchers develop models and applications that are very robust to accommodate these limit and heterogeneity, which lead to low capacity of our transport systems. With the advent of the connected and automated vehicles (CAV), the cooperation among vehicles becomes possible and, as a result, the limit and the heterogeneity can be controlled through developing a cooperative vehicle motion controlling system that

is able to smooth our traffic flow dynamics (Zhou, Qu & Jin 2016; Zhou, Qu & Li 2017).

There are a few studies analysing the influences caused by work zones. Adeli and Jiang (2003) used a neuro-fuzzy logic model to estimate the work zone capacity on the freeway. Jiang and Adeli (2004) used clustering-neural network models to estimate the work zone capacity on the freeway with less than 10 per cent error and applied object-oriented model to estimate the freeway work zone capacity, as well as queue delay. Meng and Weng (2011) proposed an Improved Cellular Automata Model (ICAM) to simulate the work zone traffic flow dynamics. Weng and Meng (2014) proposed a methodology to estimate the rear-end crash possibility on the work zone merging area, and it is found that this possibility increases as a result of late merging which is an instant merging maneuver with short front gap to the activity area in a work zone. Weng and Yan (2016) established a truncated lognormal distribution method to estimate the traffic capacity due to the presence of work zone. To the best of our knowledge, there is no research that applies the CAV on smoothing work zone traffic flow dynamics. The CAV are able to make immediate reaction to the deceleration of the preceding vehicle; therefore, shorter headways are required. Moreover, an embedded computer is able to compute the optimal safe speed as well as sliding distance to narrow the front gap, which is almost impossible for human drivers to calculate. As such, the average travel time to go through the work zone and the speed oscillation are anticipated to be reduced as the percentage of the CAV goes up if a proper collaborative mechanism is well designed. In this research, to bridge this void, we propose a cooperative cellular automaton model (CCAM) based on the ICAM developed by Meng and Weng (2011).

The research is organized as follows. In Section 3.2, the configuration of work zone from cellular automata model and a study area on Pacific Highway are demonstrated, followed by a review of ICAM with an amendment at the end. Section 3.3 describes the proposed microscopic traffic flow model for the CAV with the cooperative component among vehicle illustrated in detail. Section 3.4 presents the performance indicators, including traffic delay, safety and vehicle emission, under various penetration rates of the CAV. The last section concludes the paper.

Nomenclature

$G_{n,t}$	= The front gap of vehicle *n* at time *t*
x_{wz}	= The longitudinal location of work zone
$x_{n,t}$	= The longitudinal location of left front point on vehicle *n* at time *t*
$y_{n,t}$	= The lateral location of left front point on vehicle *n* at time *t*
L_t	= The length of transition area
l_n	= The length of vehicle *n*
$t_{n,t}$	= The headway of vehicle *n* at time *t*
t_{acc}	= The interaction headway
$a(V_{n,t})$	= The acceleration rate of vehicle *n* at time *t*
$B_{n,t}$	= The brake status of vehicle *n* at time *t*
$V_{n,t}$	= The velocity of vehicle *n* at time *t*
$V_{limit,n,t}$	= The speed limitation of vehicle *n* at time *t*
$G_{eff,n,t}$	= The effective front gap of vehicle *n* at time *t*
$G_{wz,n,t}$	= The distance from the front bumper of vehicle *n* to work zone at time *t*
G_{safety}	= The safety distance
$p(f_L, f_H, L_a, L_t)$	= The randomization probability within work zone
f_L	= The traffic flow volume of light vehicles
f_H	= The traffic flow volume of heavy vehicles
L_a	= The length of activity area
$G_{n,f,t}$	= The front gap of vehicle *n* with front neighbouring vehicle at time *t*
P_{merge}	= The possibility of merging maneuver
$\delta_{n,t}$	= Maximum allowable deceleration of vehicle *n* at time *t*
TTC	= The time to collision
$D_{comfort}$	= The comfortable deceleration rate

3.2 MODEL DEVELOPMENT TO SIMULATE MOVEMENTS OF MANNUALLY DRIVEN VEHICLES

3.2.1 Site description

This research is established on the basis of a two-lane (in one direction) freeway with a work zone at the Lane 1 starting from longitudinal location x1 to x4 as shown in Figure 3-1(a). The speed limit on this freeway is 110 km/h before vehicle entering advance warning zone that is from longitudinal location x0 to x1. The speed limit turns to 80 km/h after reaching the advance warning sign that is located at x0, and it then reduces to 60 km/h when vehicles enter the work zone. Figure 3-1(b) shows a photo of a work zone located on Pacific Highway around Coolangatta airport, where the number of lanes drops from two to one because of a large scale of construction tasks as indicated by the circle.

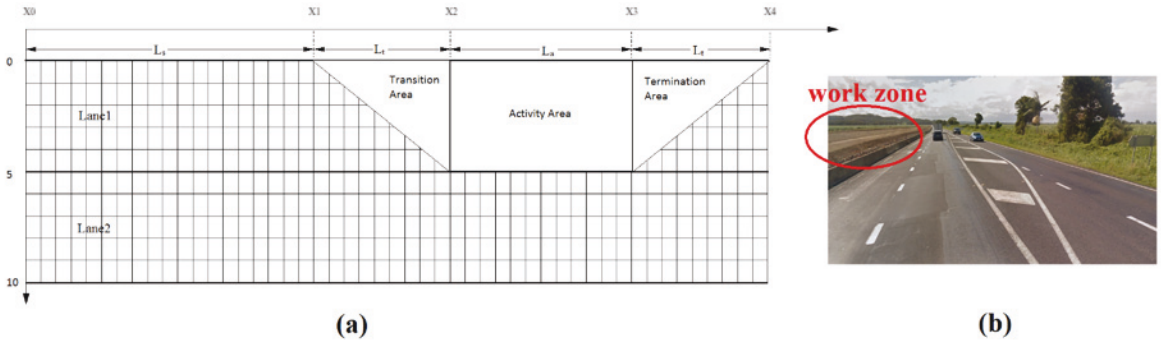

Figure 3-1 A plan view of freeway section around a work zone and a work zone on Pacific Highway

3.2.2 Modified ICAM

To simulate the traffic flow dynamics of MV, the ICAM was employed with modified incentive criterion and safety criterion. According to the ICAM, lanes were divided into cells of 0.5 meter in length and 0.7 meter in width. For any two consecutive vehicles

$$G_{n,t} = x_{n-1,t} - x_{n,t} - l_{n-1} \tag{3.1}$$

where $G_{n,t}$ denotes the front gap between vehicle n and its preceding vehicle n-1 or the remaining distance to the work zone at time t. Similarly,

$$G_{wz,n,t} = x_{wz} - x_{n,t} + y_{n,t} \times \frac{L_t}{5} \tag{3.2}$$

where $G_{wz,n,t}$ denotes the front gap between vehicle n and the work zone ahead.

3.2.2.1 Acceleration

The acceleration rule stipulated two application scenarios. The first scenario is when time headway $t_{n,t}$ is greater than interaction headway t_{acc}, and the second one requires that neither vehicle *n* nor its preceding vehicle *n-1* has braked during the previous simulation interval *t-1*. When either of these two scenarios happens, vehicle *n* accelerates with an acceleration rate $a(V_{n,t})$. Namely, if $(B_{n,t-1} = 0 \ \wedge \ B_{n-1,t-1} = 0) \ \vee \ t_{n,t} > t_{acc}$,

$$V_{n,t} = \min\{V_{n,t-1} + \ a(V_{n,t}), V_{limit,n,t}\} \tag{3.3}$$

Here, $a(V_{n,t})$ is a function of current speed $V_{n,t}$, and the values with regards to various speeds are demonstrated in Table 3-1. $V_{limit,n,t}$ denotes the speed limit of the road section.

Table 3-1 General coefficients

Variable	Condition	MV	CAV
Acceleration rate (cell/s^2)	$V_{n,t-1} \leq 11cell/s$	4	4
	$11cell/s < V_{n,t-1} \leq 22cell/s$	3	3
	$V_{n,t-1} > 22cell/s$	2	2
Deceleration rate (cell/s^2)		6	6
Comfortable deceleration rate (cell/s^2)		6.8	6.8
Interaction headway (s)		6	6
Safety distance (cell)		9	9
Maximum speed (cell/s)	Freeway	Based on Eq. (3.23)	60
	freeway work zone	Based on Eq. (3.23)	45

3.2.2.2 Deceleration

Compared with the original CA model, the ICAM proposed the effective front gap, taking the travel distance of vehicle *n-1* into account.

$$G_{eff,n,t} = G_{n,t} + \max\{0, \min(V_{n-1,t-1},\ G_{n-1,t}) - G_{safety}\} \tag{3.4}$$

where the component $\min(V_{n-1,t-1},\ G_{n-1,t})$ denotes the anticipated velocity of the preceding vehicle. It was applied to predict the minimum distance that the vehicle *t-1* can travel during the current simulation interval.

If $G_{eff\ n,t} < V_{n,t}$, vehicle n decelerates to avoid a rear-end crash with its preceding vehicle or the merging vehicle. The target velocity for the deceleration period is $G_{eff\ n,t}$ instead of $G_{n,t}$ which is too conservative, namely,

$$V_{n,t} = \min(V_{n,t}, G_{eff,n,t}) \tag{3.5}$$

If $V_{n,t} < V_{n,t-1}$, vehicle n decelerated with brake status being activated, namely, $B_{n,t} = 1$.

3.2.2.3 Randomization probability

Randomization probability was firstly proposed in Nagel-Schrechenberg's CA model to simulate the excessive brake and acceleration delay, which simulates the human limit as traffic flow forwards (Nagel & Schreckenberg 1992). Meng and Weng (2010) pointed out that the randomization probability was a function of traffic flow of light vehicles, traffic flow of heavy vehicles, the length of activity area and the length of transition area. The randomization probability can be formulated as

$$P(f_L, f_H, L_a, L_t) = \mathrm{a}f_L + bf_H + cL_a + dL_t + e \tag{3.6}$$

Parameters in Eq. (3.6) were calibrated by Meng and Weng (2011) using a trial-and-error method as demonstrated in Table 3-2.

Table 3-2 Parameters in randomization probability equation

coefficient	p_{in}	p_{out}
a	-1.24×10^{-4}	-6.80×10^{-5}
b	-1.30×10^{-4}	-1.28×10^{-4}
c	-3.00×10^{-5}	0
d	0	0
e	0.425	0.541

(Meng & Weng 2011)

3.2.2.4 Incentive criterion

The incentive criterion is one of the most significant two components in CA-based lane-change rule. In the ICAM, Meng and Weng (2010) proposed two incentive criteria, and the criteria referred to a larger following gap in the target lane and a slower preceding vehicle in the ego lane which can be denoted by $V_{n,t} > G_{n,t} \wedge V_{n,t} > V_{n-1,t}$ and $G_{n,t} < G_{n,f,t}$ respectively. Nonetheless, it is believed that the dominating incentive is the distance to the transition area when a vehicle is approaching a work zone. In that case, vehicles are encouraged to merge into the through lane when $G_{wz,n,t}$ reaches a critical value. Hidas (2002) announced that lane-changing action became essential when the headway to a lane blockage was less than 8 seconds. As such, we proposed Eq. (3.7) to calculate the possibility of lane-changing action in this chapter.

$$P_{merge} = \begin{cases} 0, & if\ G_{wz,n,t} > 8 \times V_{limit,n,t} \\ 1, & if\ G_{wz,n,t} \leq 8 \times V_{limit,n,t} \end{cases} \tag{3.7}$$

3.2.2.5 Safety criterion

As mentioned in the ICAM, the value of the gap between vehicle *n* and its back neighbouring vehicle in the target lane need to be greater than the value of the maximum speed, namely, $G_{n,b,t} > V_{limit,n,t}$ (Meng & Weng 2011). However, this safety criterion excluded the gap between subject vehicle and its anticipated preceding vehicle (APV), which is unrealistic. To avoid rear-end crash during merging period, a merging vehicle has to maintain a sufficient gap with its anticipated preceding vehicle; therefore, this gap needs to start from a reasonable value to accommodate the speed difference.

We proposed a new safety criterion in CCAM, that is, the front gap with the anticipated preceding vehicle from through lane has to be greater than $R_c(V_{n,t} - V_{alv,t}) + G_{safety}$ to accommodate the speed difference. Here, R_c denotes the reaction time, and it was assumed to be one second. With regards to lateral movement, the speed was limited to be less than 2 cells per second according to the ICAM (Meng & Weng 2011). However, merging maneuver was assumed to be completed within one second in CCAM, which means vehicles were able to merge into the target lane during the next simulation interval as long as safety criterion being fulfilled. To better

compare the performances of ICAM and CCAM, the MV were assumed to be able to finish merging maneuver with one second as well, and the main differences between the ICAM and the CCAM were compared as shown in Table 3-3. Compared with the ICAM, CCAM assigned different allowed maximum speeds with regards to type of the vehicles. It worth noting that the speed of the HDV can be affected by the change of the local density as illustrated in Eq. (3.23). Another difference between ICAM and CCAM is related to the effective gap who included two preceding vehicles in ICAM yet the whole platoon of preceding vehicles in CCAM. In the simulations, any negative front space headway or overshooting deceleration rate was regarded as an indication of a rear-end crash. Those crashes can happen during the car-following tasks or during a lane-change attempt, and the values of the safety distance and its related coefficients need to be modified once a crash is witnessed.

Table 3-3 Comparison between ICAM and Modified ICAM

Variable	ICAM	Modifications in CCAM
Randomization probability	Both are determined by Eq. (3.6), and the parameters are demonstrated in Table 3-2.	
Allowed maximum speed	45 cell/s within a work zone 60 cell/s elsewhere	Illustrated in Table 3-1
Acceleration	Both are determined by brake status and headway	
Deceleration	Determined by effective front gap	The effective front gap is modified as shown in Eq. (3.14)
Incentive criterion	Encouraged by a larger front gap	Encouraged by the distance to the work zone
Safety criterion	Exclude the influence of the front gap with the APV	Include the influence of the front gap with the APV

3.3 MODEL DEVELOPMENT TO SIMULATE MOVEMENTS OF CONNECTED AND AUTOMATED VEHICLES

3.3.1 Following model

3.3.1.1 Maximum allowable deceleration

In this model, we proposed a concept named the maximum allowable deceleration. The maximum allowable deceleration represented by $\delta_{n,t}$ can be defined as the maximum disturbance that two consecutive vehicles could accommodate. The

deceleration represented by $d_{n,t}$ is caused by the disturbance that vehicle n encountered at time t. If the preceding vehicle is slower than its following vehicle owing to the disturbance, namely $V_{n+1,t} > V_{n,t} - d_{n,t}$, there will be a risk of collision between these two consecutive vehicles. If the preceding vehicle is still faster than its following vehicle after decelerating, a collision is unlikely to happen. Hence, we only applied the maximum allowable deceleration when $V_{n+1,t} > V_{n,t} - d_{n,t}$.

When both vehicles maintain the unchanged speed after the deceleration, the time to collision (TTC) under such disturbance is calculated as:

$$TTC = \frac{G_{n+1,t}}{V_{n+1,t} - \left(V_{n,t} - d_{n,t}\right)} \tag{3.8}$$

Let τ be the threshold of time to collision (Kuang, Qu & Wang 2015). Only if $\frac{G_{n+1,t}}{V_{n+1,t}-(V_{n,t}-d_{n,t})} \geq \tau$ can a crash be avoided. Rearranging the equation gives

$$d_{n,t} \leq (V_{n,t} - V_{n+1,t}) + \frac{G_{n+1,t}}{\tau} \tag{3.9}$$

Thus, the right-hand side of the Eq. (3.9) are regarded as the maximum disturbance that a car-following scenario can accommodate, namely,

$$\delta_{n,t} = (V_{n,t} - V_{n+1,t}) + \frac{G_{n+1,t}}{\tau} \tag{3.10}$$

This disturbance can be further applied to determine the optimal acceleration as described in the next section.

3.3.1.2 Optimal speed increment

On the purpose of narrowing the car-following distance, a CAV is expected to adopt an optimal acceleration rate by which the CAV is able to not only reduce the headway at highest efficiency but also avoid rear-end crash even when its preceding vehicle encounters a disturbance. In our simulations, a speed difference between two consecutive simulation intervals delivered by the optimal acceleration is regarded as the optimal speed increment. The worst condition refers to when the preceding CAV applies the maximum deceleration rate that is calculated as the lesser of maximum allowable disturbance $\delta_{n-1,t}$ and the comfortable deceleration rate. The minimum stopping distance for vehicle n during the current simulation interval is approximated to be $(G_{n,t} + V_{n-1,t+1})$. Here, $V_{n-1,t+1} = V_{n-1,t} - \min\left(\delta_{n-1,t}, D_{comfort}\right)$ represents

the minimum velocity of the preceding vehicle and the target velocity of vehicle n. The maximum velocity for vehicle n narrowing the gap is $V_{n-1,t} + \Delta_{n,t}$, where $\Delta_{n,t}$ represents the optimal speed increment; thus, the equation can be written as:

$$(\Delta_{n,t+}V_{n-1,t})^2 - (V_{n-1,t+1})^2 = 2\big(G_{n,t} + V_{n-1,t+1}\big)D_{comfort} \tag{3.11}$$

That is,

$$\Delta_{n,t} = \big(2\big(G_{n,t} + V_{n-1,t+1}\big)D_{comfort} + (V_{n-1,t+1})^2 - V_{n-1,t}\big)^{0.5} \tag{3.12}$$

3.3.1.3 Effective gap

The determination of the effective gap highly depends on the type of the preceding vehicle, and therefore two cases are separately discussed. The first case refers to when the subject vehicle follows a MV. The CCAM stipulates that if the preceding vehicle n-1 is a MV, the subject CAV will not expect more information from its preceding vehicle. Thus, a same function from ICAM was used to calculate the effective gap, namely,

$$G_{eff,n,t} = G_{n,t} + \max\{0, \min\big(V_{n-1,t-1},\ G_{n-1,t}\big) - G_{safety}\} \tag{3.13}$$

In the second case, the preceding vehicle is a CAV. As two successive vehicles are both the CAV, we believed that the subject CAV was capable of accessing the effective gap of the preceding vehicle; therefore, we modified the effective gap as

$$G_{eff,n,t} = G_{n,t} + \max\{0, \min\big(V_{n-1,t}, G_{eff,n-1,t}\big) - G_{safety}\} \tag{3.14}$$

In Eq. (3.14), $V_{n-1,t}$ is used to calculate anticipated speed of the preceding vehicle instead of $V_{n-1,t-1}$ which is applied in Eq. (3.13), because the preceding CAV n-1 is able to share the speed with its surrounding CAV accurately with negligible delay. Additionally, an updated effective gap is sent from the preceding CAV n-1 to the subject CAV n for the effective gap calculation, which enables two successive CAV to travel with a shorter gap so as to increase the traffic capacity without decreasing the speed dramatically.

3.3.1.4 Deceleration

The velocity of a CAV depends on two factors that are the front gap and its derivative. The CAV will brake if its preceding vehicle decelerate and the front gap is small, namely, if $B_{n-1,t} = 1 \wedge G_{n,t} <= \alpha V_{n,t-1},\ B_{n,t} = 1$. Here, α is calibrated to be two seconds for the purpose of eliminating collisions. The rule emulates that a CAV

takes two consecutive brakes (during two consecutive simulation intervals) as potential indicator of the congestion downstream. In that case, if $G_{n,t} > 2 \times V_{n,t-1}$, there will be two possible scenarios based on the brake status.

In scenario 1, the preceding vehicle's brake status during next simulation interval is not activated. $G_{n,t+1}$ is definitely acceptable for the subject vehicle to keep its following action.

In scenario 2, the preceding vehicle's brake status during next simulation interval is activated. The front gap which is more than the value of $V_{n,t-1}$ (thus the effective gap is definitely greater than the current velocity) is enough for a CAV decelerate.

Trajectories extracted from simulations illustrated that rear-end crash diminished when α was equal to two. If $G_{eff,n,t} < V_{n,t}$, vehicle n decelerates to $G_{eff,n,t}$ avoid rear-end crash with its preceding vehicle n-1, namely $V_{n,t} = \min(V_{n,t}, G_{eff,n,t})$; moreover, a CAV will decelerate if its surrounding vehicles need cooperation as illustrated in the lane-changing model. If $V_{n,t} < V_{n,t-1}$, vehicle n decelerated with brake status activated ($B_{n,t} = 1$).

3.3.1.5 Narrowing the front gap

G_{safety} was introduced into CCAM from the ICAM to ensure that the CAV can decelerate to a safe speed before rear-end crash happens with a relatively small deceleration rate for comfort consideration. If vehicle n has a greater velocity than its preceding vehicle when the front gap is greater than the safety distance, the velocity of vehicle n is allowed to be greater than that of its preceding vehicle by one speed increment; however, the velocity should be less than the effective gap to avoid a rear-end crash. Namely, If $G_{n,t} > G_{safety} \wedge V_{n,t-1} > V_{n-1,t}$,

$$V_{n,t} = \min\left(V_{n-1,t} + \Delta_{n,t}, G_{eff,n,t}\right) \tag{3.15}$$

At the same time, vehicle n can avoid the necessity of excessive brakes.

If the velocity of vehicle n is less or equal to that of vehicle n-1 when the front gap is greater than the safety distance, there are two scenarios that are:

In scenario 1, when the brake status of vehicle n is not activated, vehicle n accelerates by acceleration rate proposed in the ICAM, however the speed difference should not

be greater than one speed increment, namely, If $G_{n,t} > G_{safety} \wedge B_{n,t} \neq 1 \wedge V_{n,t-1} \leq V_{n-1,t}$,

$$V_{n,t} = \min\left(V_{n,t-1} + a\left(V_{n,t-1}\right), V_{n-1,t} + \Delta_{n,t}\right) \tag{3.16}$$

In scenario 2, when the brake status is activated, vehicle n keeps a lesser speed of $V_{n,t-1}$and $V_{n-1,t-1}$, that is, If $G_{n,t} > G_{safety} \wedge B_{n,t} = 1 \wedge V_{n,t-1} \leq V_{n-1,t}$,

$$V_{n,t} = \min\left(V_{n,t-1}, V_{n-1,t-1}\right) \tag{3.17}$$

3.3.2 Lane-change model

The lane-change model was established based on the types of APV and anticipated following vehicle AFV, and we defined the scenarios by three cases. In the first case, the APV and the AFV are CAV, where the APV and AFV denotes the preceding vehicle and the following vehicle respectively after the subject vehicle merging into the target lane. If the net distance to the APV and AFV are not less than the safety distance, namely, $G_{n,apv,t} \geq G_{safety} \wedge G_{n,afv,t} \geq G_{safety}$, vehicle *n* is able to start merging. Otherwise, when the net distance to the APV is shorter than the safety distance, namely, $G_{n,apv,t} < G_{safety}$, the ego vehicle will decelerate to increase the gap. As shown in Eq. (3.18) the deceleration is restricted by comfortable deceleration rate and the maximum allowable deceleration rate.

$$V_{n,t} = V_{n,t-1} - \min\left(D_{n,CAV},\ D_{comfort}, \delta_{n,t}\right) \tag{3.18}$$

When the net distance to the AFV is shorter than the safety distance, namely, $G_{n,afv,t} < G_{safety}$, the AFV will decelerate with a well-controlled deceleration rate as shown in Eq. (3.19).

$$V_{afv,t} = V_{afv,t-1} - \min\left(D_{afv,CAV},\ D_{comfort}, \delta_{afv,t}\right) \tag{3.19}$$

$G_{n,alv,t}$ and $G_{n,afv,t}$ denote the gaps with the APV and the AFV respectively. If a CAV receives a message indicating the existence of a work zone from the first vehicles of the platoon, a lane-change maneuver will be indicated. At the meanwhile, its APV and AFV will receive the message of this lane-change maneuver. When a CAV starts merging, the APV updates its maximum allowable deceleration by taking $G_{n,apv,t}$and $V_{n,t}$ into account. At the same time, AFV also updates its front gap to $G_{n,afv,t}$. The front gap of the ego CAV is equal to the lesser of $G_{n,apv,t}$ and $G_{n,t}$; thus, maximum

allowable decelerations, optimal speed increments and effective gaps of these three vehicles are updated accordingly.

In the second case, the AFV is still a CAV, however, the ego vehicle merges to follow a MV. Similar to the first case, vehicle *n* will start merging when $G_{n,apv,t} \geq G_{safety} \wedge G_{n,afv,t} \geq G_{safety}$, but if $G_{n,alv,t} < G_{safety}$,

$$V_{n,t} = V_{n,t-1} - \min\left(D_{n,MV}, D_{comfort}, \delta_{n,t}\right) \tag{3.20}$$

Nonetheless, the difference is that the deceleration rate is determined by a more conservative effective gap as described by modified ICAM. When $G_{n,afv,t} < G_{safety}$,

$$V_{afv,t} = V_{afv,t-1} - \min\left(D_{afv,CAV}, D_{comfort}, \delta_{afv,t}\right) \tag{3.21}$$

Because the APV is driven by a human driver, it will not be notified about this lane-change maneuver. Even though it is possible that the human driver is carefully enough to notice the ongoing lane-change maneuver, the ego vehicle will not risk on continuing the lane-change task. Hence, the deceleration of the APV may interrupt the lane-change maneuver of the CAV, which makes the waiting period longer.

In the third case, the anticipated following vehicle is a MV, the anticipated preceding vehicle is either a MV or a CAV. Three different scenarios are illustrated as below:

In scenario 1, when $G_{n,apv,t} \geq G_{safety} \wedge G_{n,afv,t} \geq G_{safety} + R_c\left(V_{afv,t} - V_{n,t}\right)$, the vehicle *n* is able to start merging.

In scenario 2, when $G_{n,alv,t} < G_{safety}$, but the gap between anticipated preceding vehicle and anticipated following vehicle can accommodate the merging vehicle, namely, $G_{n,apv,t} + G_{n,afv,t} \geq 2 \times G_{safety} + R_c\left(V_{afv,t} - V_{n,t}\right)$, the velocity of merging vehicle will be adjusted according to an updated front gap that is $G_{n,t} = \min\left(G_{n,apv,t}, G_{n,t}\right)$. The subject vehicle *n* will be able to merge whenever the condition mentioned in scenario is reached.

In scenario 3, when $G_{n,afv,t} < G_{safety}$, and the gap between anticipated preceding vehicle and anticipated following vehicle cannot accommodate the merging vehicle, namely, If $G_{n,apv,t} + G_{n,afv,t} < 2 \times G_{safety} + R_c\left(V_{afv,t} - V_{n,t}\right)$, the subject vehicle *n* will have to expect to merge into a following gap, and

$$V_{n,t} = V_{n,t-1} - \min\left(D_n,\ D_{comfort}, \delta_{n,t}\right) \tag{3.22}$$

Additionally, if the AFV is followed by another CAV, this CAV will decelerate to prepare a gap for the subject vehicle n: $V_{afvf,t} = V_{afvf,t-1} - \min\left(D_{afvf},\ D_{comfort}, \delta_{afvf,t}\right)$. Here, $V_{afvf,t}$ denotes the velocity of the following vehicle of APV, and D_{afvf} denotes the deceleration rate (which is illustrated in the ICAM) of the following vehicle of APV.

To summarize, when all of these three vehicles are CAV, a well-developed collaborative strategy can guarantee a smooth merging maneuver. While the APV is the only MV among these three vehicles, the other two vehicles' collaborations can still perform well without the participation of the APV. If the AFV is a MV, only a certain condition can encourage the subject CAV merge into the gap no matter APV being CAV or not; otherwise, the collaboration will be currently terminated while the subject CAV decelerates to look for collaborations with following vehicles. The

3.4 CASE STUDY

3.4.1 Model calibration

According to traffic fundamental diagram, the speed is limited by the current density which can be transferred into current headway for individual vehicle. Greenshield's model as shown in Eq. (3.23) was applied to emulate the maximum speed that a driver may accepted under certain traffic density.

$$V = V_f - \left(\frac{V_f}{K_j}\right) \times K \tag{3.23}$$

where V_f denotes the free flow speed which is same as the maximum speed of CAV; K_j denotes the jam density which is assumed to be 60 vehicles per kilometre; V and K denote the actual speed and actual density respectively. With the decrease of the headway, drivers of MV are encouraged to drive slower than the actual speed limit to avoid rear-end crashes. In the simulation, the trajectories of all vehicles were renewed after every simulation loop, and the simulation would be terminated once a crash or an overshooting acceleration rate was witnessed. In our generated dataset, results showed that no crash or overshooting acceleration rate was witnessed after the whole simulation. To be consistent with the ICAM, the time span lane-change maneuvers were assumed to be 1 second. It is also assumed that the approaching vehicles were

impacted by the work zone from as least 8 second away from the work zone. Other assumptions including the selection of the value of the τ and the values of the coefficients ahead of the safety distance from the CCAM were determined to avoid the rear-end crashes, where the values were approximated into the nearest integers respectively.

3.4.2 Deterministic indicators

To precisely and comprehensively illustrate the relationship between the performance of cooperative lane-change and the penetration rate, we conducted 14 microscopic simulations for each penetration rate. The headways are consistently set to be 3 seconds. The distributions of CAV and MV are different through these 14 simulations so that all scenarios of lane-change cooperation can be covered; moreover, curve fittings are conducted to clearly demonstrate the trends.

Six deterministic indicators selected to demonstrate the traffic performance are as follows:

- Travel time: this is an essential criterion to evaluate traffic performance according to traffic jam economic cost (Zhou, Qu & Jin 2016). The average travel time is the average duration starting from a vehicle travels exiting the 8,000th cells to entering the 10,000th cells;

  Excessive brake: it describes the quantity of overshooting deceleration that discomfort the passengers. It was believed that the main reason is the aggressive (forced) lane-change at the entrance of the work zone. We took 6.8 cell/s^2 as the threshold of distinguishing the excessive brakes and the ordinary brakes, which was suggested by AASHTO (2004) to be the comfortable deceleration rate. Hence, the quantity of excessive brake is counted on the basis of whether the deceleration rate is greater than 6.8 cell/s^2.

- Merge delay: it represents the duration starting from when the merging indication is activated to whenever the merging maneuver is finished. On the other hand, it demonstrates the average time needed for lane-change vehicles to find the lane-change opportunities.

- Speed standard deviation: this is an indicator for speed oscillation which may cause passengers' dissatisfaction, and the speed standard deviation for vehicle *n* can be calculated by the Eq. (3.24):

$$SD_n = \sqrt{\frac{\sum_{t=1}^{N}(V_{n,t} - \bar{V})^2}{N}} \tag{3.24}$$

- The duration of immobility: it represents the cumulative time span when one vehicle stops. The immobility is either caused by congestion before reach the work zone or the failure of lane-change at the entrance of the work zone.
- The quantity of emission: it is generated by VT-micro emission model that was proposed by Ahn et al.(2002) as shown in Eq. (3.25), where velocities and accelerations are the key factors that affect the emission.

$$\ln(MOE_e) = \begin{cases} \sum_{i=0}^{3}\sum_{j=0}^{3}\left(L_{i,j}^{e} \times s^i \times a^j\right) & a \geq 0 \\ \sum_{i=0}^{3}\sum_{j=0}^{3}\left(K_{i,j}^{e} \times s^i \times a^j\right) & a < 0 \end{cases} \tag{3.25}$$

Where MOE_e denotes the instantaneous fuel consumption (l/s.) or emission rate (mg/s), $L_{i,j}^{e}$ and $K_{i,j}^{e}$ represent the coefficients calibrated via the regression of the fuel consumption and the emission data in these two scenarios, while *a* and *s* denote acceleration and speed respectively as shown in Table 3-4. The field data were collected by the Environment Protection Agency of the Automotive Testing Lab in Ohio and in Michigan respectively in 1997 mainly focusing on the emission of the HC, CO, NO_x, and CO_2, while a total of 101 vehicles (including heavy vehicles and light vehicles) were involved in the experiment.

As shown in Figure 3-2(a), a concave descending trend can be witnessed when the penetration rate kept increasing. The average travel time was reduced by 25 % when the penetration rate came to 34.1%, while only half of the original travel time was needed when penetration rate came to 62.25%. In Figure 3-2(b), the quantity of the excessive brakes concavely decreased from 3103 to 271 when penetration rate rose from 0% to 100%. It showed that drivers and CAV were more comfortable with the disturbances caused by the lane-change maneuvers when more CAV were involved into the traffic network. In Figure 3-2(c), the cumulative merge delay for all vehicles showed a non-monotonic decrease from around 3561 seconds to 9 seconds. The reason is that vehicles were able to find the lane-change opportunities due to the high-level collaborations. Figure 3-2(d), the standard deviation decreased with the increase of

penetration rate, and it was proved that the collaborations provided by the CAV were capable of reducing the traffic oscillations. In Figure 3-2(e), the duration of immobility showed a concave decrease trend when penetration rate increased, and there were no vehicle stopping at the end of the transitional taper as a result of high-level collaborations when the penetration rate came to 98.5%. As shown in Figure 3-2(e), the y-axis denotes the total emission during the entire time span, and the quantity of emission continued decreasing with the increase number of the CAV being involved. The trend was relatively steep when penetration rate rose from 50 % to 80 %, which means the CAV can contribute more to reduce emission if they take the majority of vehicles. When the MV was the major component, the CAV had to give priorities to the MV frequently; thus, the collaboration that the CAV provided is relatively limited. This result showed that the CAV is not only fuel-economic but also environmental-friendly.

Table 3-4 Coefficients of VT-micro emission model

Coefficients	**Constant**	**Speed**	**Speed^2**	**Speed^3**
Positive acceleration				
Constant	-0.87605	0.03627	-0.00045	2.55E-06
Acceleration	0.081221	0.009246	-0.00046	4.00E-06
Acceleration^2	0.037039	-0.00618	2.96E-04	-1.86E-06
Acceleration^3	-0.00255	0.000468	-1.79E-05	3.86E-08
Negative acceleration				
Constant	-0.75584	0.021283	-0.00013	7.39E-07
Acceleration	-0.00921	0.011364	-0.0002	8.45E-07
Acceleration^2	0.036223	0.000226	4.03E-08	-3.5E-08
Acceleration^3	0.003968	-9E-05	2.42E-06	-1.6E-08

3.4.2.1 Disaggregated trajectory analysis

By extracting the trajectories from the entire traffic network, we can find more detailed demonstrations of the lane-change collaborations. Figure 3-3 gives the car-following trajectories of two different types of vehicles. Compared to the following MV, the following CAV were shown to be capable of tolerating much shorter headways, and it demonstrated much fast reaction to the deceleration of the preceding vehicle. This explains why the increase of density did not reduce the average speed. Due to the high sensitivity to the change of speed, the CAV demonstrated a synchronized trajectory with its preceding MV, and almost no delay of CAV's

accelerating was witnessed when the preceding vehicle accelerated. This advantage is even clearer when the CAV were in a platoon as shown in Figure 3-4. While MV suffered from the speed variations and over-braking, the CAV were able to keep very stable car-following motions. Consequently, not only was the average travel time reduced, but road users' comfort was guaranteed.

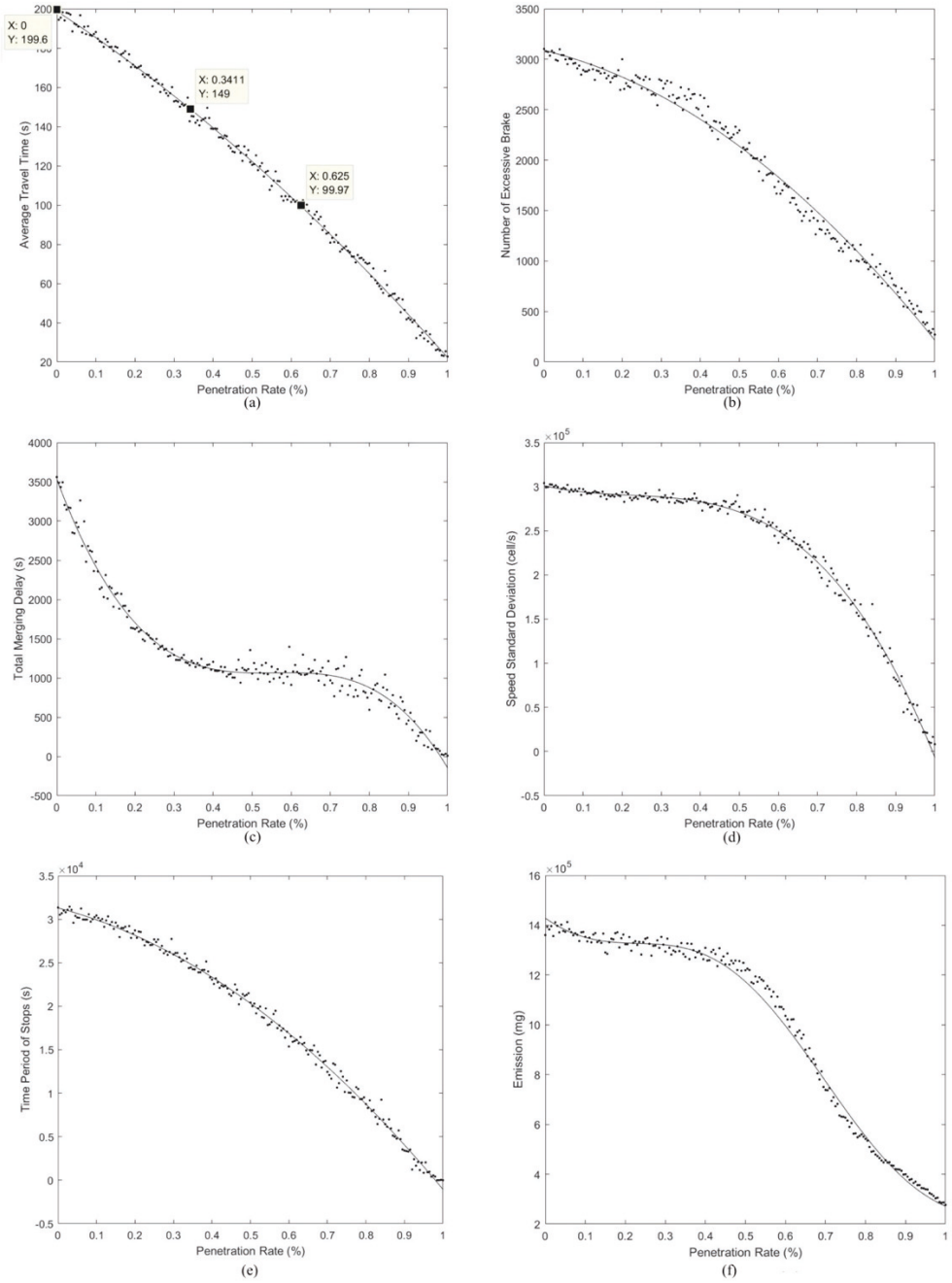

Figure 3-2 The deterministic indicators of the traffic performance: (a) Average travel time. (b) Quantity of Excessive brakes. (c) Cumulative merge delay. (d) Speed standard deviation. (e) Duration of Stopping. (f) Emission.

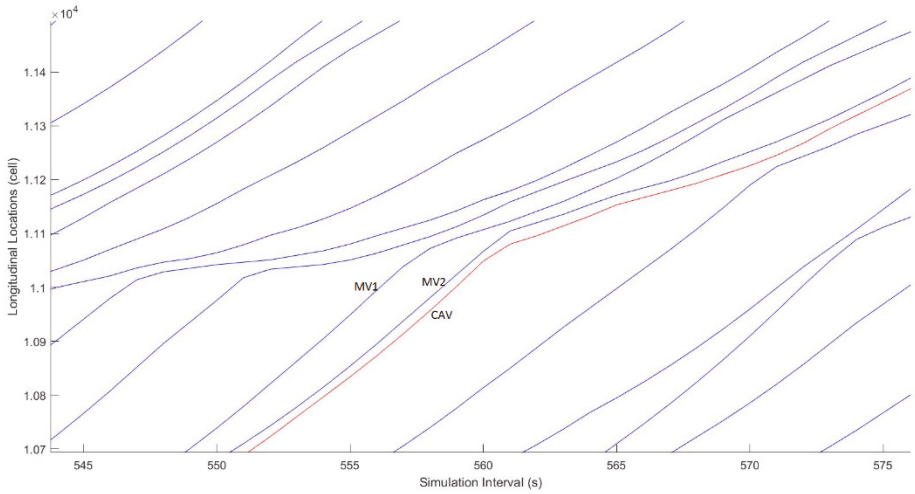

Figure 3-3 Following front gap comparison based on trajectories

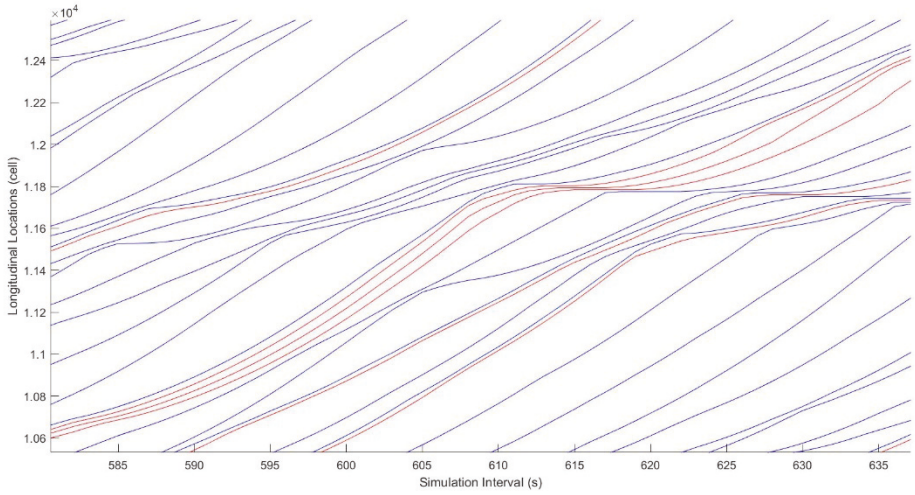

Figure 3-4 Following model performance analysis based on trajectories.

As shown in Figures 3-5 and 3-6, the dash lines record the trajectories when vehicles were travelling on the origin lane, while solid lines records the trajectories after vehicles merged into the target lane, and the green circles represent the starts and the ends of the lane-change maneuvers. In Figure 3-5, a CAV was shown to be capable of determining whether to merge in front of or behind its adjacent vehicle according to their relative position. Figure 3-6 demonstrates how CAV facilitated the MV's lane-change maneuvers. When a MV sent a lane-changing indication to the anticipated following CAV, the CAV in the target lane will give priority to the MV to facilitate the pending lane-change maneuver.

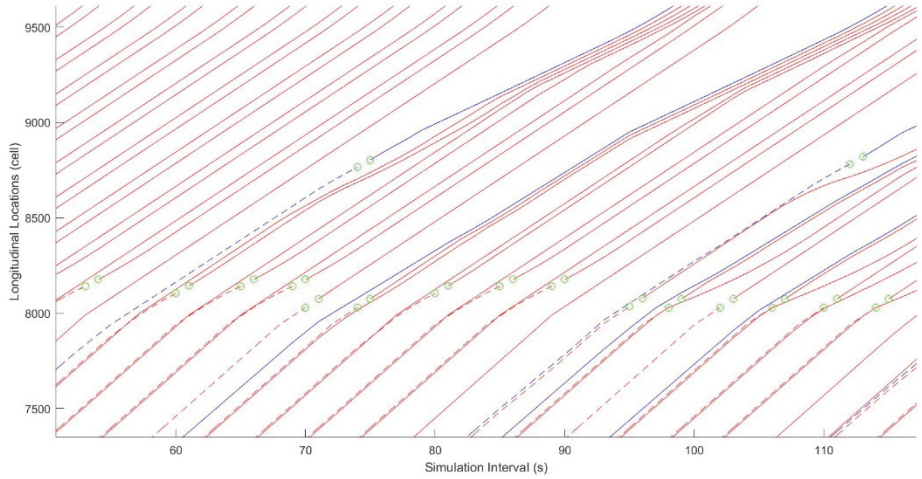

Figure 3-5 Priority analysis during lane-changing period

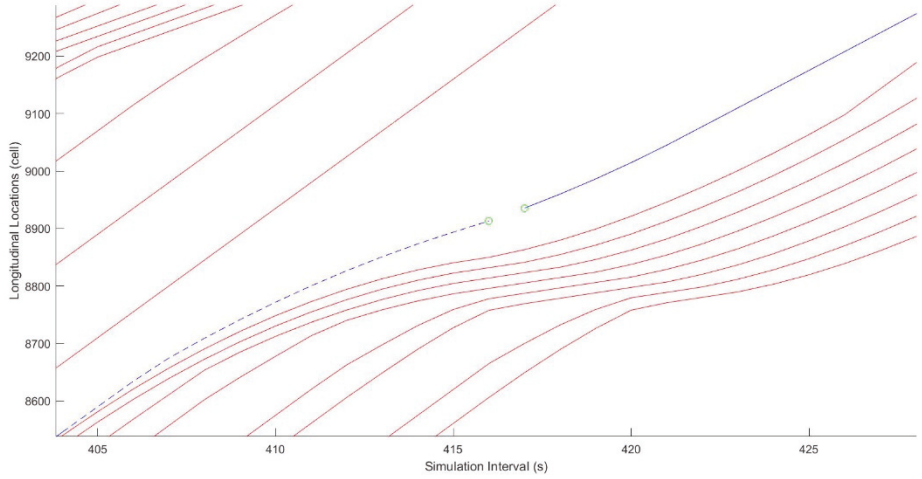

Figure 3-6 Cooperation between CAV and MV during lane-changing period

Figures 3-7 and 3-8 illustrate the trajectories when penetration rate are 0 and 100% respectively. When there was no CAV participating in the simulation, the merging maneuvers brought severe disturbances to the following vehicles, and the disturbance then evolved into the wide moving jam. By incorporating the CAV, collaborations among the CAV can solve this problem effectively. Figure 3-8 shows the resultant trajectories where regulated collaborations were demonstrated.

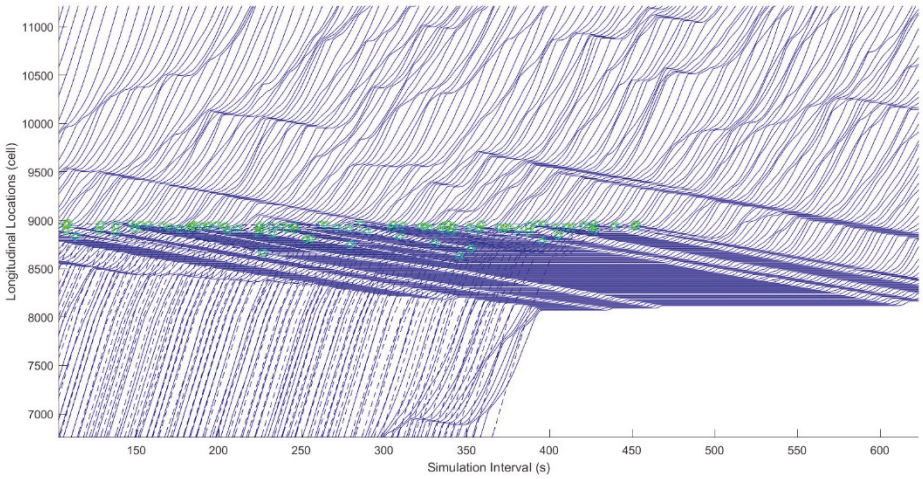

Figure 3-7 Trajectories without CAV's participation

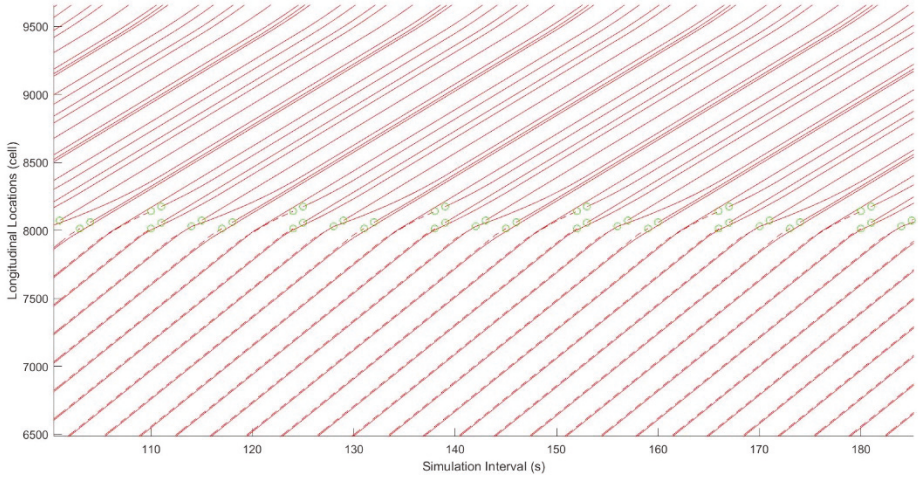

Figure 3-8 Trajectories with penetration rate being 100%

3.4.3 Probabilistic indicators

Figure 3-9 shows the average travel time collected from more than 2,000 simulations, and the average travel time variation decreased with the penetration rate, which means that the traffic condition can be predictable in a more deterministic manner with the increase of CAV' penetration rate. Similarly, a similar trend appeared on emission prediction as shown in Figure 3-10. The variation kept decreasing, and the quantity is negatively related to penetration rate. The main source of the randomness was the conflicts among heterogenous human drivers either during the car-following tasks or the lane-change tasks. Even tiny oscillation created between two drivers can cumulate into a huge congestion, especially in the work zone where the

traffic density can be usually higher. One of the most significant reasons for the decreasing randomness was that the deterministic features of the CAV vehicles can filter plenty of redundant accelerations and decelerations, therefore, the velocities would be kept on a relative stable level when the penetration rate increased. Additionally, the collaborations among vehicles during the lane-change tasks can avoid many aggressive merge behaviours, and thus mitigating the impacts on the target lanes. In that case, the vehicles from the target lane can traverse without significantly decreasing the speed even though other vehicles merge ahead of them. It should also be mentioned that both figures are depicted with a three-second initial headway.

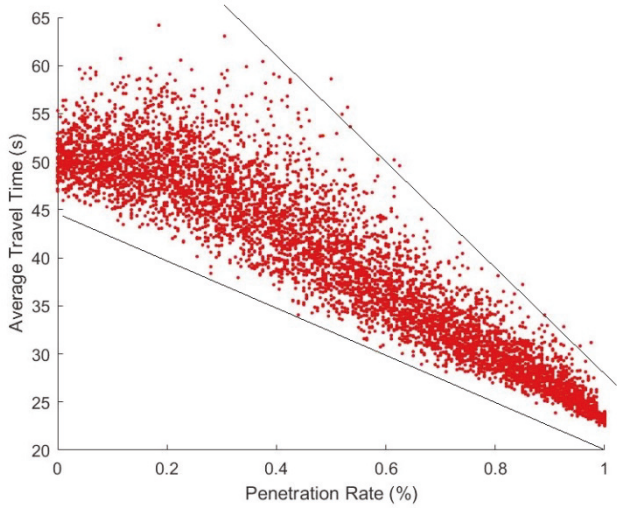

Figure 3-9 Massive illustration of average travel time over penetration rate

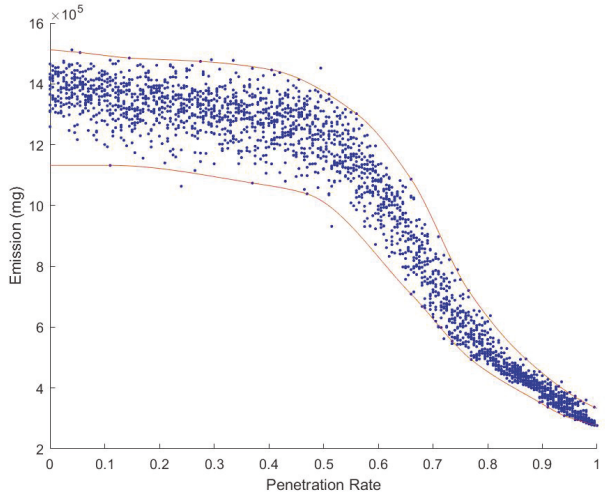

Figure 3-10 Massive illustration of emission over penetration rate

3.4.4 Traffic phase analysis

Figures 3-11to 3-14 demonstrate the velocities over longitudinal positions at the work zone under various CAV' penetration rates of 0 %, 30 %, 50 % and 80 % respectively. Their sub-figures illustrate the velocities of the 50^{th} vehicle and the 150^{th} vehicle representing the downstream vehicles and upstream vehicles respectively. The velocities of their surrounding CAV are also demonstrated for comparison purpose when penetration rate is 50 % and 80 %. As shown in Figure 3-11, a severe traffic jam appeared in the work zone area, and most of vehicles kept travelling with low speeds even though they had passed the work zone by 500 cells. As can be seen from two sub-figures, the upstream vehicles represented by sub-figure 2 suffered a more severe disturbance than downstream vehicles represented by sub-figure 1 because disturbances propagated along the platoon, which is consistent with the traffic-phase theory. In Figure 3-12, it is shown that vehicles were able to accelerate to relatively high speed after suffering a severe disturbance even though vehicles were still within the work zone area with the help of a few (around 30 % of total number of vehicles) CAV' collaborations; however, the speeds were still lower than normal speed limit after passing the work zone, but this problem was alleviated when there were more CAV in the platoon as shown in Figure 3-13. With the collaboration provided by CAV, MV suffered less disturbances as shown in sub-figure 1. Sub-figures 2 and 3 illustrate the velocities of two successive vehicles that consisted of a preceding CAV and a following MV, and the main differences are highlighted by the circles in the figure. The CAV had higher peak speed than the MV at same condition because CAV can handle shorter front gap after precise calculations. In that case, the vehicle can narrow the front gaps effectively. When penetration rate came to a relatively high level, most of disturbances were able to be avoided at high level (80%) of penetration rate. In Figure 3-14, sub-figures 1 and 2 and sub-figures 3 and 4 illustrate two pairs of successive vehicles both consisting of a preceding MV and a following CAV. The circled parts in sub-figure 3 and 4 illustrate the advantage that CAV can decelerate with a relatively small deceleration rate to avoid passengers' dissatisfaction while avoiding the rear-end crash at the same time. Hence, disturbances cumulated along the platoon can be effectively avoided; moreover, most of vehicles can accelerate to its original speed after leaving the work zone. Detailed illustrations of speed evolvement over longitudinal positions are shown in Appendix B, where a clear alleviation of disturbance can be witnessed. At the meanwhile, it can be clearly witnessed that the

participation of the CAV was very effective on dampening the traffic oscillations by comparing all figures with varying penetration rates.

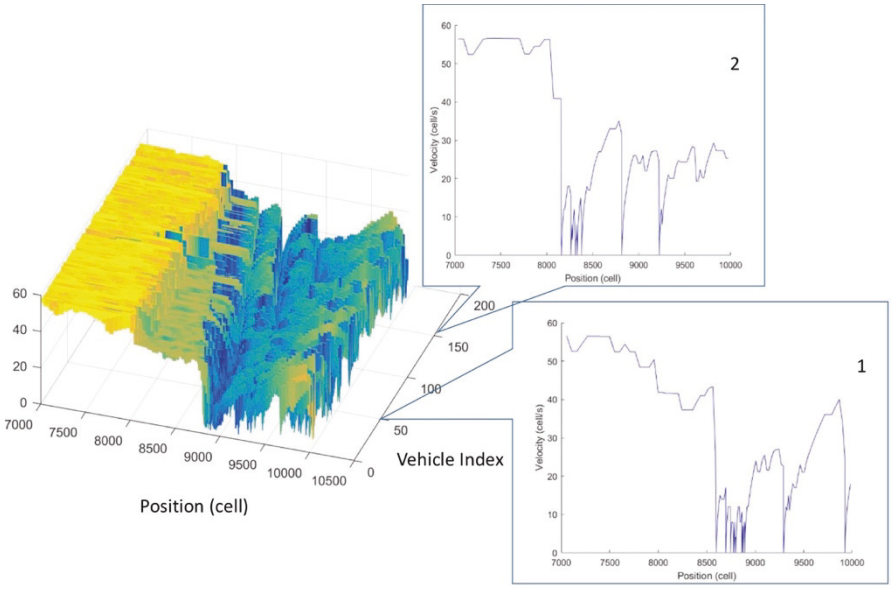

Figure 3-11 Velocities over longitudinal positions when penetration rate = 0 % with sub-figures illustrating the velocity-location relationships of (1) the 50th vehicle which is a MV; (2) the 150th vehicle which is a MV respectively

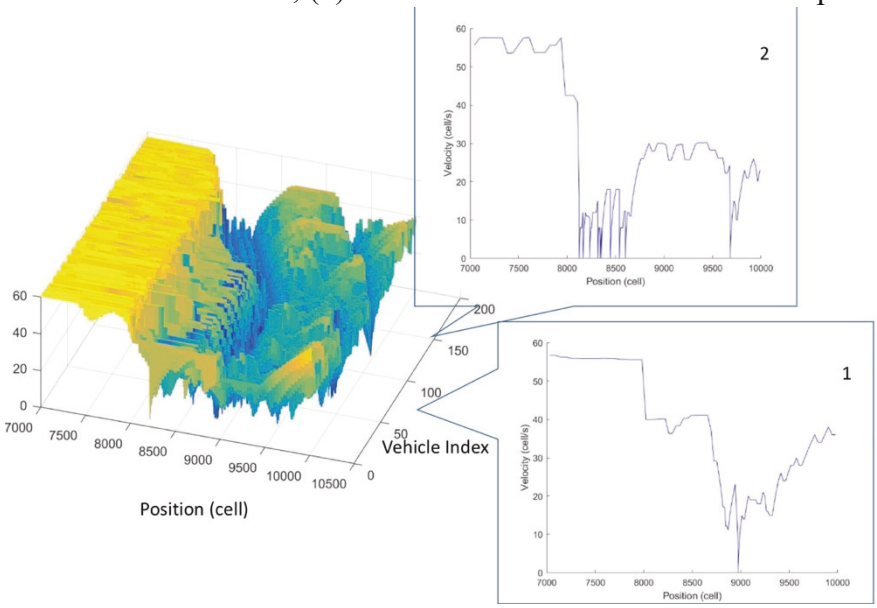

Figure 3-12 Velocities over longitudinal positions when penetration rate = 30 % with sub-figures illustrating the velocity-location relationships of (1) the 50th vehicle which is a MV; (2) the 150th vehicle which is a MV respectively

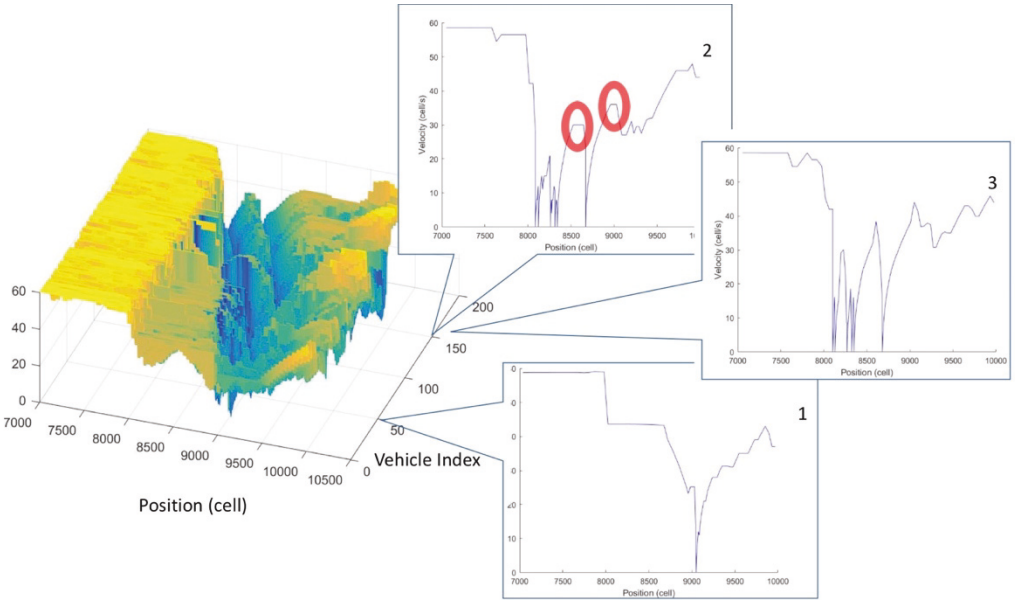

Figure 3-13 Velocities over longitudinal positions when penetration rate = 50 % with sub-figures illustrating the velocity-location relationships of (1) the 50th vehicle which is a MV; (2) the 150th vehicle which is a CAV; (3) the 151th vehicle which is a MV respectively

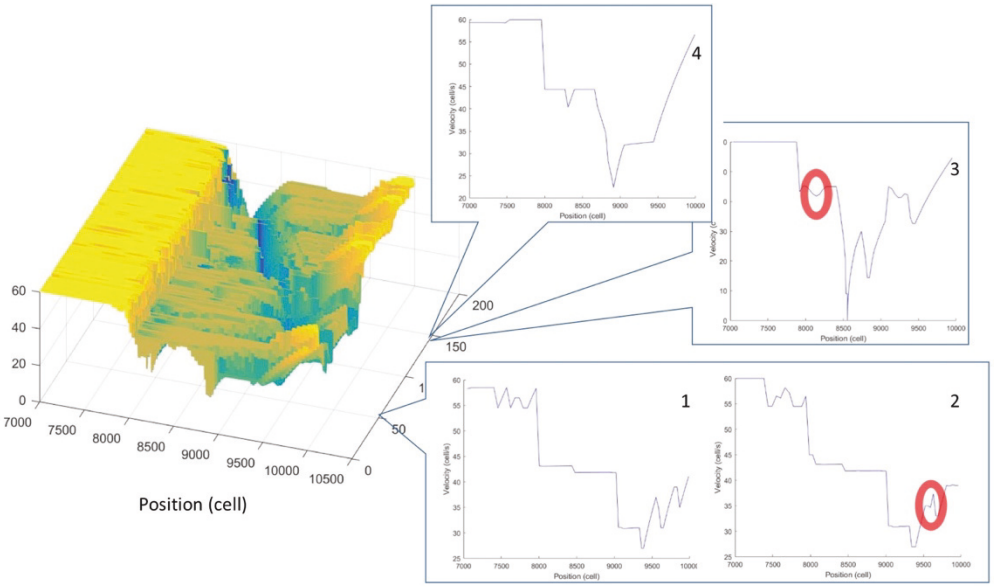

Figure 3-14 Velocities over longitudinal positions when penetration rate = 80 % with sub-figures illustrating the velocity-location relationships of (1) the 49th vehicle which is a MV; (2) the 50th vehicle which is a CAV; (3) the 150th vehicle which is a CAV; (4) the 149th vehicle which is a MV respectively

3.5 SUMMARY

Work zones bring negative impact on freeway traffic, and a number of problems emerge, such as long travel time, high speed variation, driver's dissatisfaction and traffic congestion. In this research, for the first time, we develop a cooperative cellular automata model introducing a collaborative component of connected and automated vehicles to simulate a highway work zone system. Results are collected from different penetration rates for comparison purposes, and positive effects are demonstrated. The average travel time decreases by 25% and 50% when penetration rate reaches 34.1% and 62.25% respectively. The variabilities of these indicators also show significant decrease trend as the penetration rate of connected and automated vehicles goes up. We also extract some of the trajectories in order to analyse the reason for these improvements, and it clearly reveals how connected and automated vehicles harmonize traffic flow dynamics. It can be expected that the work zone traffic will no longer bring severe negative impacts on our current traffic network even during the rush hour with reasonable amount of CAV's participation, because the CAV are looked forward to address the most significant source of the congestion which are the oscillations and the lane-change conflicts.

Compared to other CA-based model, the CCAM can deliver more continuous trajectories without boost computational load; furthermore, it included intelligent contents which could emulate the collaborative manner of the CAV. The CAV regulated by the CCAM were able to avoid redundant reactions to the change of the surroundings while safety level was guaranteed at the same time. Thanks to the effective gaps, more preceding vehicles can be involved to determine the optimal following velocities, so the oscillations during the car-following maneuvers can be effectively reduced. The CCAM also demonstrated a good compatibility to the work zone traffic simulation where the change of headway and density can be significant.

This study mainly focused on the traffic flow in the freeway, where the speeds of the vehicles are relatively high, and the number of the entrances and the exits is very limited compared to the other road types, therefore, the CCAM is only suitable for simulating the freeway traffic. In the future researches, more development based on the CCAM are expected to make it compatible with more road types. The limitation of CCAM is that the information topology adopted in car-following model only involves three homogenous vehicles in a platoon, thus, a heterogenous traffic system will be

considered, and more communication topologies will be adopted to improve the platoon stability and scalability in the future research; moreover, a time-dependent driver behaviour model needs to be considered in order to examine the feasibility of CCAM under a more realistic scenario.

Chapter 4: Congestion Dispersion under Emergency Service

4.1 INTRODUCTION

Transportation has been playing an extremely significant role in modern societies from people's daily routines to the economy of countries. A smooth traffic can bring high satisfaction to all participations in our society, while a traffic jam can significantly impact the functionality of a city. Unfortunately, the truth is that our traffic systems are usually unstable with the presence of incidents, such as traffic accidents or vehicle breakdowns. Other incidents, like public events, that partially take up road surface can also bring similar impacts. In that case, lanes are likely to be either fully blocked or partially impacted creating bottlenecks to the surrounding traffic system; therefore, the traffic capacity would dramatically reduce due to the closure of the lanes. Emergency services after severe traffic accidents usually require much larger space than the incident-affected area, and thus lead to more lane closures. In this research, the emergency service refers in particular to the existence of the emergency vehicles, for instance, the ambulance, the wrecker, etc. Under the aforementioned situations, vehicles on the blocked lane will be forced to execute lane-change activities; otherwise, they will have to stop at the merging point, which inversely influence the lane-change maneuver. It is found that both lane closures and lane-changing activities impact the traffic capacity significantly (Laval & Daganzo 2006; Qu, Wang & Zhang 2015). With the decreasing of traffic capacity, road users may experience longer travel time, higher speed variation and traffic congestion (Zou & Qu 2018). Freeways, as a specific scenario where the number of entry and exit is relatively limited compared to other traffic system, are extremely vulnerable to aforementioned bottlenecks. Once an incident occurs on the freeway, drivers cannot avoid the bottleneck via reconfiguring the route, alternatively, they have to queue upstream of the incident area until incident being cleared. Apart from wasting tremendous amount of time on queuing, there is also a high possibility that drivers experience the stop-and-go traffic condition and poor collaborations from other drivers.

To have an in-depth understanding of the impact brought by incidents, researcher have done a large quantity of simulations both macroscopically and microscopically.

Among these researches, microscopic simulation models demonstrate a better performance over macroscopic simulation models with regards to reproducing the cooperation among vehicles, furthermore, the microscopic simulation model can demonstrate how vehicles are impacted by lane-change motion individually and detailly (Zheng 2014). Car-following model and lane-change model as two essential components of microscopic simulation models are wildly discussed. FVD model as one of the most prevalent car-following models has been applied and modified to simulate the driving behaviour under single-lane traffic (Tang et al. 2014). The development of FVD model can date back to 1995 when Bando et al. (1995) proposed the Optimal Velocity (OV) model. In the OV model, an optimal following velocity is calculated for every vehicle by substitute the following gap to their proceeding vehicle into

$$\ddot{x}_n(t) = \kappa[V(s) - \dot{x}_n(t)] \tag{4.1}$$

where κ denotes the sensitivity constant, $V(s)$ denotes the optimal velocity under the current following gap, $\dot{x}_n(t)$ denotes the current velocity of vehicle n, $\ddot{x}_n(t)$ denotes the acceleration rate during the following simulation interval. It was then calibrated by Helbing and Tilch (1998) based on field data, and a function was developed as

$$\mathrm{V(s)} = V_1 + V_2 \tanh[C_1(\Delta x - l) - C_2] \tag{4.2}$$

Table 4-1Calibrated parameter of confined FVD

Parameters	Values
$\boldsymbol{V_1}$	14.300
$\boldsymbol{V_2}$	15.997
$\boldsymbol{C_1}$	0.066
$\boldsymbol{C_2}$	1.508

However, it was soon found that OV model can result in unrealistically high acceleration rates and deceleration rates (Jiang, Wu and Zhu 2001). To limit the acceleration rate and deceleration rate into a realistic range, Jiang et al. (2001) proposed the FVD model taking the velocity difference of two successive vehicles into account. However, Yu et al. (2019) found that large acceleration and deceleration rates are still observable, thus, he proposed a confined FVD model and calibrated the optimal velocity function based on field data collected from NGSIM. The calibrated values are demonstrated in Table 4-1.

Due to the similarity of researched area (freeway) between Yu's research and ours, we adopted his calibrated parameter to simulate the car following motion of single-lane traffic, and the function of adopted FVD model is

$$\ddot{x}_n(t) = \kappa[V(s) - \dot{x}_n(t)] + \lambda\Delta\dot{x} \tag{4.3}$$

where $\Delta\dot{x}$ denotes the velocity difference between two successive vehicles, λ denotes the sensitivity as

$$\lambda = \begin{cases} 0: & \Delta x \leq critical\ gap \\ 0.5: & \Delta x > critical\ gap \end{cases} \tag{4.4}$$

Although there existed a large quantity of researches on the car following models, researchers paid much less attention on lane changing model at same time, fortunately, lane-change model has been attracting more and more attention recently, because researchers have been gradually noticing that (1) drivers are prone to make mistake during lane changing motions and (2) lane changing motions bring native impacts on traffic capacity, reducing the bottlenecks discharge rate (Zheng 2014). Based on the field observations, Hidas (2005) grouped the lane changing maneuvers into free lane change, forced lane change and cooperative lane change, and he discussed the difference among these three types of lane changing maneuvers and illustrated the procedures of each lane-change maneuver in detail. Hidas (2005) also proposed a lane-change model comparing the space gap between the preceding vehicle and the following vehicle respectively with the minimum required space gap, however, Hidas (2005) made an assumption that lane changing maneuvers are executed instantaneously, thus the time span of the lane changing motion was taken as 1s which is equal to the simulation interval. This assumption is not always realistic, especially under complex lane changing situation when subject vehicles travel much more slowly than vehicles on the target lane so that the drivers cannot make the lane changing decision immediately and determinedly. It is obvious that this model did not discuss the trajectories when vehicles execute lane changing task, thus, it is necessary to develop a lane changing model taking lane changing trajectories into account.

In our research, we developed a four-lane microscopic model simulating the traffic dynamics on a four-lane freeway with an incident blocking one lane as shown in Figure 4-1. Once the drivers see the emergencies, they will start lane-change maneuvers.

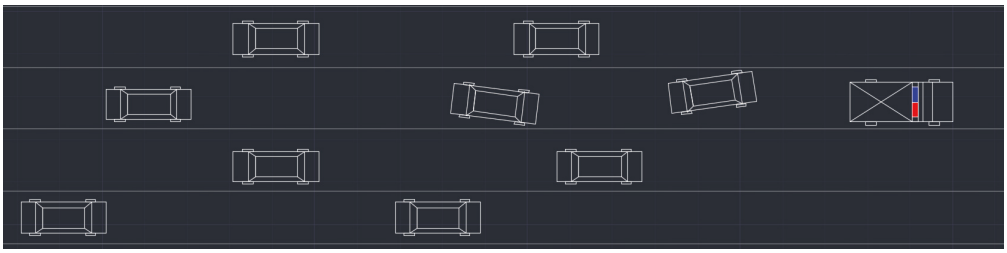

Figure 4-1 Demonstration of researched four-lane freeway

4.2 MODEL DEVELOPMENT

4.2.1 Car-following model

FVD model as one of the most prevailing car-following models has been widely researched, and it has been proved that FVD model is able to reproduce the car following motion both microscopically and macroscopically (Jiang, Wu & Zhu 2001; Yu, Jiang & Qu 2019). Hence, we adopted FVD model as the car following model as illustrate in Eqs. (4.1) to (4.4), and we introduced the calibrated parameters from Yu et al. (2019) due to the similarity between two researched cases. In order to simulate the deceleration motions when the vehicles were approaching the bottleneck, we proposed a quadratic equation to demonstrate the relationship between remaining distance to incident and the velocity. Because the existence of the bottleneck was the main reason for the deceleration motions, we assumed that the velocity limit was determined by the remaining distance to the bottleneck impacted by an incident. We, therefore, introduced a velocity cap to limit the maximum velocity of an approaching vehicle as

$$\mathrm{VC}\big(x(t)\big) = a_1(x(t) - x_{start})^2 + a_2(x(t) - x_{start}) + a_3 \qquad (4.5)$$

where $\mathrm{VC}\big(x(t)\big)$ denotes the velocity cap owing to the incident, $x(t)$ denotes the longitudinal location at time t, x_{start} denotes the longitudinal location where drivers start to decelerate, a_1 , a_2 and a_3 are constants. Before calibrating these parameters, we must clarify the location where vehicles will start to be affected by the incident. We, therefore, assumed that the distance was consist of the length of advanced warning area L_{aw} and the visibility distance L_{vd}. As L_{aw} and L_{vd} are highly dependent on road geometry, we assumed that approaching vehicles start to decelerate when they are 300 meters away from the incident area, at the meanwhile, the closer the vehicles get the

higher the deceleration rates are supposed to be applied. VC are supposed to fulfil the requirement of

$$\begin{cases} VC(x_{start}) = 16.7 \\ VC(x_{incident}) = 0 \end{cases} \quad and \quad \begin{cases} \dot{VC}(x_{start}) \approx 0 \\ \dot{VC}(x_{incident}) \geq -D_{limit} \end{cases} \tag{4.6}$$

where D_{limit} denotes the maximum deceleration, which is assumed to be 2.7 m/s^2 (Zheng 2014), $x_{incident}$ denotes the longitudinal location of incident area. Thus, the Eq. (4.5) is calibrated based on the highest approaching speed as

$$\mathrm{VC}\big(x(t)\big) = -1.86 \times 10^{-4}(x(t) - x_{start})^2 + 16.7 \tag{4.7}$$

4.2.2 Lane-change model

Lane-change models as an essential component of traffic dynamics simulation model are capable of reproducing the interaction among vehicles at complex traffic conditions (Zheng 2014). Lv et al. (2011) proposed a lane changing model based on FVD car following model, but the model is oversimplified for two reasons: (1) the critical acceptable gaps are constant determined by safety distance; (2) the lane-change maneuvers are finished instantaneously. In Lv's model, drivers are encouraged to execute lane-change maneuvers either by anticipating higher velocity or a larger front gap, while assumption are made in many other bottleneck-related researches that vehicles on the through lane do not merge into the blocked lane, and the only stimulation for lane change is the distance to the bottleneck (Hidas 2002; Meng and Weng 2011; Zou & Qu 2018). Zheng (2014) classified the impact brought by lane changing motion into three groups by their occurrence period which are anticipation, insertion and relaxation. As we assumed that driver will commence merging into the target lane without any hesitation as long as the immediate preceding gap and following gap are acceptable, drivers on target lane are unlikely to be disturbed during the anticipation period. However, we did include the reaction time in our lane-changing model by adding a term $C_r V_{platoon}$ which depicted the distance that the platoon in the target lane travelled during the reaction period. Hence, the critical acceptable gaps can be calculated via

$$\begin{cases} g_{p,min} = a_p l + C_r V_{platoon} \\ g_{f,min} = a_f l + C_a V_{platoon} \end{cases} \tag{4.8}$$

where $g_{p,min}$ and $g_{f,min}$ denote the minimum acceptable preceding gap and following gap respectively, l denotes the length of vehicles, C_r denotes the reaction factor which

is assumed to be 0.25 seconds, C_a denotes the coefficient related to the acceptable gap, a_p and a_f are the constants which are assumed to be 1 and 2 respectively (in that case the safety distance is equal to the length of vehicles). As long as the preceding gap and following gap are greater than the respective minimum acceptable gap, drivers commence lane change determinedly.

4.2.3 Lane-change trajectories

As many previous models being established under the assumption that lane changing motion is finished within one simulation interval, they inevitably ignore the lane changing trajectories (Hidas 2002; Meng & Weng 2011; Zheng 2014; Zou & Qu 2018; Lv, Song & Fang 2011). Slege and Marshek (1998) innovatively introduced the concept of emergency lane-changing trajectories, and Slege and Marshek (1998) proposed that an ideal lane changing trajectory need to be continuous and smooth with optimal curvature and minimum longitudinal span. Gackstatter et al. (2010) approximated the lane changing trajectories into polynomials. Kasper et al. (2012) introduced a lane change model with third order polynomial trajectories as

$$\mathrm{y} = A_3(x(t) - x_{start})^3 + A_2(x(t) - x_{start})^2 + A_1(x(t) - x_{start}) + A_0 \qquad (4.9)$$

where $A_3 = \frac{-2(y_{end} - y_{start})}{D^3}$, $A_2 = \frac{3(y_{end} - y_{start})}{D^2}$, $A_1 = 0$, $A_0 = y_{start}$, y_{start} and y_{end} denote the lateral position at the start and the end of the lane change respectively, x_{start} denotes the longitudinal location when vehicle commence lane-change, D denotes the longitudinal distance of the lane-change trajectory, and it is restricted by

$$\mathrm{D} \geq \dot{x}(t)\sqrt{\frac{6|y_{end} - y_{start}|}{|\ddot{y}_{max}|}} \qquad (4.10)$$

where $\ddot{y}_{max}$denotes the maximum lateral acceleration rate. In order to demonstrate a smooth trajectory, the value of $\dot{x}(t)$ was nailed down as the velocity when vehicle starts a lateral shift.

4.3 RESULT AND DISCUSSION

In the simulation, we hypothesized an incident occurs on the outmost middle lane denoted by lane 2, and the incident was located at the longitudinal position of 450 meters. Vehicles on the blocked lane started to be impacted by the existence of incident from the point of 100 meters based on the visibility distance and the deployment of

roadside signs. It is also assumed that vehicles on through lane will not execute lane-change motion due to a lack of necessity. Figure 4-2 to 4-6 demonstrate the trajectories of four-lane freeway, where left-top, right-top, left-bottom and right-bottom sub-figures represents the trajectories on lane 1 to lane 4 respectively. The trajectories from the blocked lane were highlighted with the red lines, while the other trajectories were depicted with the blue lines. The y-axis of each sub-figure represents the longitudinal location of vehicles, and the x-axis denotes the simulation intervals whose unit is 0.1 second. As vehicles on lane 3 did not merge into lane 4, the trajectories on lane 4 can be regarded as undisturbed trajectories. When we applied regular lane-change criteria that is illustrate in Eq. (4.8), eight out of thirty vehicles failed to execute the lane-change motions before they stopped at the incident-affected zone. Among the twenty-four successfully merged vehicles, seven of them started lane-change maneuvers when their velocities were much lower than those of vehicles on the through lanes, which brought great impacts to their surrounding vehicles as shown in Figure 4-2. When we improved the inter-vehicle communication by eliminating the negative effect of drivers' reaction time, only three out of thirty vehicles merged at relatively low speed, causing much fewer negative effects on the through lane; however, there were still 6 vehicles failed to merge as shown in Figure 4-3. Alternatively, we reduced the $g_{f,min}$ by $\frac{V_{platoon}}{2}$ and depicted the trajectories in Figure 4-4. Even though the lane-change motions seemed to be smooth, it brought much greater impact on the through lane, and that might be the result of over-aggressive lane changing maneuvers. In Figure 4-5, we combined the two methods to smooth the lane changing maneuvers, results show a great improvement. This might be explained by the concept proposed by Hidas (2005) that the large velocity difference can increase difficulty of the lane changing. In our case, even short gaps encouraged driver to merge before velocity difference boost, so vehicles were able to merge without disturbing the through lanes. When we reduced the acceptable gap to the minimum requirement, almost all of the vehicles were able to commence merging immediately after drivers being inform of the occurrence of incidents as demonstrated in Figure 4-6. It was also found that solely reducing the preceding or following minimum acceptable gap requirement cannot improve the performance of the traffic system, thus, the inter-vehicle communication with the preceding vehicles and following vehicles of target lanes are equally important. By comparing Figures 4-2 to 4-6, it is not difficult to find out that incorporating the close

cooperation can not only boost success rate for lane-change but reduce the negative impact to the target lanes. Figure 4-7 demonstrates the lateral trajectories from origin lane to the two target lanes, and it is clear that these trajectories varied on shape which was determined by the drivers' heterogeneities and the lane-change conditions.

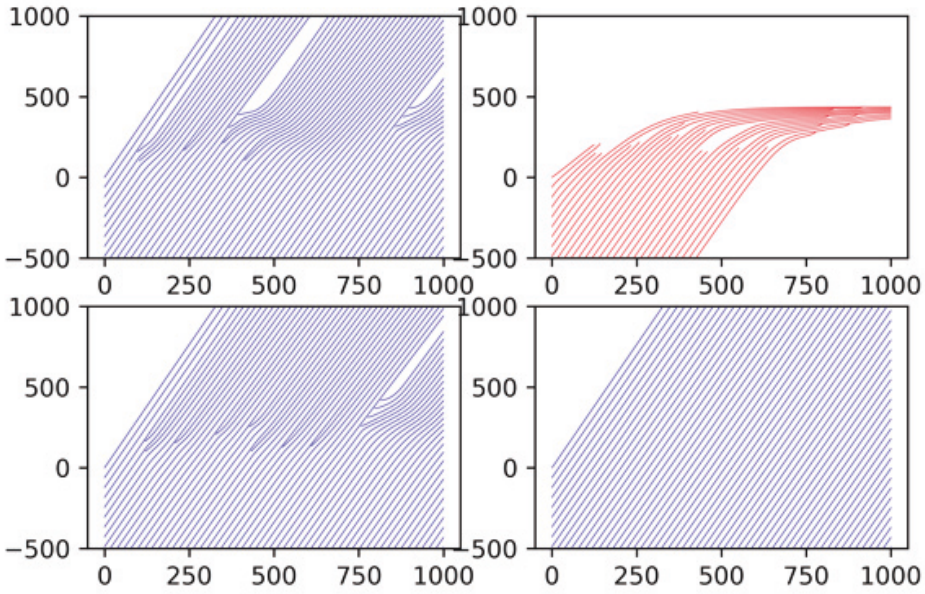

Figure 4-2 Vehicle trajectories with reaction time and regular minimum acceptable gap

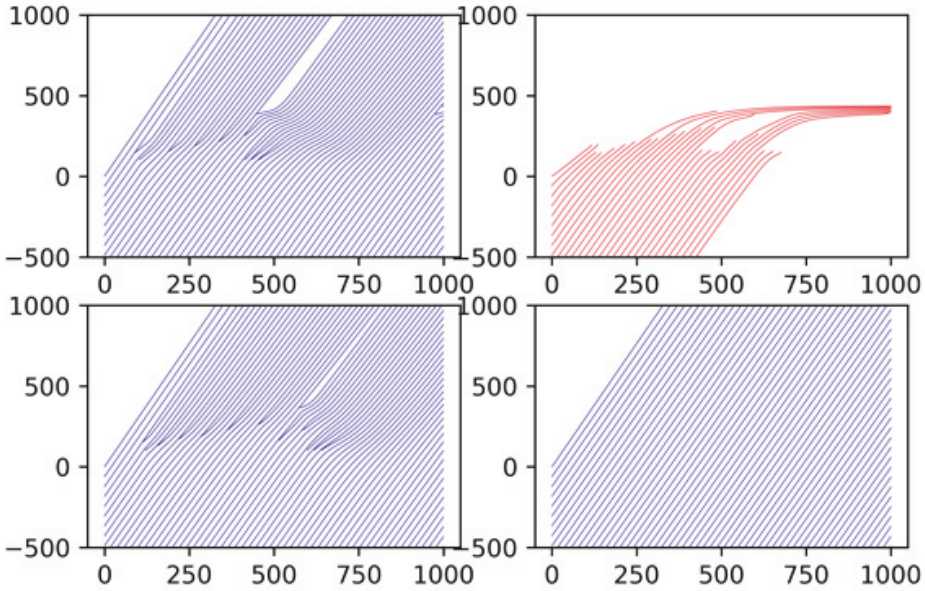

Figure 4-3 Vehicle trajectories ignoring the reaction time

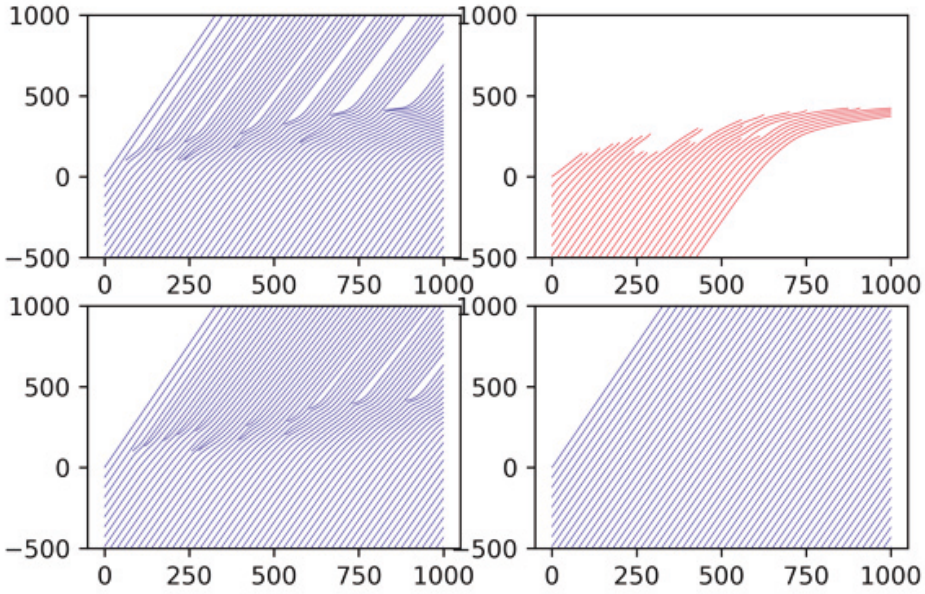

Figure 4-4 Vehicle trajectories with reduced the minimum acceptable following gap

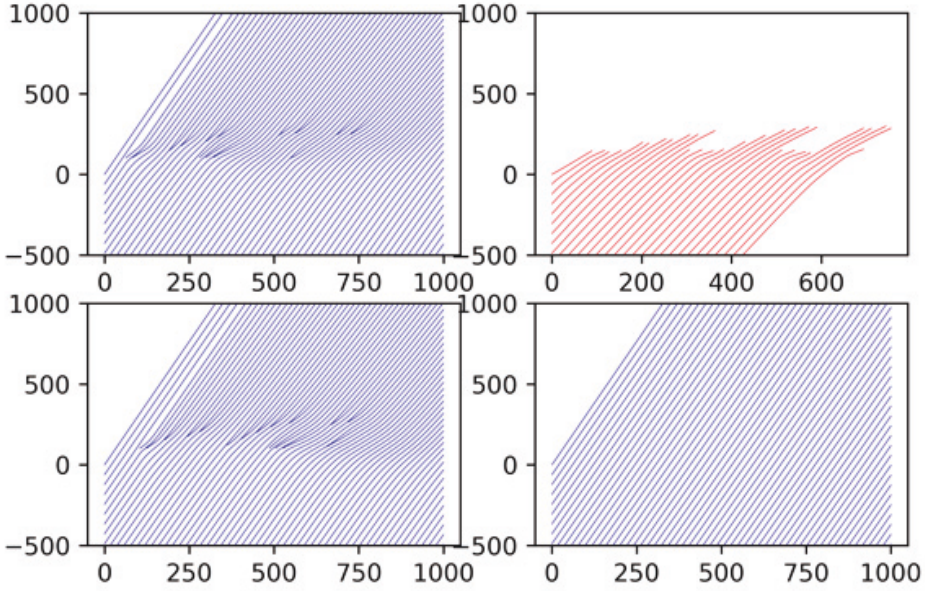

Figure 4-5 Vehicle trajectories with reduced minimum acceptable following gap while ignoring the reaction time

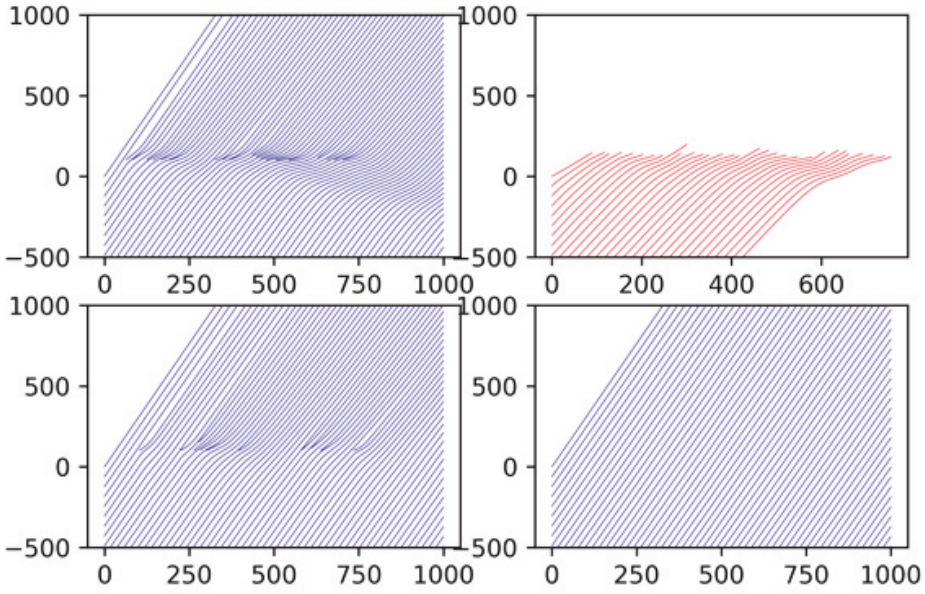

Figure 4-6 Vehicle trajectories with ideal cooperation

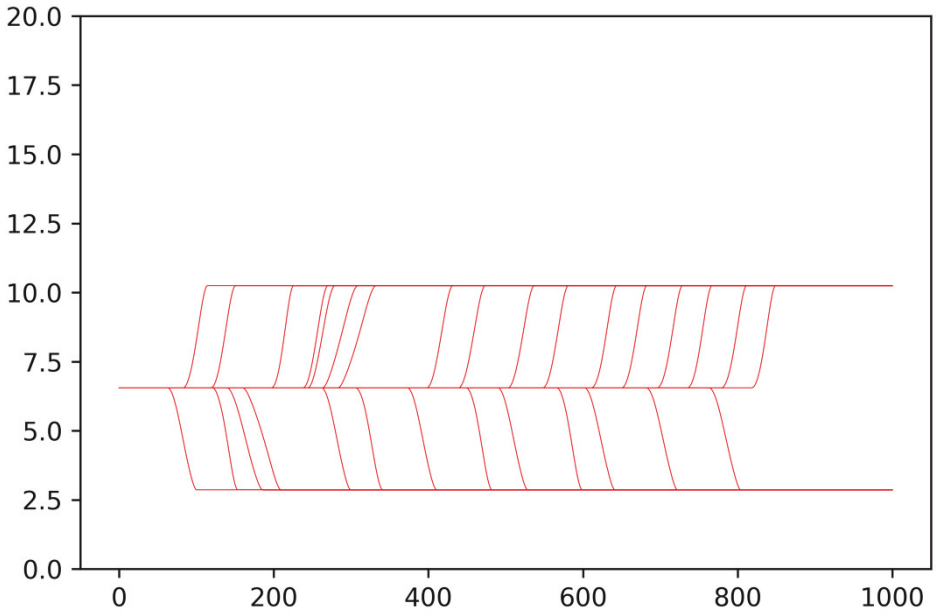

Figure 4-7 Lateral movement with ideal cooperation

4.4 SUMMARY

In this chapter, we developed a four-lane traffic dynamic model and microscopically demonstrated the impact brought by bottlenecks on the freeway. One

of remarkable improvements was that our model incorporates a realistic FVD-based lane-change trajectories by approximating the clothoids into cubic polynomials. Therefore, the time span of lane changing maneuver did not have to be equate with one simulation interval, instead, more realistic time spans were determined by the velocities and lane changing trajectories of vehicles. Moreover, the inter-vehicle communication was indicated by the reduction of minimum acceptable gap, because inter-vehicle communication can bring connected and automated vehicles and drivers the confidence when they were executing lane changing maneuvers. It was found that the communication with the preceding and the following vehicle of target lane can be equally important when we plan to improve the overall traffic performance. However, there are some more in-depth researches yet to be done, for instance, how cooperation among vehicles function need to be further researched. Additionally, the cooperative lane-change when the following vehicle actively decelerate to encourage lane-change are to be discussed, because the mechanism of our current model is based on free lane change and force lane change.

Chapter 5: Lane-change prediction in Re-organizing Traffic Flow

5.1 INTRODUCTION

The rule-based microscopic simulations are effective and economical tools to estimate the dynamics of traffic flow, while more and more researchers focus on non-parametric models which are established on the basis of historical traffic data. One of the most significant reasons is that the real traffics are full of complexity and stochasticity that almost no single model can illustrate the traffic flow realistically. It will require a large quantity of parameters and functions if all heterogenous road participators are expected to be reproduced. Many researchers have endeavoured to apply non-parametric models on predicting the lane-change trajectories. In 1994, Hunt and Lyons(1994) intuitively applied the neural network to model drivers' the lane-change decisions on a dual carriageway. Results showed a great success when training and predicting based on manually generated data; however, a lack of large-scale data at that time resulted in a poor training process of real-life traffic data and then a unsatisfactory prediction. In 2010, Tomar et al. (2010) applied the large-scale historical data to predict the lane-change trajectories with neural network. They extracted historical trajectories from NGSIM database to incorporate uncertainties and behaviours into their prediction model. It was found that the surrounding vehicles brought the major impacts to the lane-change trajectories, but their model can only predict some discrete parts of the whole trajectories accurately. It is proposed by Tomar and Verma (2012) that the lane-change trajectories are not only very sensitive to the surrounding vehicles but also affected by the subjective features of the ego drivers. The subjective feature of human drivers can lead to poor performance of lane-change predictive model, and the Tomar and Verma (2012), regarded that neural network can facilitate the prediction of lane-change trajectories. They, therefore, applied the neural network on both the short-term and the long-term prediction of trajectories on the basis of safety consideration. Tang et al. (2018) proposed an adaptive fuzzy neural network to predict the steering behaviour during a lane-change task. The data of trajectories were collected from a driving simulator, and a preceding vehicle are presented with various velocities under different scenarios.

Apart from the prediction of the lane-change trajectories, some other researchers also endeavoured to predict the lane-change decision. Zheng et al. (2014) also applied the neural network to deal with the complexity of lane-change maneuver. Different from aforementioned literature, they focus on the decision-making period. The data of trajectories were extracted from NGSIM database, more specifically, U.S. Highway 101, however, they regarded that continuous trajectories are not suitable for training this decision-making prediction model. Alternatively, they captured the data from 'cross-line' moments as the lane-change instances, and each lane-change instance are coupled with two randomly selected non-lane-change instances. Results shows that the neural network outperform the multinomial logit model on the predicting lane-change decision. Yi et al. (2016) proposed a driver situation awareness algorithm to recognize the driving states of vehicles. Both supervised learning and unsupervised learning were applied to categorize the driving environments, and NGSIM database was adopted to validate the algorithm. Hou et al. (2015) developed a lane-change assistance system based on random forest and AdaBoost. With the application of the comprehensive variables and the NGSIM dataset, their system successfully predicted the lane-keeping decisions, but the performance for predicting lane-change decisions was not very satisfactory. The Support Vector Machines (SVM) as an effective classification algorithm are also widely applied on lane-change prediction. Mandalia and Salvucci (2005) adopted five groups of features for SVM-based early lane-change prediction. The linear kernel was employed as it outperformed the other kernels including polynomial, exponential and Gaussian. Most of the aforementioned literatures focused on the free lane-change tasks and the cooperative lane-change tasks, while they seldom took into account the compulsory lane-change tasks on incident-affected road sections or bottlenecks (or lane drops). Dou et al. (2016) combined the SVM and the Artificial Neural Network (ANN) to analyse the feasibility and possibility of lane-change tasks with the present of lane drops on the highway. Three features were extracted from the NGSIM database with regards to speed differences, gaps and positions. Similar to the other researches, Dou et al. (2016) used the data of U.S. Highway 101 and the Interstate 80 Freeway; however, they focused on the vehicles from auxiliary lanes. The trajectories were analysed on 1-second interval basis, and they regarded that continuously approaching to the lane mark was the signal of the lane-change task. It showed a good performance on non-merge prediction while a relatively poor accuracy rate was witnessed for merge prediction. Hou et al. (2013) combined the Bayes

classifier and decision tree to predict the lane-change decision, and it showed that the combined algorithm outperform each single algorithm. Wang et al. (2014) proposed minimum Bayes risk decision and minimum error Bayes decision based on the Bayesian network to establish lane-change model and predict the lane-change decision-making. Li et al. (2015) applied the BP neural networks and the Bayesian filters to forecast the drivers' lane-change intentions. Balal et al.(2014) analysed the related parameters from free lane-change tasks on the safety basis, and it was found that one or few parameters would be sufficient enough to evaluate the risk of lane-change tasks. This is also true for the lane-change prediction as the more parameters considered the more noised need to be deal with. Although a lot of researchers have use non-parametric model to predict the human drivers' lane-change decision, few of them applied the model on enhancing the collaboration during the cooperative lane-change within a microscopic simulation. Furthermore, there is not an explicit criterion extracting the merge and non-merge instances from the large-scale database.

In this chapter, we intuitively introduced the lane-change prediction algorithm into the microscopic simulation. The CAV who are embedded with this prediction model from the target lane are able to encourage the ego vehicle to execute the lane-change task through a collaboration where the requirement of headways and relative speeds are to be fulfilled to an acceptable extend that the vehicles on the target lane do not need to sacrifice too much on travel time. Even though the impact of lane-change on the traffic system is inevitable, our model is looked forward to mitigating the massive disturbances on the target lane and therefore gradually addressing the congestion problem owning to the bottlenecks. Non-merge instances are extracted from trajectories based a criterion rather than randomly selecting cruising moments.

5.2 DATA DESCRIPTION AND PROCESS

In this research, the trajectories were extracted from one of the most prevailing open-access datasets in the NGSIM database. Trajectories data from a 2100-foot section of southbound of U.S. Highway 101 (see Figure 5-1) and a 1650-foot section of Interstate 80 Freeway (see Figure 5-2) were adopted to train and test the Bayes classifier prediction model. Data of the U.S. Highway 101 were collected for three pieces that start from 7:50 am, 8:05 am and 8:20 am, and each piece contains data for a 15-minute time span. Data from the Interstate 80 Freeway were collected for three

pieces that start from 4:00 pm, 5:00 pm and 5:15 pm, each piece also contains data for a 15-minute time span.

Among all the trajectories we only selected those affected by the non-through lanes, more specifically, the auxiliary lane on the U.S. Highway 101 and the sixth lane of the Interstate 80 Freeway. Vehicles traversing on the auxiliary lane will have to merge to the adjacent lane, otherwise they will continue traversing on the auxiliary lane till leaving the highway. In that case, vehicles face a similar scenario with the non-through lane, and vehicles traversing on the sixth lane on the Interstate 80 Freeway experience the same scenario that drivers who want to stay on the freeway have to merge into the adjacent lane to avoiding exiting through the off-ramp. Table 5-1 and Table 5-2 demonstrate the number of vehicles from the U.S. Highway 101 (refer to US-101 in the table) and the Interstate 80 Freeway (refer to I-80 in the table) respectively, including the original database and the number after the first and the second filter. Through the first filtering process, only the vehicles who executed lane-change tasks from 'non-though' lanes were kept. Through the second filtering process, any lane-change involving trucks or motorcycles were eliminated to remove vehicles' heterogeneities.

Table 5-1 The number of vehicles in the US-101

	7:50 – 8:05	8:05 – 8:20	8:20 – 8:35
Raw	2169	2017	1915
1st filter	134	127	141
2nd filter	130	122	140

Table 5-2 The number of vehicles in the I-80

	4:00 – 4:15	5:00 – 5:15	5:15 – 5:30
Raw	2052	1836	1790
1st filter	174	156	156
2nd filter	171	150	154

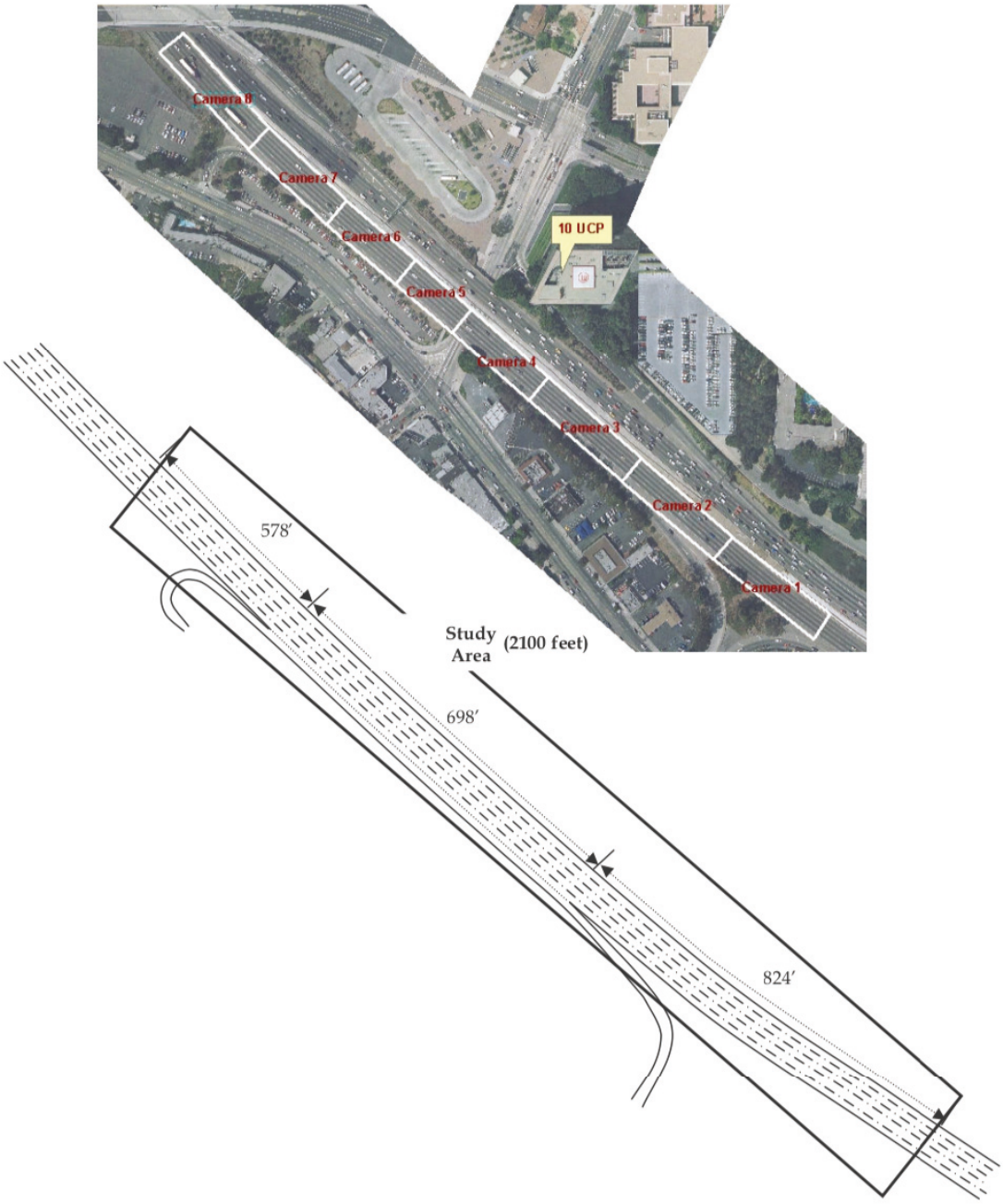

(Cambridge Systematics 2005)

Figure 5-1 Study Area of U.S. Highway 101

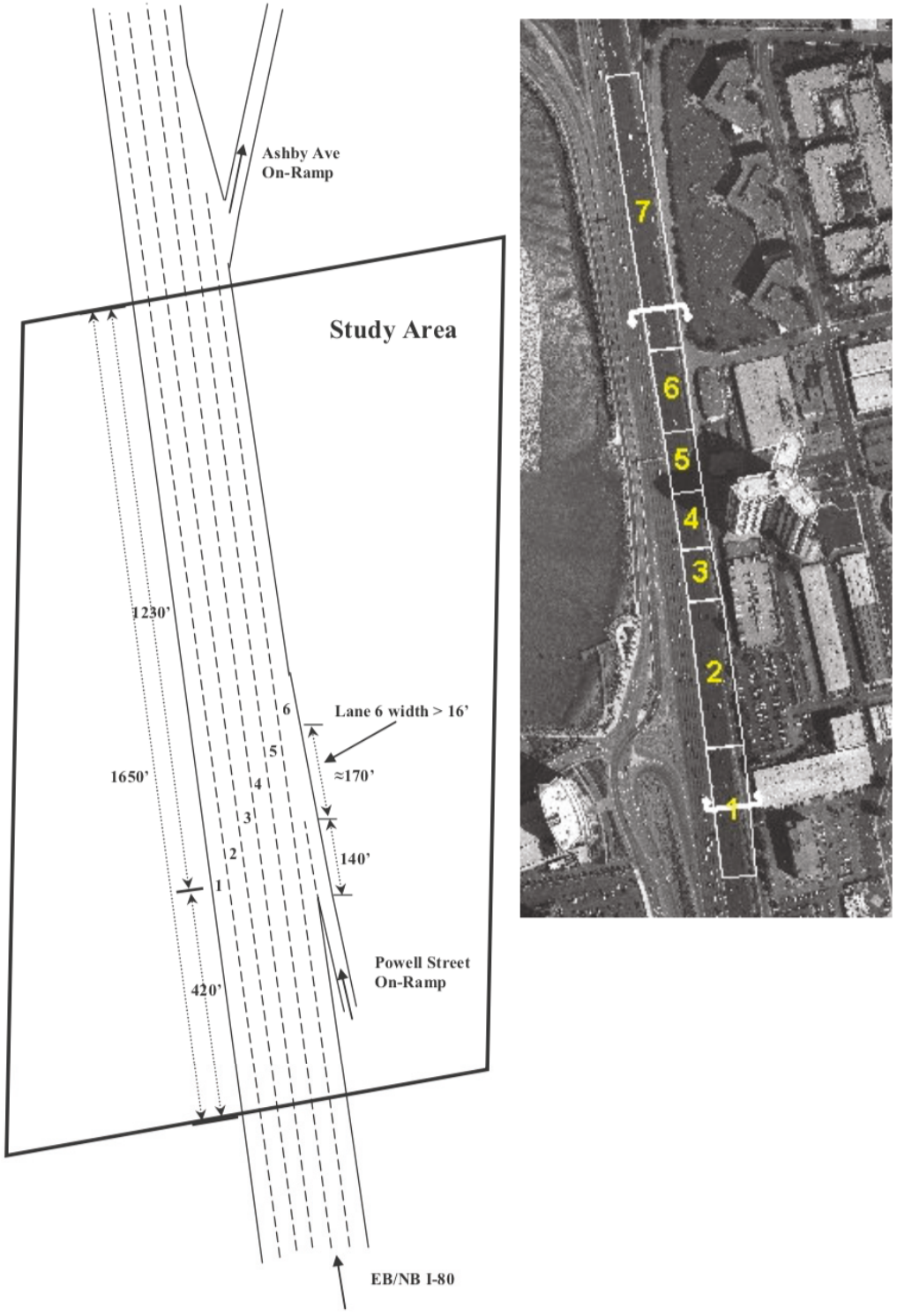

(Cambridge Systematics 2005)

Figure 5-2 Study Area of Interstate 80 Freeway

Literatures showed that the NGSIM contains many noises (Punzo, Borzacchiello & Ciuffo 2009; Ossen & Hoogendoorn 2008; Duret, Buisson & Chiabaut 2008; Kesting & Treiber 2008; Thiemann, Treiber & Kesting 2008). The trajectories were

collected based on the camera over the highway sections, and the velocities and accelerations were derived from the positions. Hence, any deviation on reading the position can lead to huge errors on the velocities and the acceleration. To avoid the overshooting velocities and accelerations, we applied a moving average smoothing algorithm to eliminate the random errors from the trajectory data. It was looked forward that the smoothing method can also eliminate the unrealistic oscillations of the trajectories. In this research, a symmetric exponential moving average filter (sEMA) was adopted to smooth the longitudinal position, velocity and acceleration, while the lateral position, velocity and acceleration was not smoothed because the moving average would affect the high-frequency components from data with regards to finding windows (Punzo, Borzacchiello & Ciuffo 2009).

Consider X_j as the j^{th} original position of a n-dimensional position matrix and x_i as the i^{th} smoothed position of a n-dimensional position matrix. The smoothed position can be calculated by Eq. (5.1) (Thiemann, Treiber & Kesting 2008).

$$x_i = \frac{1}{\sum_{j=i-W}^{i+W} e^{-\frac{|i-j|}{D}}} \sum_{j=i-W}^{i+W} X_j e^{-\frac{|i-j|}{D}} \tag{5.1}$$

where $D = \frac{T}{dt}$, $T = 0.5$ denotes the smoothing width, $dt = 0.1$ represent the simulation intervals in the NGSIM database. W denotes the smoothing window width, and $W = \min(3D, i-1, n-i)$ can ensure that the smoothing window is always symmetric with respect to the X_i even near the boundary of the matrix. To avoid the substantial computational load, we directly derived the velocities and accelerations from the smoothed position data rather than applying the sMEA to the original data of velocities and accelerations as shown in Eq (5.2) and (5.3).

$$\dot{x}_i = \frac{X_{i+1} - X_{i-1}}{2dt} \tag{5.2}$$

$$\ddot{x}_i = \frac{X_{i+1} - 2X_i + X_{i-1}}{dt^2} \tag{5.3}$$

Figure 5-3 displays the smoothed longitudinal positions, and only slight differences between the smoothed data and original data can be seen. Even so, the outcome of smoothing the velocities is distinct as shown in Figure 5-4. The lateral positions, lateral velocities and lateral acceleration rates were also smoothed by sMEA as demonstrated in Figures 5-5 to 5-6. It is worth noting in Figure 5-6 that the extremely large positive

and negative accelerations before the 400th interval result from that the vehicles were initially travelling on the on-ramp that great lateral speed changes along the lateral direction are need when the vehicle enter the freeway. For all these, the following unrealistically large accelerations are effectively eliminated.

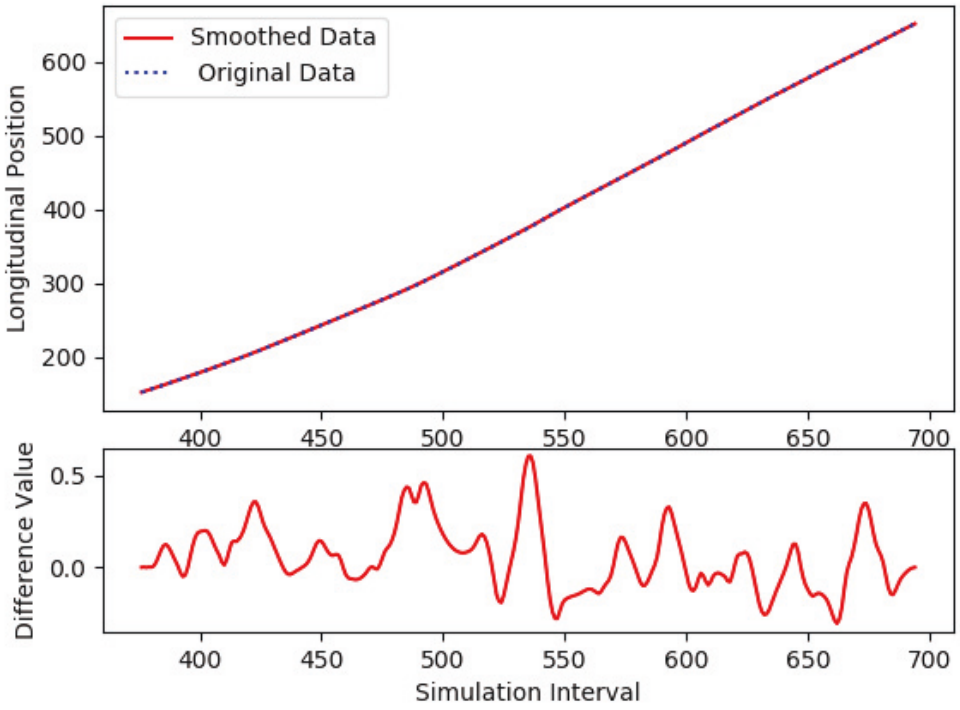

Figure 5-3 Smoothed longitudinal positions compared to the original longitudinal positions

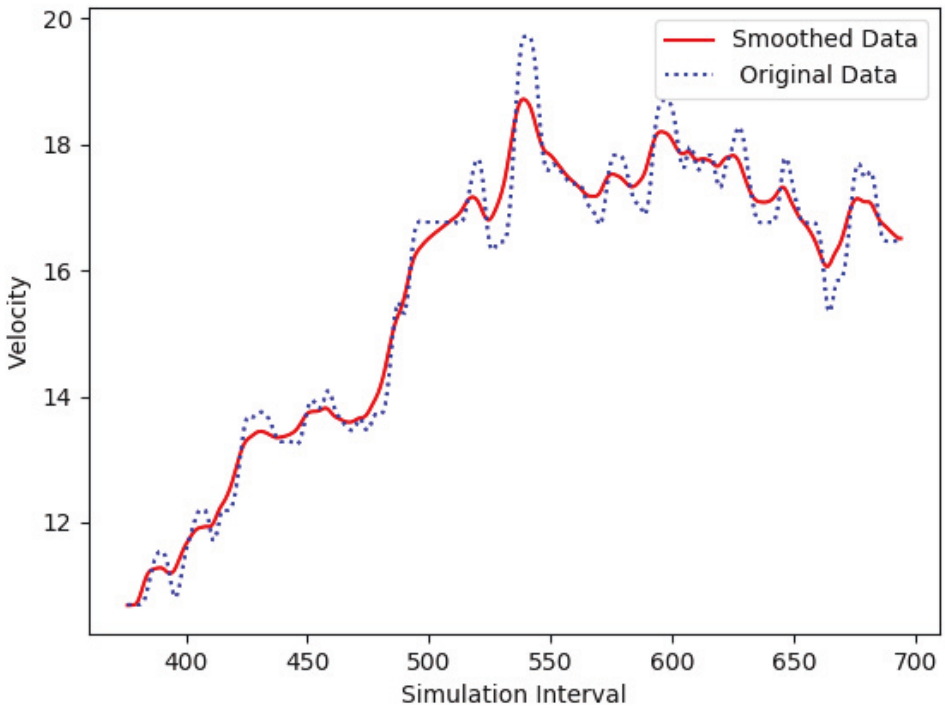

Figure 5-4 Smoothed velocities compared to the original velocities

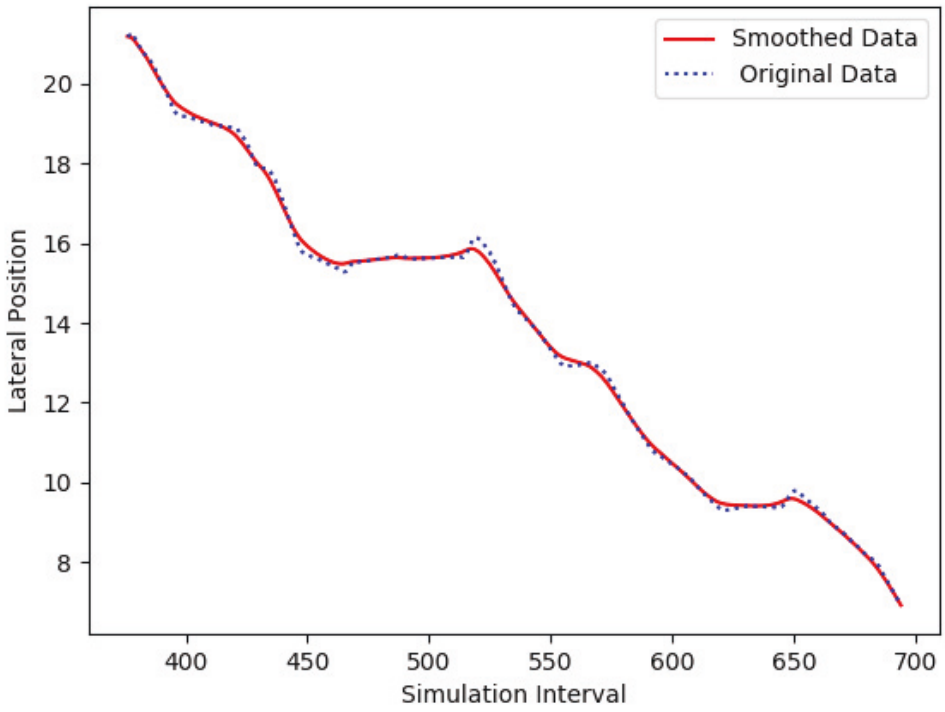

Figure 5-5 Smoothed lateral positions compared to the original lateral positions

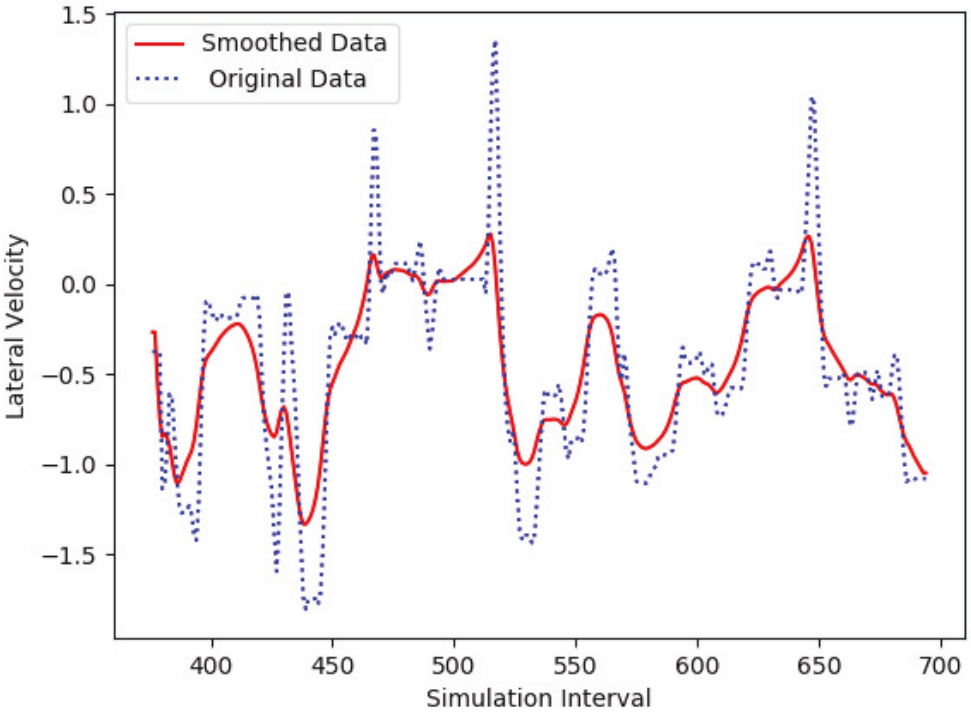

Figure 5-6 Smoothed lateral velocities compared to the original lateral velocities

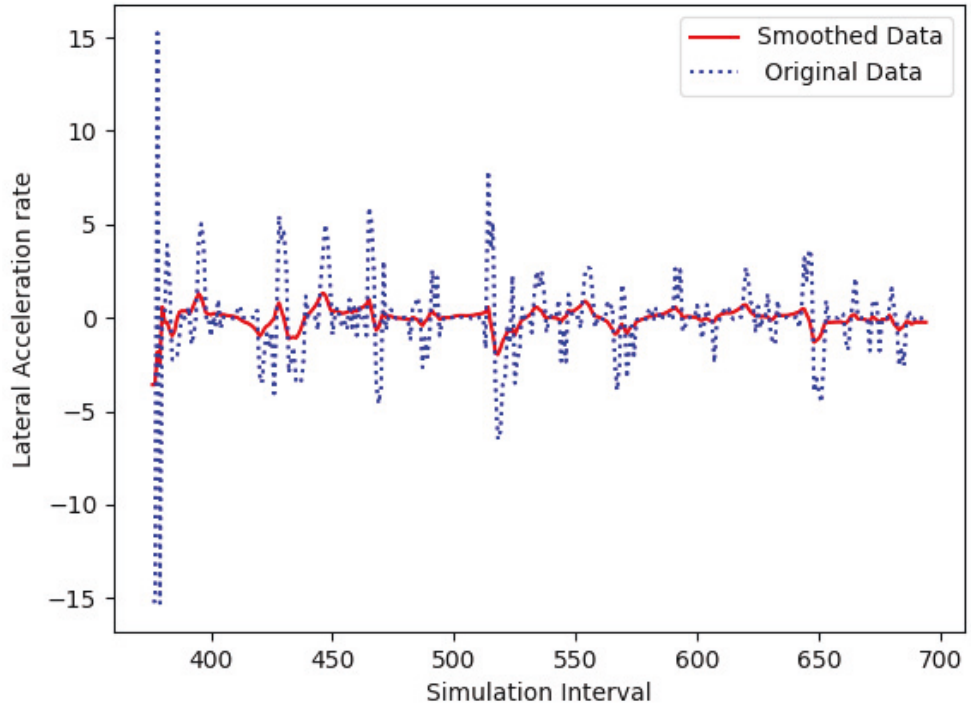

Figure 5-7 Smoothed lateral acceleration rates compared to the original lateral acceleration rates

After eliminating the noises, we focused on categorizing the accepted lane-change instances and the rejected lane-change instances. An accepted lane-change instance refers to the scenarios where a driver is able to make lane-change decision and execute the lane-change task immediately, while a rejected lane-change instance presents when a driver is not able to start a lane-change maneuver. It has been widely acknowledged that the start of a continuous movement can be regarded as the accepted lane-change instance when a vehicle continuously moves to and passes the lane mark (Dou, Yan & Feng 2016; Hou, Edara & Sun 2013); however, there is not an explicit criterion to standerize the rejected lane-change instances. At the begining, we took the previous interval of when a negative velocity exists before the accepted lane-change instance as the indication; however, it came that the moment of a rejected lane-change instance is too close to its corresponding accepted lane-change instance that the feature, such as gap and relative speed, is not distinctive, which reduces accuracy of lane-change prediction. Alternatively, we selected the rejected instance by searching for a directly previous negative acceleration that represents a 'steering' action back to the origin lane. The negative acceleration is triggered when a lane-change attempt is rejected by its surrounding vehicles.

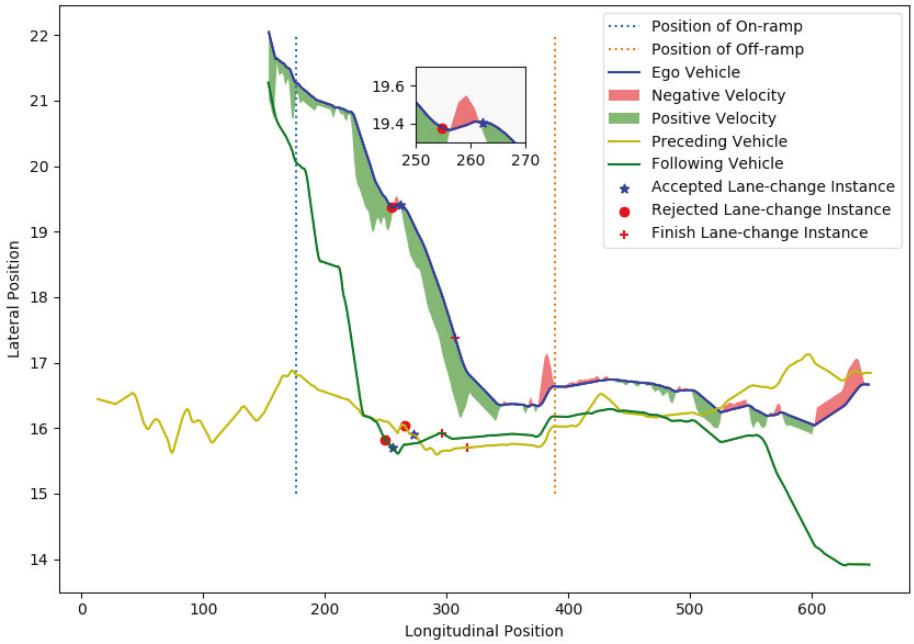

Figure 5-8 Original trajectory of the vehicles involved in a lane-change tasks

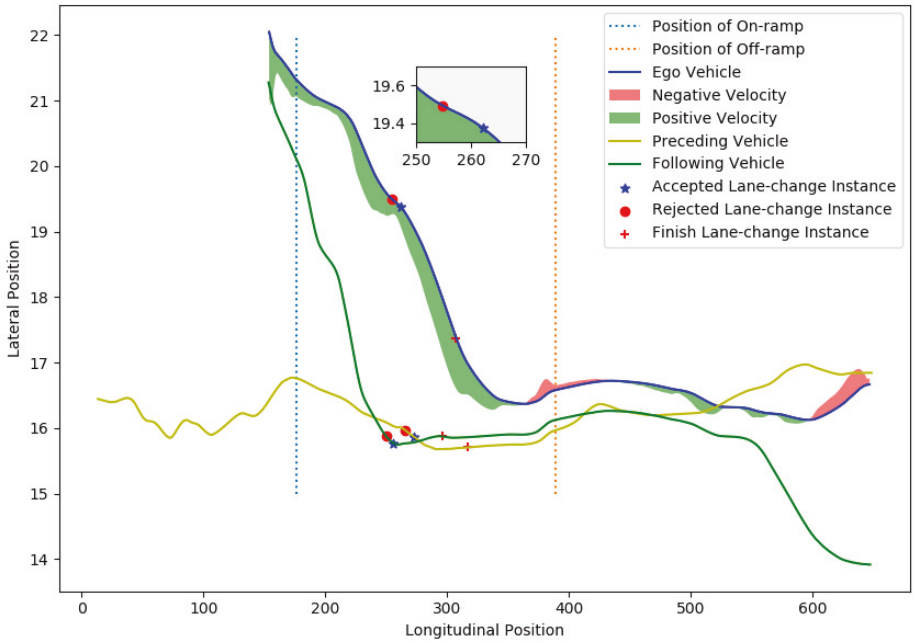

Figure 5-9 Smoothed trajectory of the vehicles involved in a lane-change tasks

The original trajectories and the smoothed trajectories of the lane-change vehicle, its adjacent preceding vehicle and its adjacent following vehicles are depicted in Figure 5-8 and 5-9 respectively. Longitudinal positions of entrance and exit of the freeway is highlighted by the dash lines. The longitudinal positions of these three vehicles are marked for the accepted instance, rejected instance and the finish instance. The lateral velocities of the ego vehicle are also illustrated on the ego vehicle's trajectory. By comparing the magnified sub-figures, we can easily tell that a large quantity of steering actions of the driver are filtered after applying the sMEA to the lateral features. There is no doubt that applying the sMEA decrease the fidelity of the dataset; therefore, we decide to only apply sMEA to the longitudinal features of the trajectories.

Finally, we abandon the data for any of the features being unable to be demonstrated. The absent of a data may because the adjacent preceding vehicle or the adjacent following vehicle was too far from the ego vehicles that the records abandoned them. Due to the fact the researched zone in Interstate 80 Freeway did not include the end of the sixth lane, we only applied data collected from U.S. Highway 101.

5.3 METHODOLOGY

In our research, we adopted six features from NGSIM database to forecast the drivers' lane-change intention:

Feature 1: Ego speed—the velocities of the researched vehicle who is expecting a lane-change requirement being accepted;

Feature 2: Distance to the end of the lane—the remaining distance to the activity area of a work zone or the obstructed area of an incident-affected area.

Feature 3: Speed difference with the adjacent preceding vehicle—the speed difference between adjacent preceding vehicle and the ego vehicle, and it can be calculated by $(v_{apv} - v_{ev})$;

Feature 4: Speed difference with the adjacent following vehicle—the speed difference between adjacent ego vehicle and the adjacent following vehicle, and it can be calculated by $(\dot{x}_{ev} - \dot{x}_{afv})$;

Feature 5: Net distance with the adjacent preceding vehicle—net longitudinal distance can be calculated by $(x_{apv} - l_{apv} - x_{ev})$ where l_{apv} denotes the length of the adjacent preceding vehicle;

Feature 6: Net distance with the adjacent following vehicle—net longitudinal distance can be calculated by $(x_{ev} - l_{ev} - x_{afv})$ where l_{ev} denotes the length of the ego vehicle.

Consider $\boldsymbol{X}$ as 6-dimension input vector; y_a denotes the corresponding output of an accepted instance; y_r denotes the corresponding output of a rejected instance. Taking the prediction of accepted instance as an example, the core function Bayesian classifier are (Wang, Chai & Cao 2014):

$$P(y_a|\boldsymbol{X}) = \frac{p(\boldsymbol{X}|y_a)P(y_a)}{p(\boldsymbol{X})} \tag{5.1}$$

where $P(y_a|\boldsymbol{X})$ denotes the probability of an accepted instance when given a matrix of input features $\boldsymbol{X}$. If the calculated $P(y_a|\boldsymbol{X})$ or $p(\boldsymbol{X}|y_a)P(y_a)$ is greater than $P(y_r|\boldsymbol{X})$ or $p(\boldsymbol{X}|y_r)P(y_r)$, the given output of the input features can be regarded as an accepted instance, and vice-versa. $p(\boldsymbol{X}|y_a)$ denotes class conditional probability

density function which can be calculate by K-nearest neighbour (k-NN) (Buturović 1993), an effective tool for nonparametric estimation, as shown in Eq. (5.2).

$$p(\boldsymbol{X}|y_a) = \frac{k}{N_a V_a} \tag{5.2}$$

where N_a denotes the gross number of accepted samples in the dataset; k denotes the number of nearest samples chosen for prediction the intention, and V_a denotes the 6-demision hypersphere whose centre is located at $\boldsymbol{X}$ in the hyperspace as shown in Eq. (5.3). The radius of the hypersphere is determined by the distance of $\boldsymbol{X}$ to its farthest point of these k points. The selection of k is essential to the prediction as too much or too few will lead to high computational load and low accuracy respectively.

$$\mathrm{V}_a = \frac{\pi^3}{6} r^6 \tag{5.3}$$

$P(y_a)$ denotes the percentage of the accepted samples in the dataset, and it can be easily calculated by Eq. (5.4).

$$P(y_a) = \frac{N_a}{N} \tag{5.4}$$

The distance between a sample $\boldsymbol{X_i}$ and the input $\boldsymbol{x}$ can be determined by a weighted Euclidian distance as illustrated in Eq. (5.5)

$$D(\boldsymbol{X_i}, \boldsymbol{x}) = \sqrt{\sum_{j=1}^{6} W_j \left(X_{i,j} - x_j\right)^2} \tag{5.5}$$

where W_i denotes the weight of the j^{th} feature, which can be calculated by support vector machines (SVM) (Buturović 1993) as shown in Eq. (5.6) (Domeniconi, Gunopulos & Peng 2005).

$$W(q)_j = \frac{\left(R(q)_j\right)^t}{\sum_{k=1}^{6} (R(q)_k)^t} \tag{5.6}$$

where t is a positive integer, and $t = 1$ shows the best performance in all predictions. $R(q)_j$ can be calculated by Eq. (5.7).

$$R(q)_j = \left| e_j^T \nabla f(p) \right| \tag{5.7}$$

As a linear kernel is applied, $f(p)$ can be written as the linear hyperplane $w\boldsymbol{x} - b = 0$ if the samples are separable, otherwise, $f(p) = \sum_i w_i y_i x_i^T x - b$. $\nabla f(p)$ denotes the gradient vector, and e_j is a canonical unit vector. Figure 5-10 demonstrates the process of the lane-change prediction.

5.4 DISCUSSION AND ANALYSIS

Table 5-3 demonstrates the weights of each feature in the hyperspace. It is shown that the distance to the end of the lane contributes most to the lane-change intentions. We applied both the traditional Bayes classifier and the weighted k-NN Bayes classifier to predict the lane-change decision-making. After three levels of filters, we finally have 514 groups of data. We adopted k=5 as the number of nearest neighbours for the consideration of efficiency. Table 5-4 shows that the weighted k-NN Bayes classifier can predict both the accepted lane-change instances and rejected lane-change instances with relatively high accuracy. The overall accuracy is 84.44%, and the misclassification rate of lane-change intention is 6.74. The misclassification rate of inappropriate lane-change conditions is 42.19 % that more than 40 % of inappropriate conditions will be recognized as lane-change conditions. This may bring very high risks of collision if the model instructs the ego vehicle on lane-change tasks, but this model is established for lane-change collaborations. Imagine the ego vehicle is travelling on a non-through lane, and it will definitely need to merge into the through lanes. The difficulty for the collaboration is to predict when the driver is going to merge and what kind of condition (headway) can encourage the driver to start a merging task. Our model will instruct the adjacent to create suitable gaps, and then facilitate the lane-change maneuver. Table 5-5 demonstrates the prediction accuracy (the rate of the correct predictions over total predictions) of traditional Bayes classifier, and it can be seen that the weighted k-NN Bayes classifier outperforms that traditional Bayes classifier. Even so, the traditional Bayes classifier show a better performance than neural network who only successfully predict 65 % of the instances. When we applied a misclassification cost, where misclassifying the rejected instances costed 1.5 times more than misclassifying the accepted instances, to the weighted k-NN Bayes classifier, the accuracies were improved as shown in Table 5-6. As a result of the misclassification cost, any prediction of the accepted instance would receive more punishment if the lane-change is actually rejected, so the misclassification rate of rejected instance reduced from 42.19 % to 28.12 %. Compared with the rule-based

lane-change model, the proposed lane-change model can provide more flexible lane-change criteria without affected by the threshold of each factor. To be specific, the proposed model enabled the CAV to collaborate with different driver via various models which had been developed on basis of the driver's historical trajectories, while most of the current lane-change models mainly focus on the difference between each feature and the corresponding predetermined threshold. By applying the prediction model, it would be much easier to deal with the human drivers' heterogeneities. Figure 5-10 demonstrates a rough process of model development. The first two steps are to input the NGSIM database and to extract the lane-change trajectories that started from the non-through lane to the through lane. According to extracted trajectories, the accepted lane-change instances and the rejected lane-change instances can be discriminated as described in section 5.2. Based on the scenarios vary on the presence of the surrounding vehicles, features are selected to prediction the lane-change decision. An ANN (developed in Simulink) was first employed to predict the lane-change decisions, but it showed poor result on the prediction accuracy. Hence, the ANN was only adopted as a comparison group for the other two Bayes-classifier-based algorithms. The second method employed the Bayes classifier as illustrated in Eqs. (5.1), (5.3) and (5.4) where the Eq. (5.3) varied with the number of the features. The SVM was adopted to figure out the weights of each feature which were related to the distance to the dividing hypersurface as illustrated in Eqs. (5.5) to (5.7), at the meanwhile, a fixed number of nearest datasets were extract from the whole data space. The calculated weights and the extracted datasets would then be substituted into the Bayes classifier to further improve the prediction accuracy. Finally, the whole database was divided into two groups: model development group and the validation group, and the algorithm with higher accuracy was selected for the prediction model.

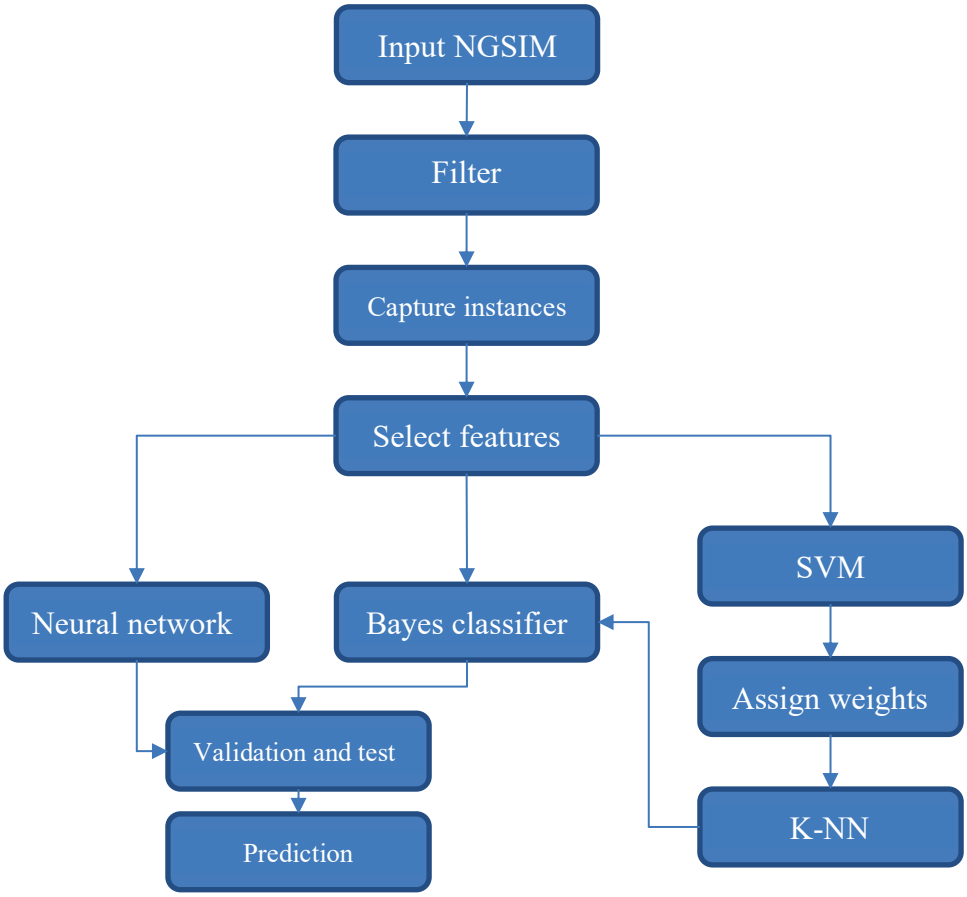

Figure 5-10 Process of lane-change prediction

Table 5-3 Weight of each feature by SVM

Feature	1	2	3	4	5	6
Weight	0.011608	0.020543	0.791840	0.152605	0.003744	0.019659

Table 5-4 Accuracy analysis of weighted k-NN Bayes classifier

	Accepted	Rejected
Training set	195	62
Test set	193	64
Prediction	207	50
Accuracy	86.96% (180/207)	74.00% (37/50)
Misclassification rate	6.74% (13/193)	42.19% (27/64)
Overall Accuracy	84.44%	

Table 5-5 Accuracy analysis of Traditional Bayes classifier

	Accepted	Rejected
Training set	195	62
Test set	193	64
Accuracy	81.73%	46.6%
Misclassification rate	15.68%	56.25%
Overall Accuracy	59.90%	

Table 5-6 Accuracy analysis of weight k-NN Bayes classifier with applying misclassification cost

	Accepted	Rejected
Training set	195	62
Test set	193	64
Accuracy	90.72%	73.02%
Misclassification rate	8.81%	28.12%
Overall Accuracy	86.38%	

5.5 SUMMARY

In this chapter, a weighted k-NN Bayes classifier is established to predict the lane-change maneuvers on the basis of 10Hz data. This model adopted six features, and it is able to enhance the cooperative lane-change; however, the model is not suitable to instruct the ego drivers. Vehicles in the target lane can follow the instruction to prepare acceptable gaps in order to encourage the lane-change maneuvers. The data is extracted from NGSIM database, an open-access database. The trajectories in the database is from different vehicles, therefore, the threshold is highly affected by the human drivers' heterogeneities. Imaging we collect the historical data from one single drivers, the trained model can be more representative to help instructing the lane-change collaboration. For future works, a comprehensive dataset that incorporating the drivers' information is preferred, for instance, the eyesight movement can indicate the drivers' lane-change intention. It will be easier to collect the rejected lane-change instance precisely if we know when the driver intent to merge.

Chapter 6: Improvements on Collaboration in Work Zones

6.1 INTRODUCTION

As mention in the previous chapters, the CAV are expected to improve the traffic performance by offering collaboration to their surrounding vehicle, like providing acceptable gaps to the lane-change vehicles without significant sacrifice of ego travel time, executing determined lane-change maneuvers within the safety criteria, etc. In this chapter, a lane-change prediction model was applied to assist the collaboration of cooperative lane-changes in a work zone. We conducted microscopic simulations to demonstrate the traffic performance of this road section when the penetration rates of the CAV increase from 0 % to 100 % by 10 %. Consider the road section originally has three lanes, yet one lane outmost lane is closed due to the deployment of a long-term work zone. FVD model was applied to simulate the car-following motions, and a lane-change model was established on the basis of a variable-time-span lane-change model as illustrated in chapter 4. As illustrated in the aforementioned literatures, the lane-change will inevitably impact the target lane during the cooperative lane-changes. Even with the participation of the CAV, we still believe that the traffic performance of the target will be affected more and less; however, the participation of the CAV is looked forward to mitigating the impacts and facilitating the collaboration.

6.2 MODEL DESCRIPTION

As illustrated in the chapter 5, there are six features being involved in the lane-change prediction model:

- $\Delta_{x,afv}$ denotes the longitudinal gap between the ego vehicle and the adjacent following vehicle;
- $\Delta_{v,afv}$ denotes the speed difference between the ego vehicle and the adjacent following vehicle;
- $\Delta_{x,apv}$ denotes the longitudinal gap between the ego vehicle and the adjacent Preceding vehicle;

- $\Delta_{v,apv}$ denotes the speed difference between the ego vehicle and the adjacent preceding vehicle;
- D_w denotes the distance between ego vehicle and the end of the lane that is the activity zone in this chapter;
- $\dot{x}_{ev}$ denotes the longitudinal velocity of ego vehicle;

In this chapter, we assumed that a vehicle would at least be able to connect to its surrounding vehicles or adjacent infrastructures even if the vehicle was currently driven by a human driver. If the ego vehicle is driven by a human driver, the on-board computer can extract the historical lane-change trajectories of this particular driver and predict the expected $\Delta_{x,afv}$ and $\Delta_{v,afv}$ that enable the human driver to start a lane-change maneuver on the basis of the other four features as shown in Eq. (6.1) where LPM denotes the lane-change prediction model, and then the $\Delta_{x,afv}$ and $\Delta_{v,afv}$ will be passed to the AFV.

$$\Delta_{x,afv}, \Delta_{v,afv} = LPM\left(\Delta_{x,apv}, \Delta_{v,apv}, D_w, \dot{x}_{ev}\right) \tag{6.1}$$

Then, the AFV will evaluate the required speed difference and gap to fulfil both of the requirement:

$$\begin{cases} \left(\dot{x}_{ev} + \ddot{x}_{ev}t\right) - \left(\dot{x}_{afv} + \ddot{x}_{afv}t\right) \geq \Delta_{v,afv} \\ \left(x_{ev} + \dot{x}_{ev}t + \frac{\ddot{x}_{ev}t^2}{2}\right) - \left(x_{afv} + \dot{x}_{afv}t + \frac{\ddot{x}_{afv}t^2}{2}\right) \geq \Delta_{x,afv} \end{cases} \tag{6.2}$$

where t denotes the threshold of time to collision, and $t = 3$ is applied (Kuang, Qu & Wang 2015); x_{ev}, $\dot{x}_{ev}$, $\ddot{x}_{ev}$ denote the position, velocity and acceleration of the ego vehicle respectively; x_{afv}, $\dot{x}_{afv}$, $\ddot{x}_{afv}$ denote the position, velocity and acceleration of the adjacent following vehicle respectively. At the meanwhile, $\ddot{x}_{afv} \geq -\delta$ restricts the maximum deceleration by maximum allowable disturbance between AFV and its following vehicle as demonstrated in Eq. (3.10). Otherwise, the CAV will seek for the opportunities for immediate lane-change to its adjacent lane. Alternatively, if the ego vehicle is automated, the sensor will evaluate the approaching speed of the AFV, therefore, making precise lane-change decision, e.g. accept shorter gap with the AFV. Different from human drivers, CAV need not check the gaps with it APV and AFV repetitively, which significantly decreases the reaction time. Additionally, CAV were

assumed to be capable of searching for lane-change opportunities earlier than HDV as a result of V2I.

The lane-change model in chapter 4 was further modified to demonstrate more realistic interactions among vehicles. Firstly, not only the target lane but the ego lane will be impacted when the lane-change vehicle is crossing the lane mark and the impacts can be calculated on the basis of the percentage of width invading the target lane (or ego lane). More specifically, an interpolated speed between scenarios with and without the ego vehicle are determined by the aforementioned percentage. Furthermore, the on-going lane-change vehicle will bring an immediate impact to its preceding vehicle if this preceding vehicle is seeking for merging into the same target lane.

A driver's patience factor was also proposed to simulate the decreasing of patience during finding the acceptable gap, and the Eq. (4.10) can be rewritten as Eq. (6.3):

$$\mathrm{D} \geq (\dot{x}(t) + p)\sqrt{\frac{6|y_{end} - y_{start}|}{|\ddot{y}_{max}|}} \tag{6.3}$$

With the decreasing of the minimum requirement of D, the ego vehicle will adopt a more aggressive lane-change strategy. The patience factor p decreases with the times of lane-change attempts.

6.3 RESULT AND DISCUSSION

The longitudinal trajectories and lateral trajectories are plotted in Figures 6-1 to 6-8 with 0, 30%, 60% and 90% CAV participating in the traffic flow respectively. Trajectories from other penetration rate can be found in Appendix C. The right-top, left-bottom and right-bottom sub-figures illustrates the trajectories of non-through lane (lane 1), left adjacent lane (lane 2) and the outermost lane (lane 3) respectively. The left-top sub-figure represents a comparison group when a lane is not impact by the work zone. It can be told from Figure 6-1 that almost half of the vehicles failed to merge into the target lane and had to decelerate to before entering the work zone. What made the situation worse was that drivers are increasingly aggressive with the growing times of attempts. Those drivers may accept more lateral acceleration and larger yaw angle regardless of the increasing speed difference between ego vehicle and the

vehicles in the target lane; therefore, great impacts were brought to the target lane as shown at the 500th and 750th simulation intervals. No vehicle was witnessed to merge into the outermost lane due to the low necessities as shown in Figure 6-2. Similar scenario can be seen from Figure 6-3, but the 30 % of CAV continued merging into the outermost lane creating acceptable gaps for further lane-change tasks into the middle lane. With the increasing of CAV's penetration rate, more vehicles can avoid stopping in front of the work zone as shown in Figure 6-5. In Figure 6-7, the 90 % penetration of CAV facilitated the lane-changes within 800 simulation intervals. The 100 % penetration rate of the CAV a surprising result that the traffic performance was not further improved compared to 90 % penetration rate as illustrated in the Figure C-13, which means the 90 % penetration rate has been sufficient to dampen the oscillation brought by the human drivers' heterogeneities. In contrast, it took longer for vehicles to merge into the target lane because too many early lane-changes boost the density on the target lane increasing the difficulty of lane-change on downstream. Well-organized lane-change collaborations among vehicles from the non-through lane and the left adjacent lane can be seen between the 300th to the 750th simulation intervals. It can also be told from the comparison of lateral trajectories that the more vehicles will choose gentle lane-change strategies with the increase of the penetration rate. The most distinctive and remarkable improvement of incorporating the CAV into the traffic system is that more vehicles can merge into the expected target lanes without huge drop of speed as can be seen from Figure 6-9. Imagine a three-lane traffic flow travelling through a work zone, the lane-change processes will be smooth if 80 % of vehicles activate connected and automated system. Comparing Figures 6-2, 6-4, 6-6 and 6-8 tells that the participation of the CAV had significant positive effects on assisting the lane-change collaboration. Under the situation when the amount of the CAV is low, the drivers from blocked lane experienced high difficulties on lane-change task; at the meanwhile, the drivers in the adjacent lane did not have enough motivation to change lane for smoother dispersion as shown in Figures 6-2 and 6-4. With the increasing number of the CAV, collaborations among vehicles were increasingly frequent, and all vehicles were able to finish lane-change tasks when the penetration rate reached 90 % as shown in Figure 6-8.

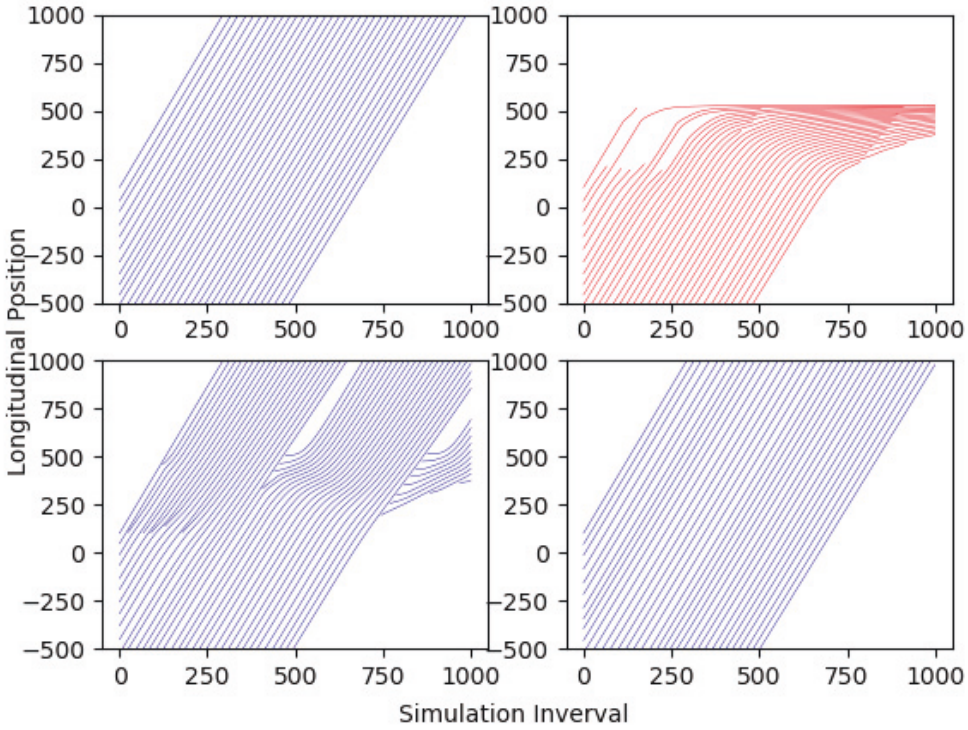

Figure 6-1 Longitudinal position with 0 % CAV penetration rate.

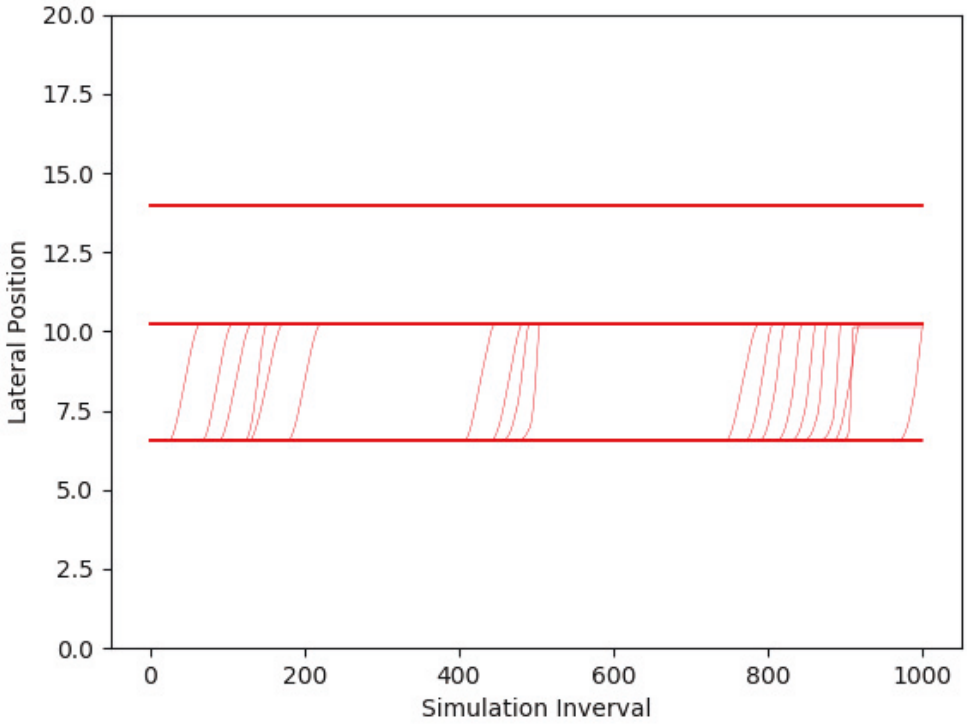

Figure 6-2 Lateral position with 0 % CAV penetration rate.

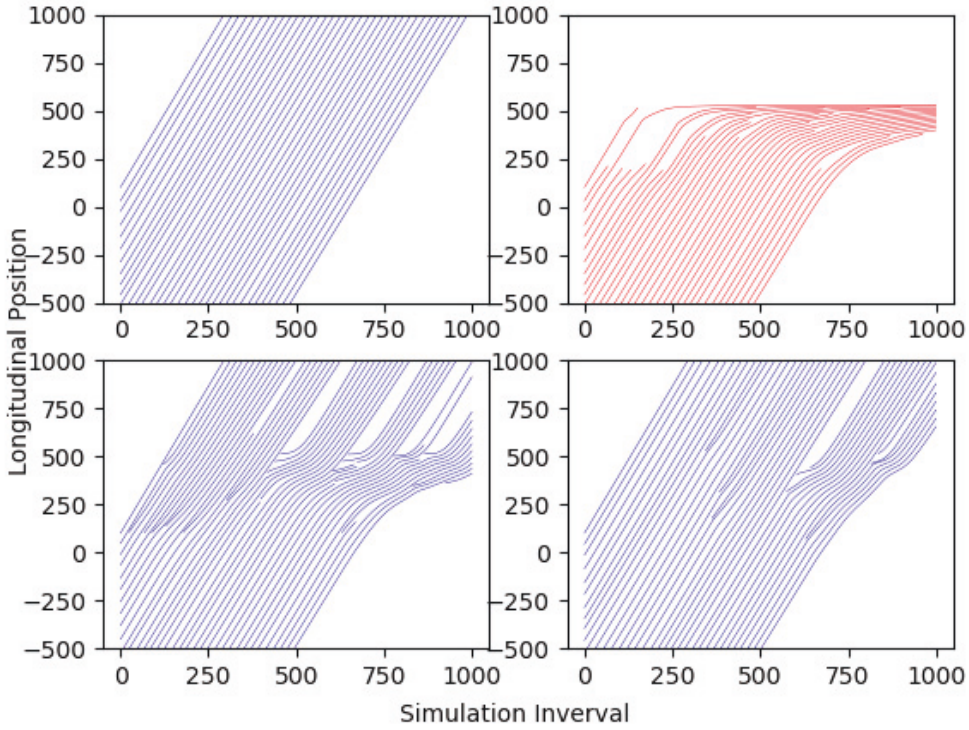

Figure 6-3 Longitudinal position with 30 % CAV penetration rate.

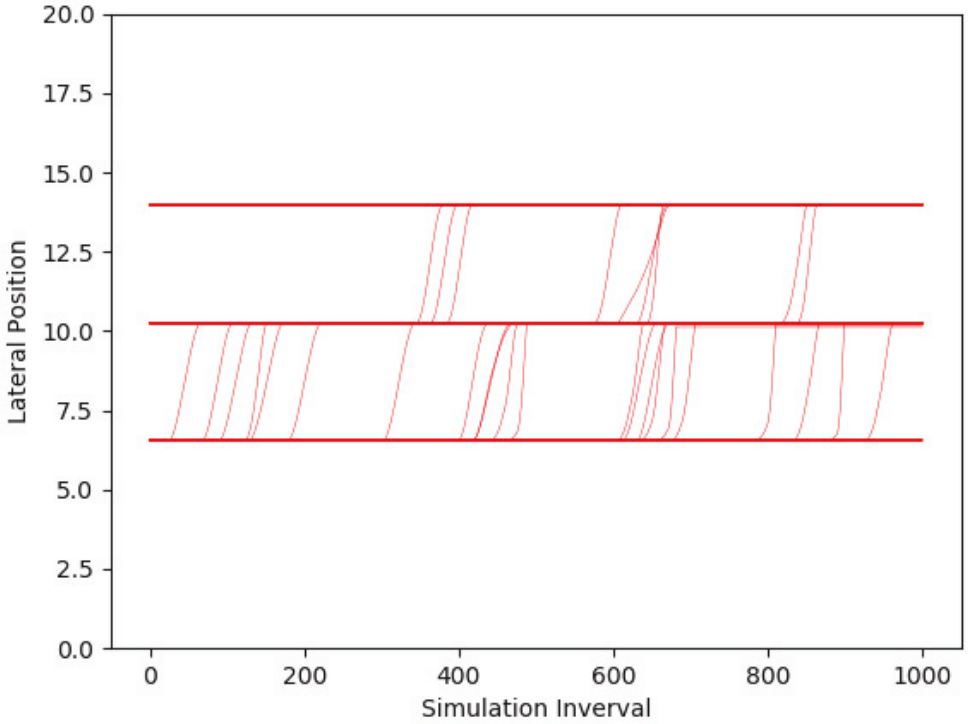

Figure 6-4 Lateral position with 30 % CAV penetration rate.

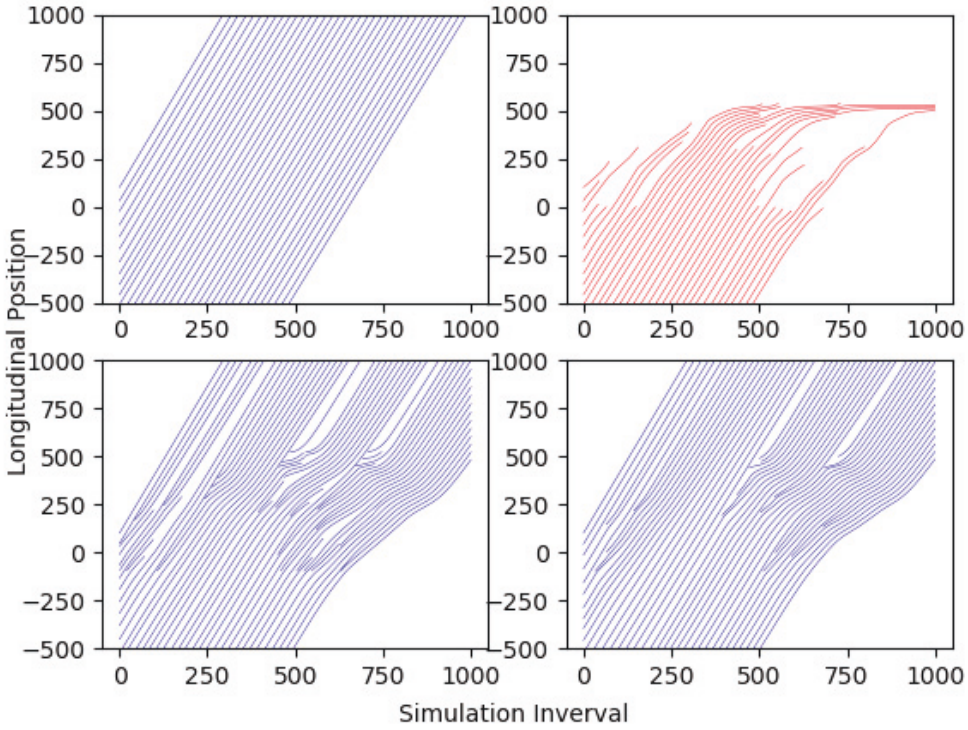

Figure 6-5 Longitudinal position with 60 % CAV penetration rate.

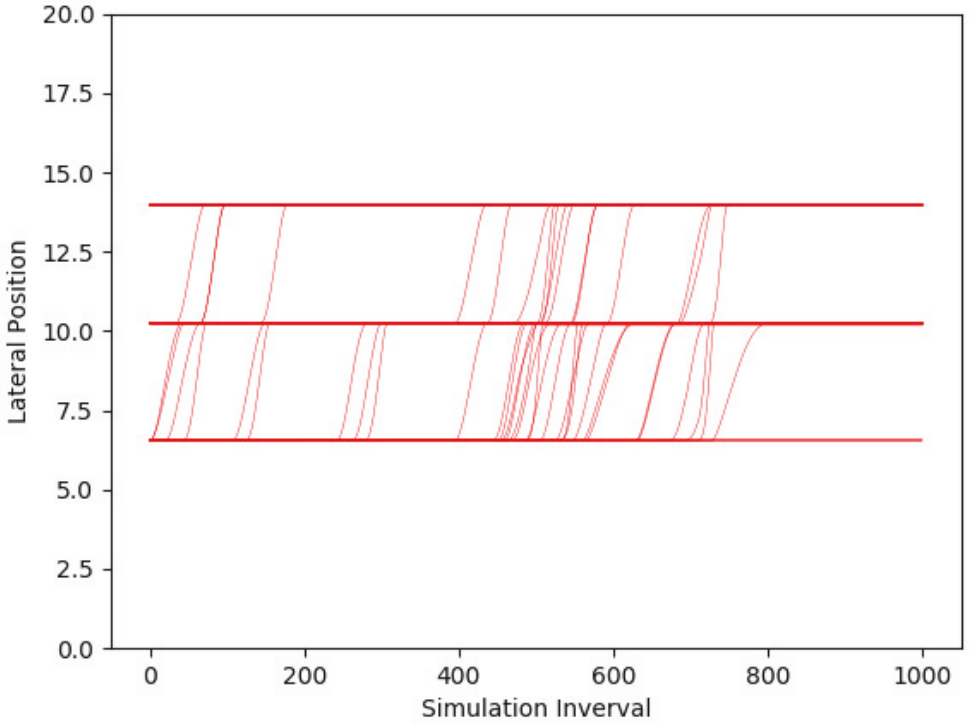

Figure 6-6 Lateral position with 60 % CAV penetration rate.

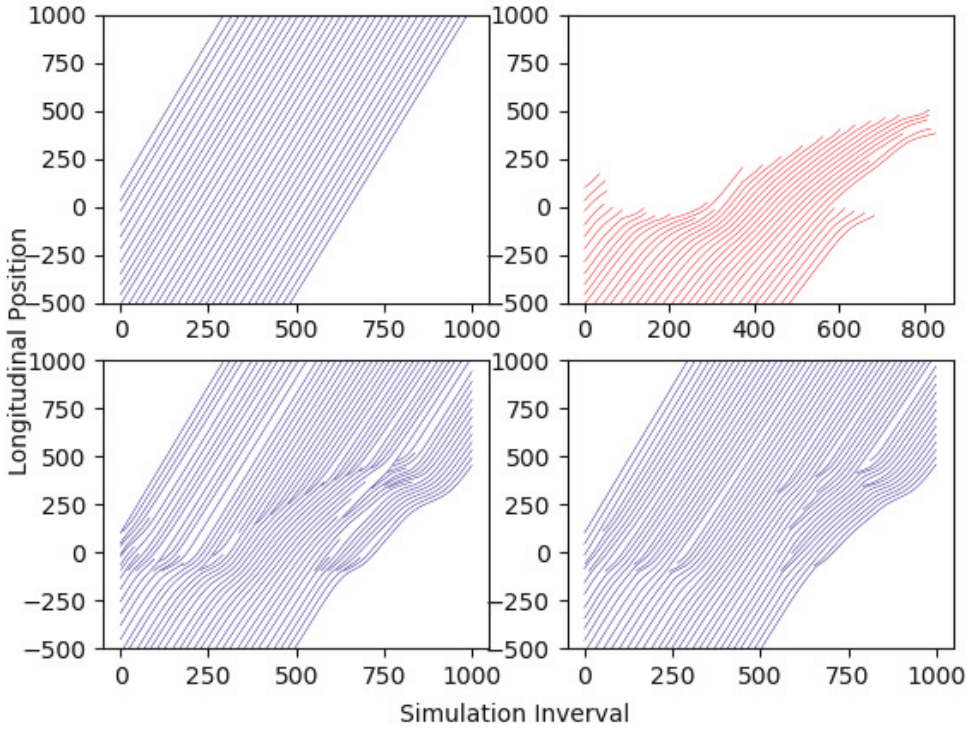

Figure 6-7 Longitudinal position with 90 % CAV penetration rate.

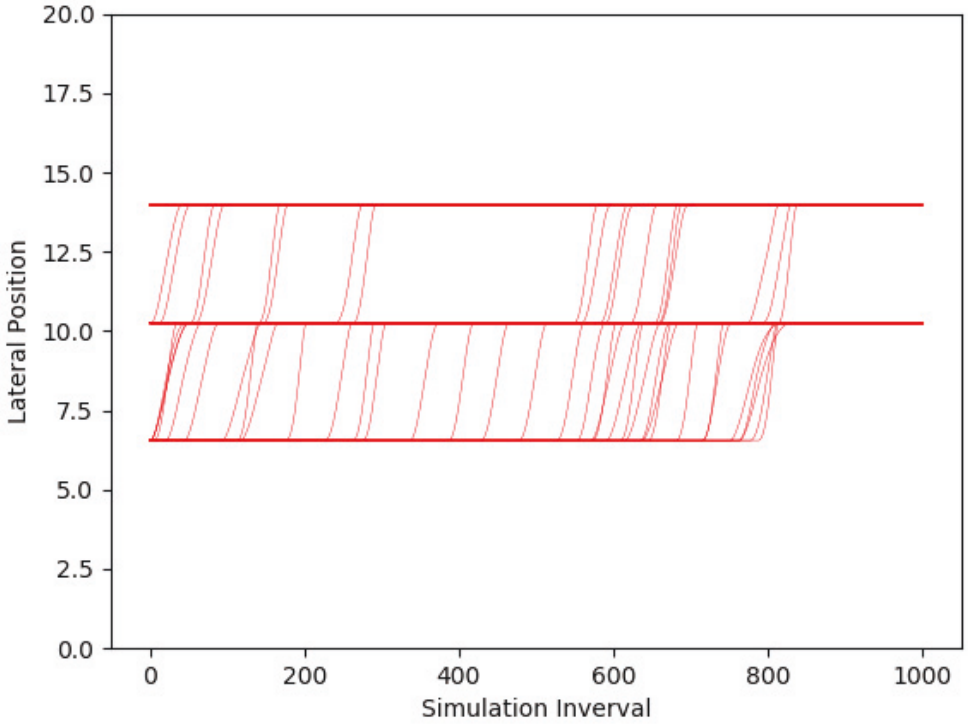

Figure 6-8 Lateral position with 90 % CAV penetration rate.

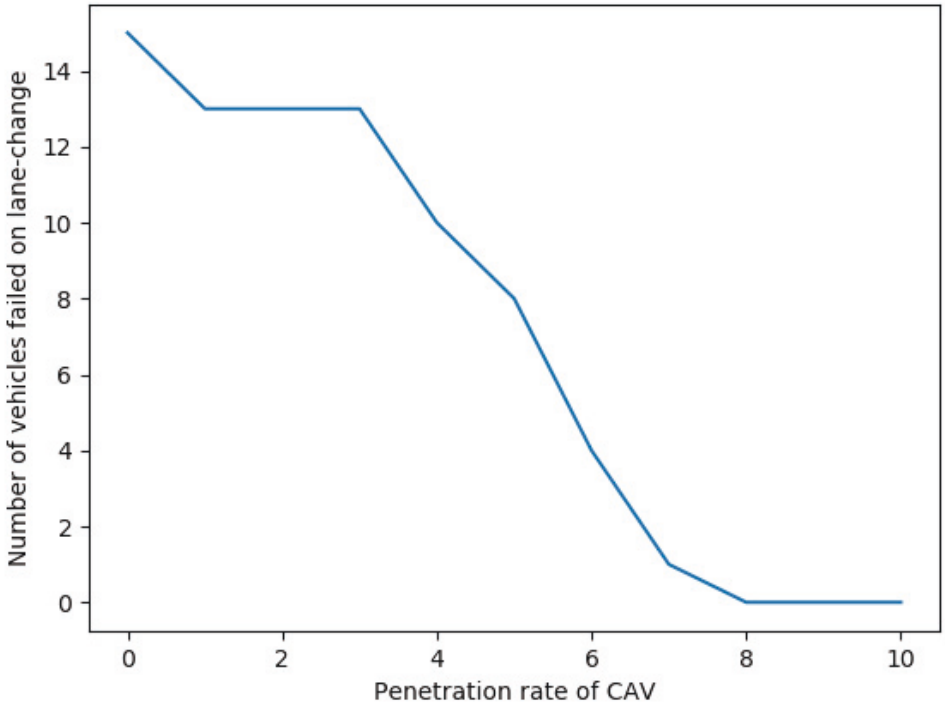

Figure 6-9 The number of vehicles failed on lane-change with the increase of the penetration rate

The emission of the 105 vehicles are calculated by VT-micro emission model which has been illustrated in Eq. (3.25). In Figure 6-10, the emission with regards to the penetration rate is displayed, and it can be seen that the emission of vehicles on lane 1 boosts with the increase number of the CAV. Nonetheless, it does not mean more jerks, on the contrary, this is right because vehicles merge into the through lanes and continue travelling through the work zone. Fortunately, it is pleasing to see that the lane-change maneuvers did not increase the emission on the target lane. Figure 6-11 shows cumulative distribution of velocities of lane 1 under different penetration rate, and large quantity of observations can be witnessed in the low-speed zone when the penetration rate is low. With more automated system being activated, the data on the low-speed zone gradually vanish, which also indicates the decrease of average travel time consumed on travelling through the work zone. Figure 6-11 summarizes the average speed of every 50-meter longitudinally span from the position of 250 meters to the position of 700 meters on lane 1. When the penetration rate is equal to 0 %, 30 % and 60 %, there are clear speed drops, while 90 % penetration rate of vehicles mitigates the impacts of work zone significantly on lane 1. Figure 6-12 showed a great effect of dampening the traffic oscillations brought by the CAV. It is clear that the positive effects grew with the penetration rate of the CAV, and the speed drops were completely mitigated at 90 % penetration rate.

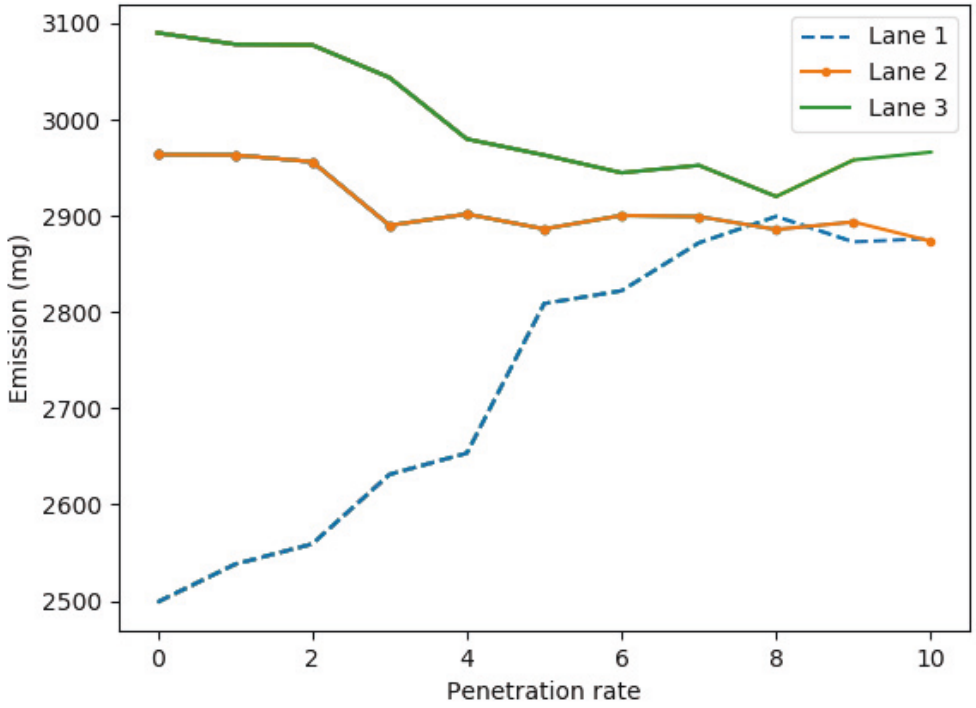

Figure 6-10 Emission of different penetration rate.

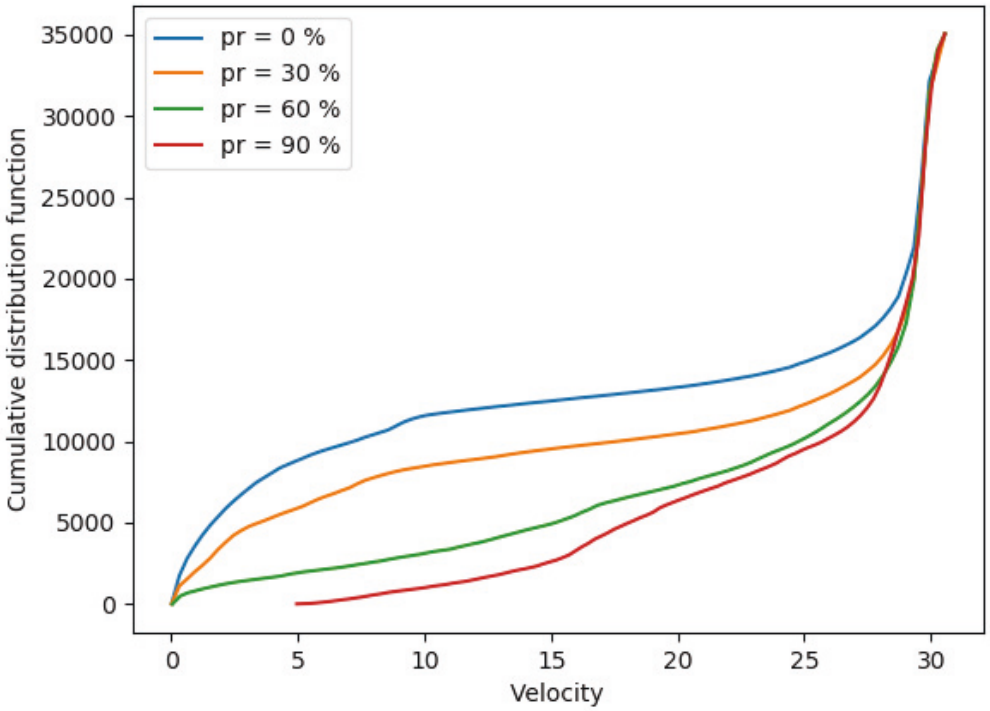

Figure 6-11 Cumulative distribution of velocities on the non-through lane.

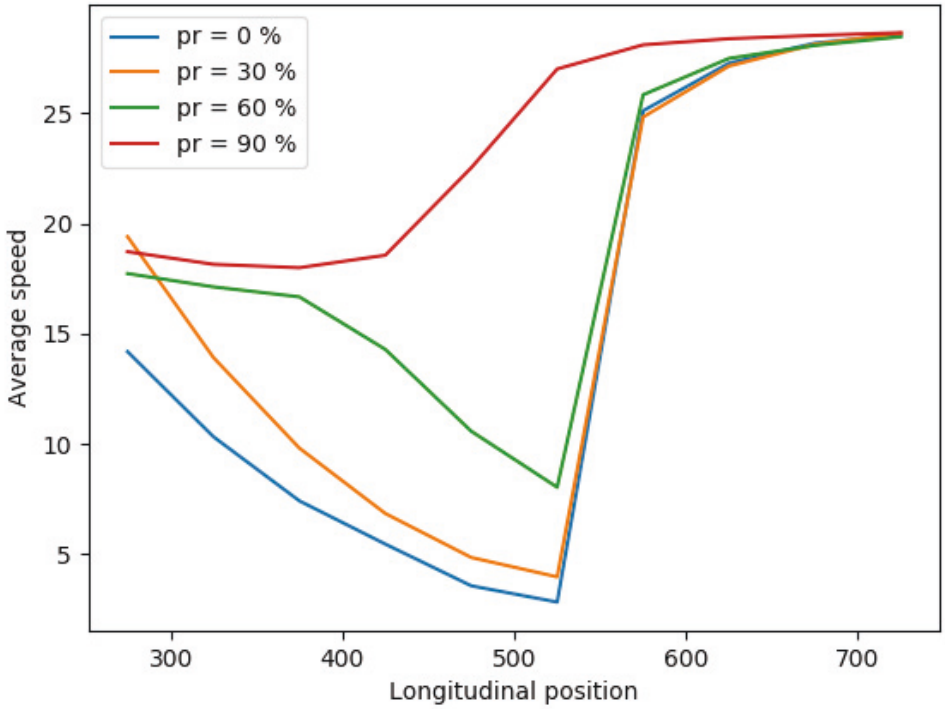

Figure 6-12 Average speed on different longitudinal positions of the non-through lane.

6.4 SUMMARY

In this chapter, the lane-change prediction model was applied to simulate the collaborative instances of the CAV. A microscopic simulation was conducted based on a three-lane traffic flow with one lane blocked by a work zone. The model of CAV was derived from the model of HDV with modification being applied to optimize the lateral movement. Results showed that the participation of the CAV can effectively mitigate the impact brought by work zones. Though the lane-change maneuvers inevitably impacted the target lane, the CAV showed great effects on reducing the disturbances. The most extraordinary benefit was decreasing number of vehicles stopped by the work zone, and it showed that traffic dispersion was perfectly done when 80 % of vehicles activated the connected and automated system. When the penetration rate reached 100 %, the time span of the traffic dispersion surprisingly grew as a result of too many early lane-changes, which indicated that 80 % penetration rate has been sufficient enough to enhance the collaborations.

Chapter 7: Improvements on Collaboration in Incident-affected Zone

7.1 INTRODUCTION

Different from work zone, an emergency incident can happen anytime in day with a long period of unsupervised traffic. Due to this characteristic, the regulation of incident-affected traffic needs to be capable of dealing with high-density traffic, sometime even heavy traffic jam. In this chapter, we conduct micro-simulation for the four-lane traffic, where the second outmost lane is blocked by the unexpected incident，and there are 45 vehicles in each lane. Vehicle on the non-through lane then have to seek for lane-change opportunities in order to avoiding stuck into the incident-affected area. Individually, stopping increase the difficulty of lane-change, while it also increases the impacts on the whole traffic system, especially the target lane. Again, the CAV are looked forward to mitigating the impacts, yet, as discussed in the previous chapter, the most penetration rate of the CAV does not mean the best performance. Hence, how many vehicles' automation systems need to be activated becomes a vital question.

7.2 MODEL DESCRIPTION

The model applied on the simulation was similar with the one illustrated in the previous chapter, and the most distinctive feature was that the ego vehicle would have two options on merging direction. The CAV and the HDV will execute lane-change tasks based on different criteria that HDV can only focus on gap on one lane, therefore, possibly missing the better gap in the other lane, but CAV will consider the lower-density lane in priority as the potential target lane.

7.3 RESULT AND DISCUSSION

The longitudinal trajectories and lateral trajectories are plotted in Figures 7-1 to 7-8 with 0, 30%, 80% and 90% CAV participating in the traffic flow respectively. Trajectories from other penetration rate can be found in Appendix D. The left-top, right-top, left-bottom and right-bottom sub-figures illustrates the trajectories of right adjacent lane (lane 0), non-through lane (lane 1), left adjacent lane (lane 2) and the

outermost lane (lane 3) respectively. The microscopic simulation depicts the dynamics of a four-lane traffic flow with lane 1 being affected by an emergency incident. Different from the simulation in the Chapter 6, vehicles had two options to avoid being stopped by the incident. We assumed that the lane-change to the right adjacent lane and the left adjacent lane require were equally accessed, but the CAV would strive for a less impact on the entire traffic. Figure 7-1 tells that the success rate of merge was not improved even though drivers can merge into both lanes. Among those who had successfully merged into the target lanes, some just caused severe delay of the following vehicles. We assumed that driving manners were not sufficient for further efforts to lane-change to the lane 3 as shown in Figure 7-2; therefore, the lane 2 would not be able to accommodate more vehicles with growing density. More connected and automated systems being activated showed great effects on facilitating the cooperative lane-change and mitigating the impact of the incident. Figure 7-9 demonstrates the number of vehicles being stopped by the incident zone, and it worth noting that the number under 90 % penetration rate is more than that under 80 % penetration rate. Comparing the trajectories from Figures 7-5 and 7-8 reveal a possible reason that the overreaction of CAV had cumulative impacts on speed reduction, therefore, increase the travel time. Nonetheless, the CAV still showed positive effects on the entire traffic flow, and the one who was not able to merge within 1,000 simulation intervals was an HDV. Different from the results in the previous chapter, 100 % penetration rate did not lead to longer dispersion period as illustrated in Figure D-13 when compared with those of the 80 % and 90 % penetration rate. The reason was that the vehicles had more than one option regarding to the target lanes; therefore, the early lane-changes did not dramatically boost the density of any single one target lane. The emission of the 180 vehicles are calculated by VT-micro emission model which has been illustrated in Eq. (3.25). In Figure 7-10, the emission with regards to the penetration rate is displayed, and it can be seen that the emission of vehicles on lane 1 boosts with the increase number of the CAV. Nonetheless, it does not mean more jerks, on the contrary, this is right because vehicles merge into the through lanes and continue travelling through the incident-affected area. In the meanwhile, the emission on the lane 2 almost levels off while other two lanes show slight decreasing trend.

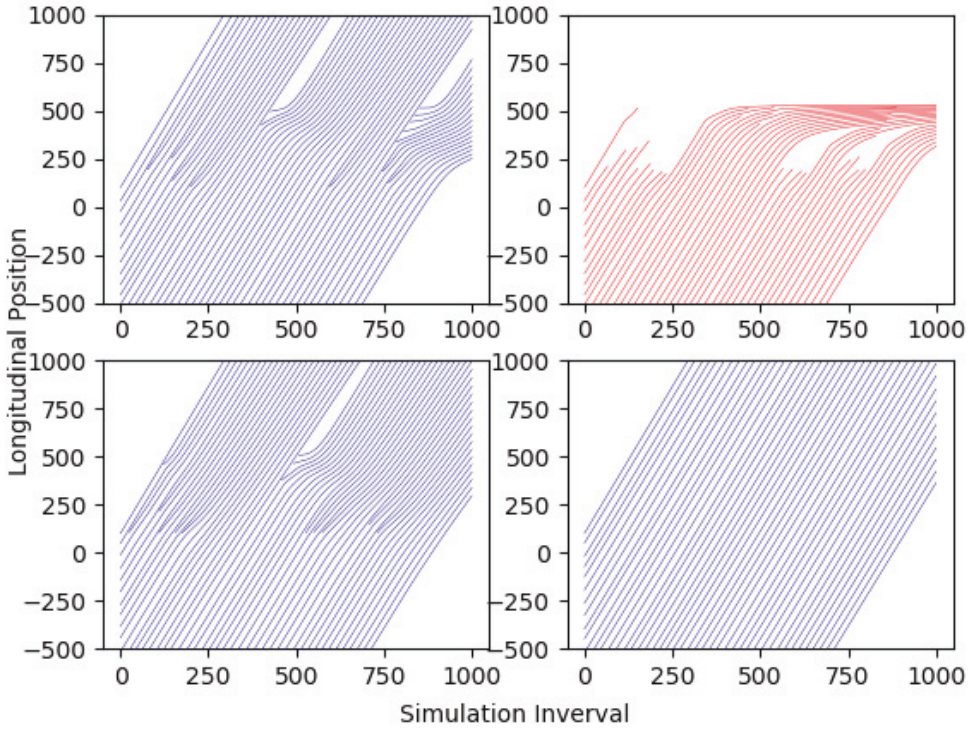

Figure 7-1 Longitudinal position with 0 % CAV penetration rate.

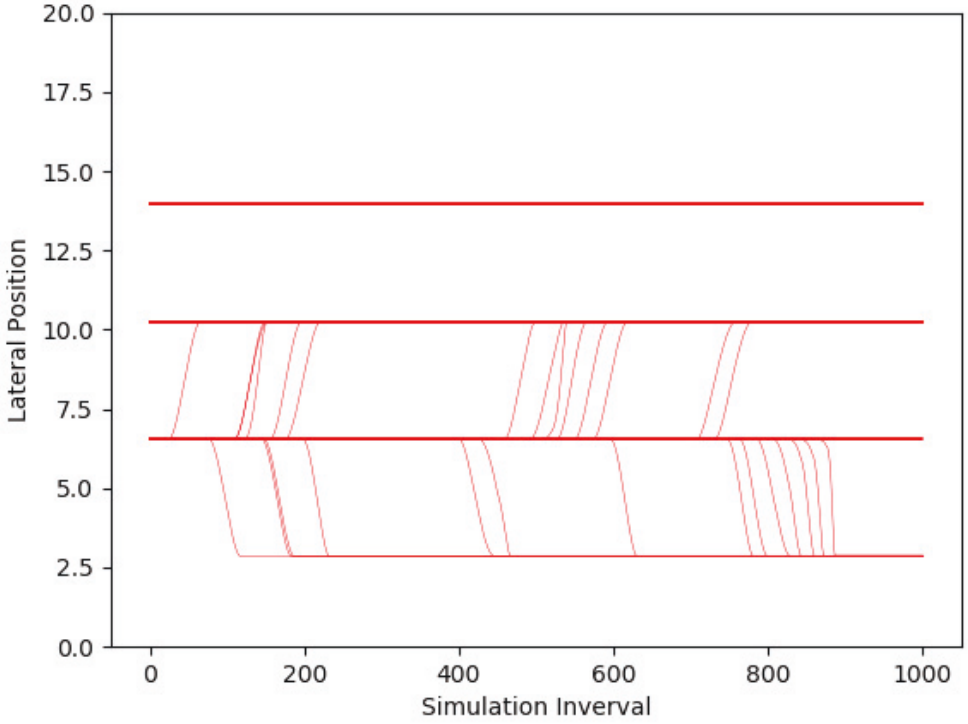

Figure 7-2 Lateral position with 0 % CAV penetration rate.

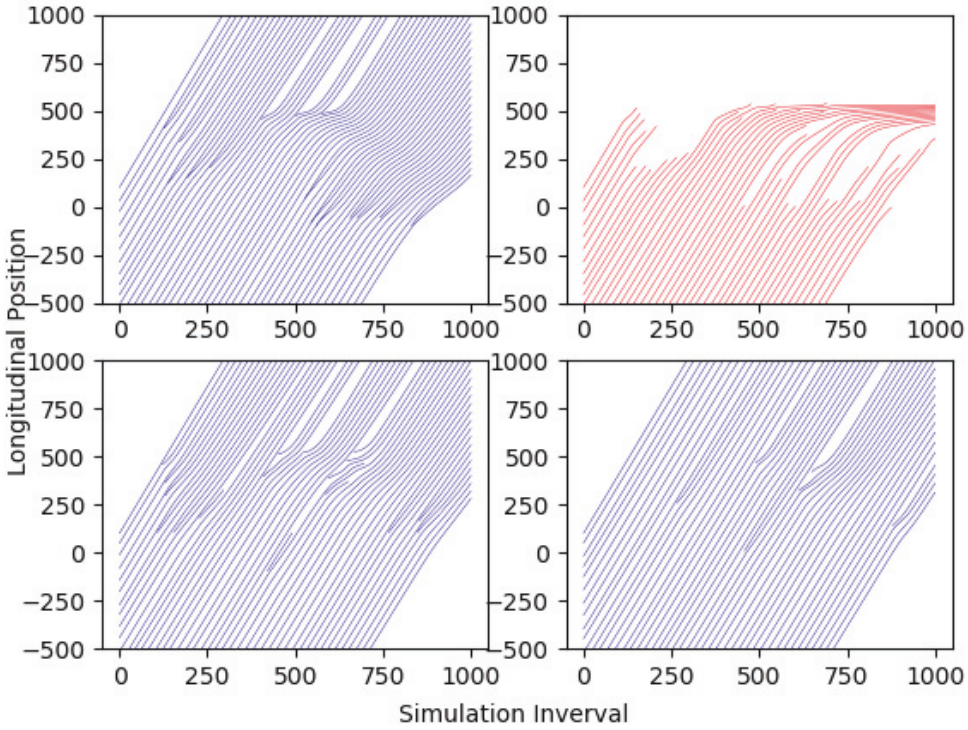

Figure 7-3 Longitudinal position with 30 % CAV penetration rate.

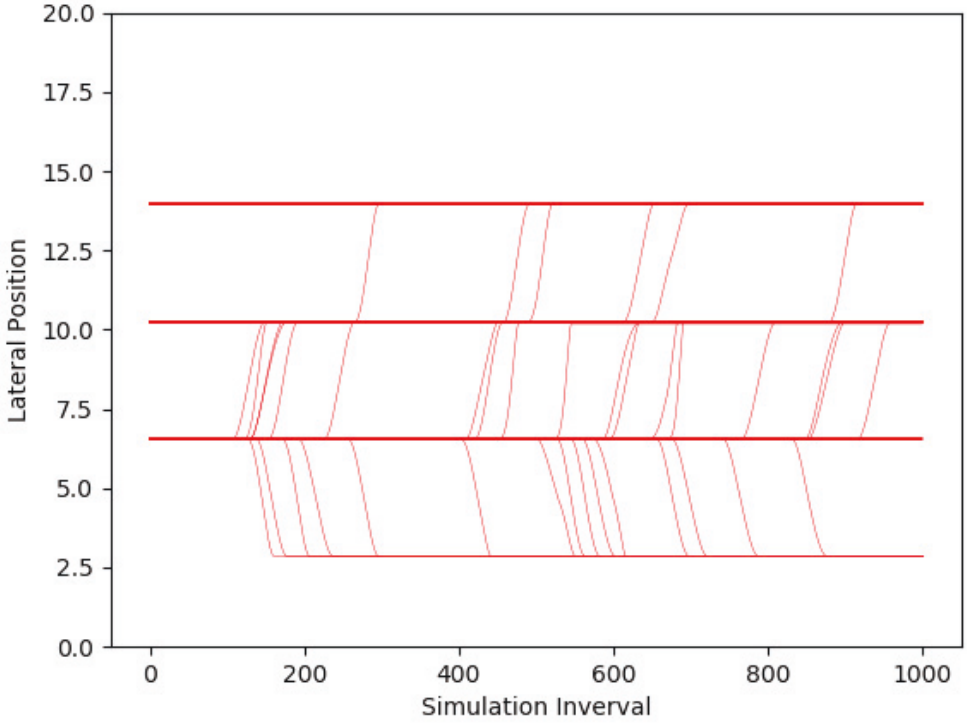

Figure 7-4 Lateral position with 30 % CAV penetration rate.

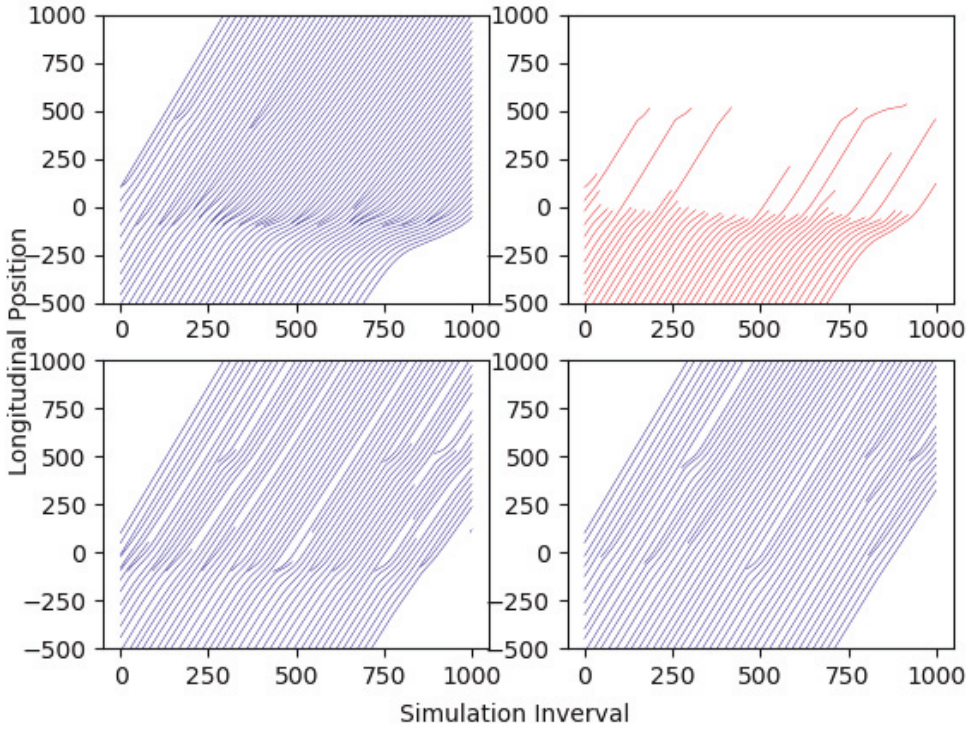

Figure 7-5 Longitudinal position with 80 % CAV penetration rate.

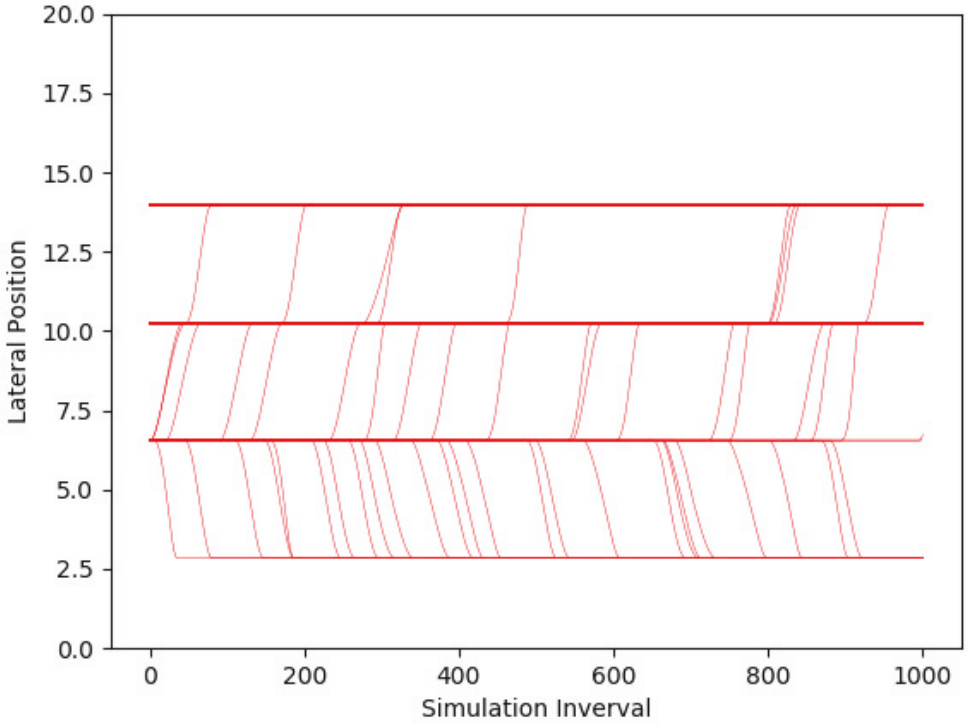

Figure 7-6 Lateral position with 80 % CAV penetration rate.

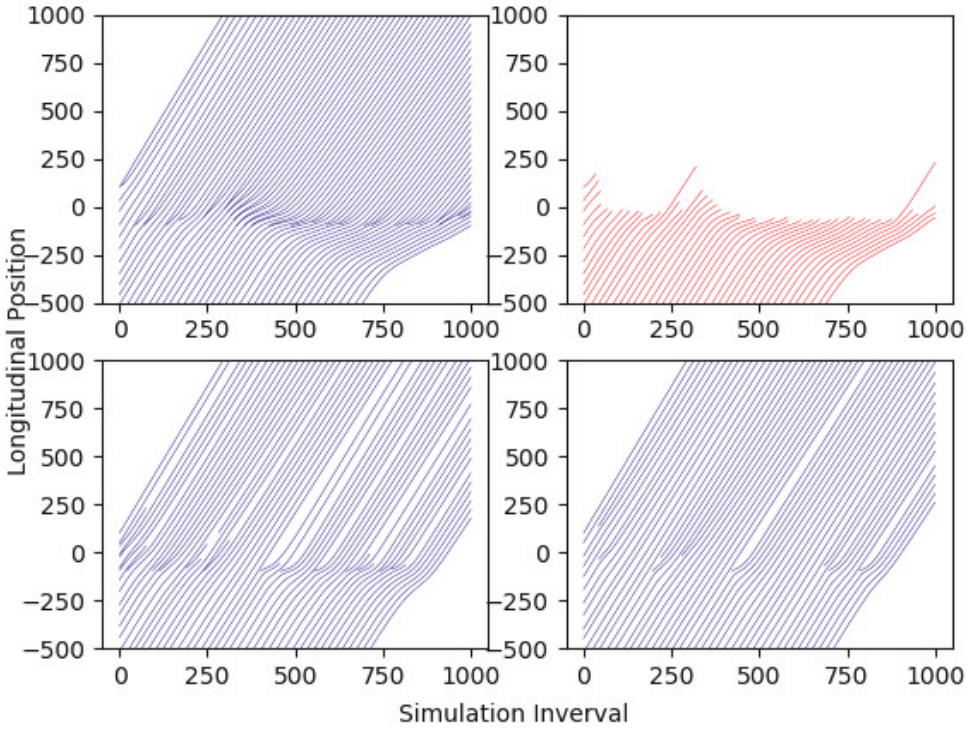

Figure 7-7 Longitudinal position with 90 % CAV penetration rate.

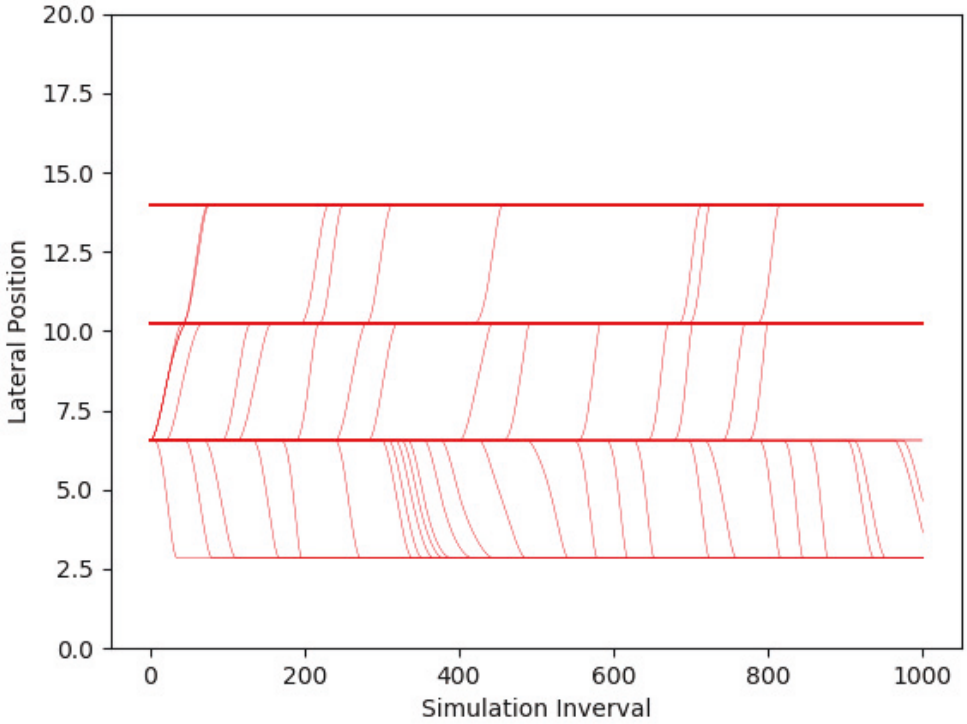

Figure 7-8 Lateral position with 90 % CAV penetration rate.

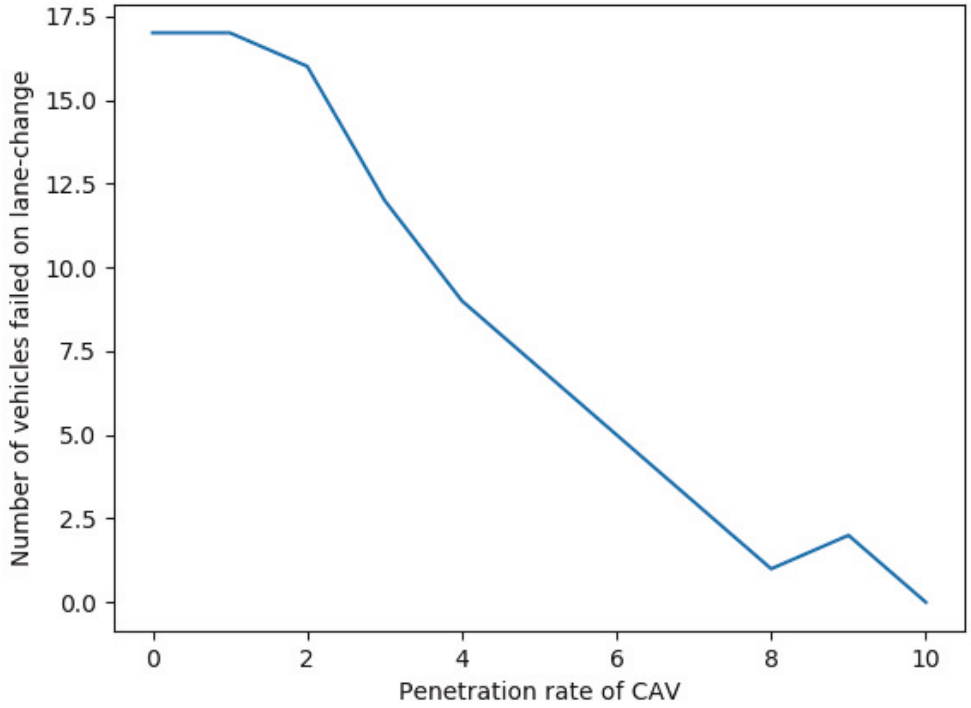

Figure 7-9 The number of vehicles failed on lane-change with the increase of the penetration rate.

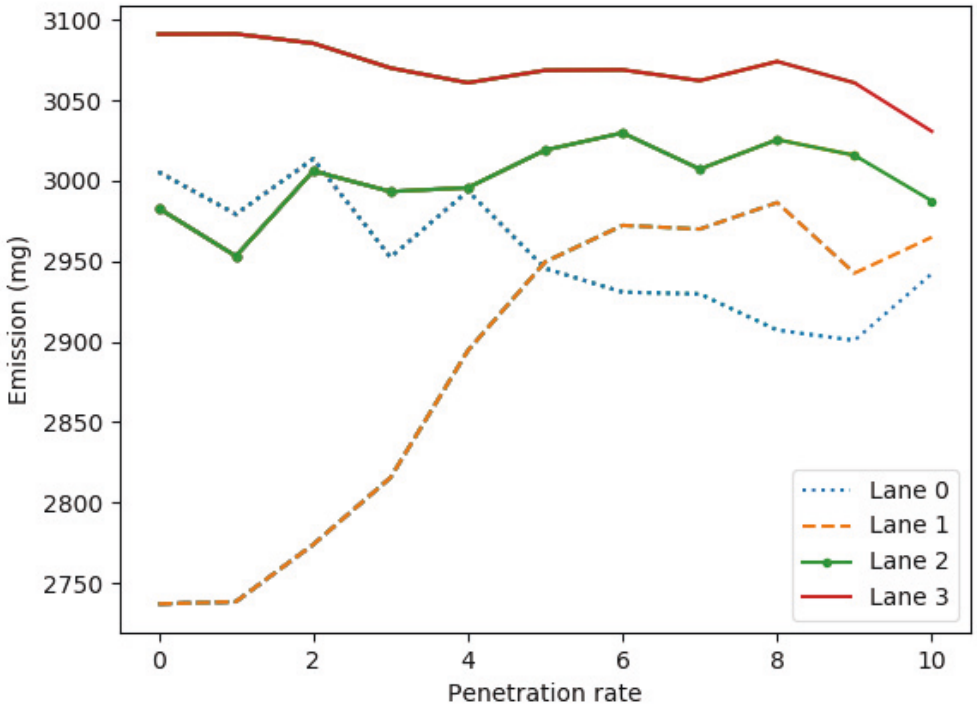

Figure 7-10 Emission for different penetration rate.

The cumulative distributions of different penetration rates display the observations of velocities from lane 1, lane 0 and lane 2 respectively in Figures 7-11, 7-12 and 7-13. When all vehicles are driven by human drivers, a large quantity of speed observations gather at the low speed zone. The observations gradually move towards the higher speed zone with the increase number of CAV in the traffic flow in lane 1. On the contrary, Figure 7-12 shows an opposite trend in lane 0 because the lane-change maneuvers inevitably bring negative effects on the target lane. On the other hand, there is much less impacts on the lane 2 owing to lane-changes from the lane2 to the lane 3. Figure 7-14 summarizes the average speed of every 50-meter longitudinally span from the position of 250 meters to the position of 700 meters on lane 1, lane 2 and lane 3 respectively. When the penetration rate is equal to 0 %, 30 % and 60 %, there are clear speed drops, while 90 % penetration rate of vehicles mitigates the impacts of work zone significantly on lane 1. It is rather clear that the participation of the CAV helped with dempening the traffic oscillation induced by the incidents.

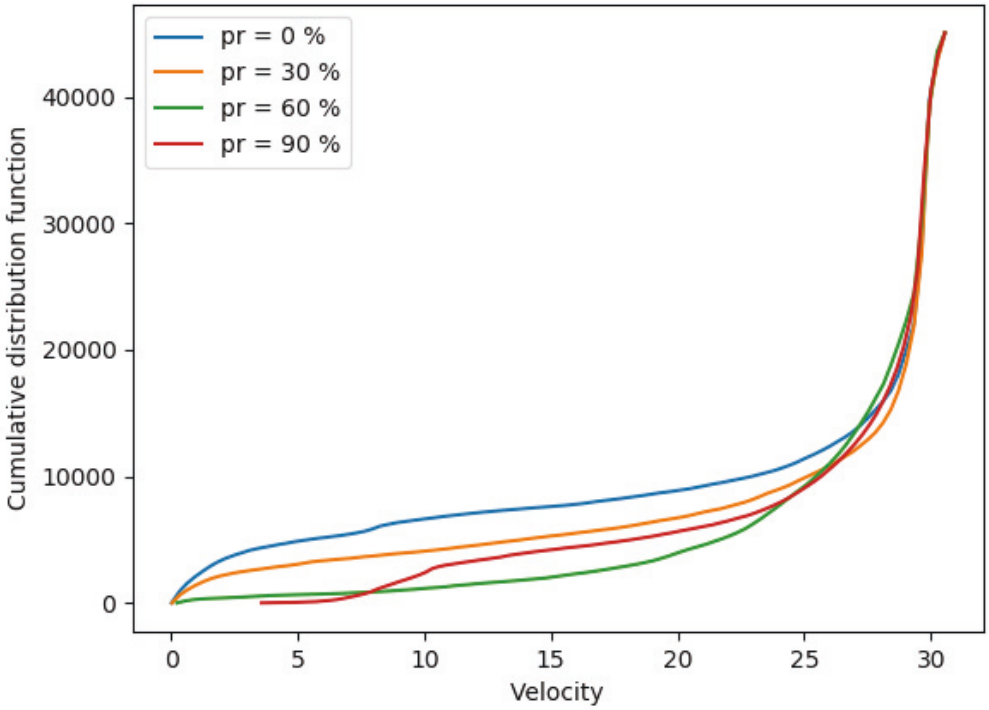

Figure 7-11 Cumulative distribution of velocities on the non-through lane.

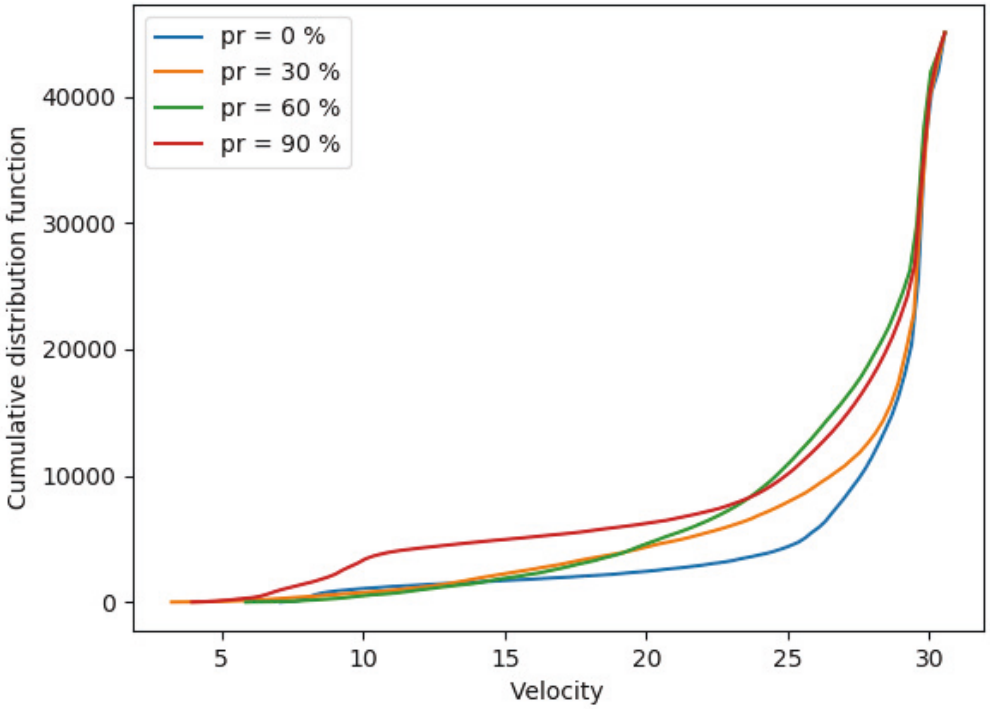

Figure 7-12 Cumulative distribution of velocities on the right adjacent lane.

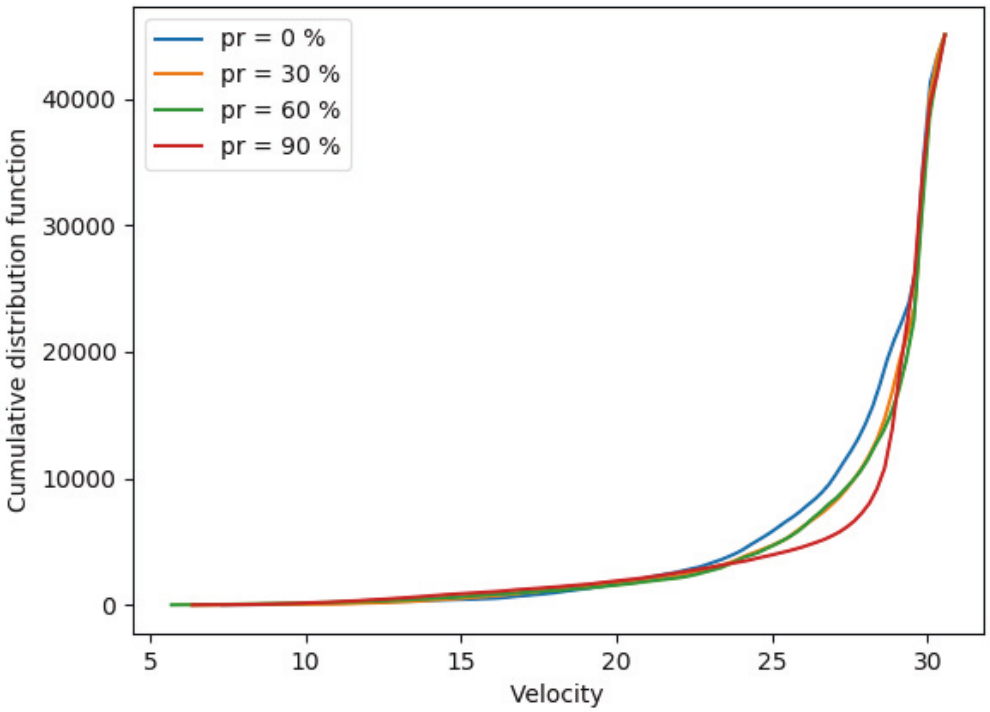

Figure 7-13 Cumulative distribution of velocities on the left adjacent lane.

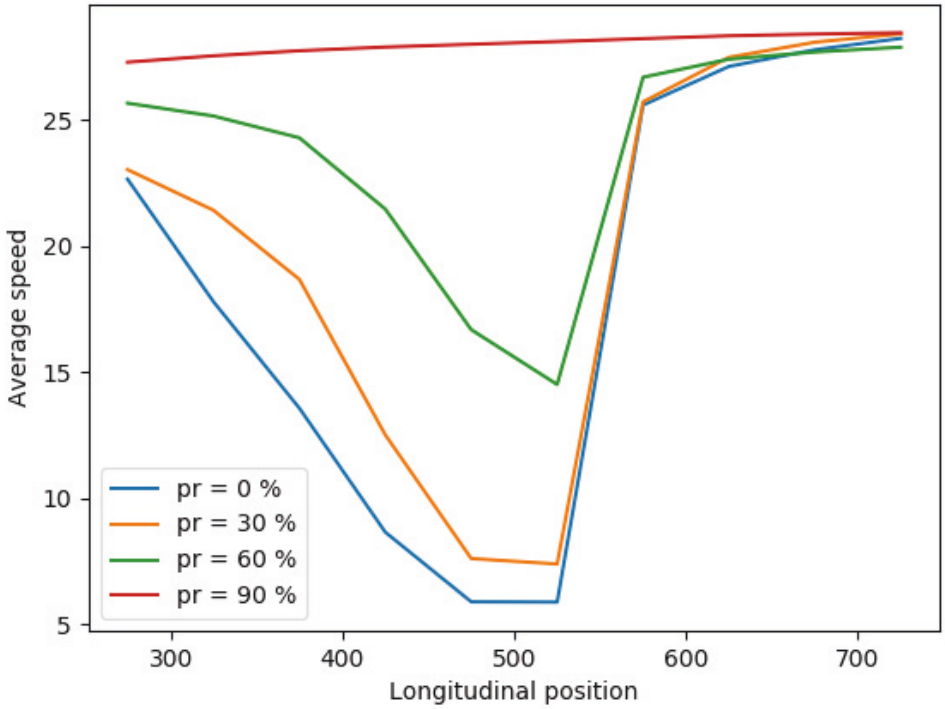

Figure 7-14 Average speed on different longitudinal positions of the non-through lane.

7.4 SUMMARY

In this chapter, the lane-change prediction model was applied to simulate the collaborative instances of the CAV, including the lane-picking criterion. A microscopic simulation was conducted based on a four-lane traffic flow with one middle lane blocked by an emergency incident. Compared to work zones, the emergency incidents need more consideration as they are non-scheduled bottleneck. The model of CAV was modified to be capable of optimizing the lane-picking and lateral movement. Results showed that the participation of the CAV can effectively mitigate the impact brought by the incident. Though the lane-change maneuvers inevitably impacted the target lane, the CAV showed great effects on minimizing the disturbances. The comparison between the lane 2 and the lane 0 demonstrates the advantages of CAV on dispersing the high-density platoon. The most extraordinary benefit was decreasing number of vehicles stopped by the incident, and it showed that traffic dispersion was sufficiently done when 80 % of vehicles activated the connected and automated system. A further increase of the penetration rate to 90 % and 100 % kept a consistent level of effect on the dispersion rate as the 80 % penetration rate.

Chapter 8: Conclusion

Our research started from an analysis on the impacts of connected and automated vehicles on work zones in a two-lane traffic based on microscopic simulations. The CA-based model was proposed to simulate the car-following and lane-change maneuvers of connected and automated vehicles, while ICAM was modified to emulate the human drivers in the work zone. Results showed that the connected and automated vehicles had distinctive effects on mitigating the traffic congestion in the work zone; however, due to the limitation of CA model, the lateral trajectories were deliberately ignored. In chapter 4, the FVD-based model combined with the Hidas-type lane-change model was introduced to emulate the traffic dynamics of a four-lane traffic flow in an incident-affected zone. Different from the CA-based simulations, realistic lane-change trajectories were incorporated into the simulations. The clothoids spirals were employed to represent the trajectories and they were further approximated into cubic polynomials. Various lane-change trajectories were depicted on the basis of human drivers' heterogeneities and the lane-change conditions; thus, it was possible to emulate the vehicles' on-going effects on the origin lane and the target lane during the lane-change maneuvers. By adjusting the reaction factors and the lane-change thresholds, an intuitive analysis on the contribution of connected and automated vehicles was demonstrated. In chapter 5, trajectories affected by lane drops were extracted from the NGSIM database, the k-NN algorithm and the Bayes classifier were combined to predict the human drivers' lane-change decision on the basis of 10 Hz trajectories data. Based on the lane-change prediction model, the connected and automated vehicles were able to collaborate with heterogenous drivers precisely. The model was then applied to simulate the cooperative lane-change in the work zone and the incident-affected zone respectively, and satisfactory outcomes were witnessed on facilitating well-regulated lane-change collaborations and improving the traffic performance.

To summarized, the connected and automated vehicles were intuitively introduced into the microscopic simulations as a solution of the congestions in the re-organizing traffic flow, especially in the work zone and the incident-affected zone. New microscopic models were proposed on the basis of the traditional car-following

and lane-change models to simulate the collaborative instances of the connected and automated vehicles, while the traditional traffic dynamic models were also modified to practically emulate the human drivers' car-following motions and lane-change maneuvers. Realistic lane-change duration and trajectories were considered; therefore, the on-going variable effects on both the ego lane and the target lane were accessed during the lane-change maneuvers. A combination of k-nearest-neighbor and Bayes classifier were presented for lane-change prediction purpose on the basis of 10 Hz trajectories dataset, which facilitated more logical and controllable cooperative lane-changes.

The microscopic simulations demonstrated the clear evolvement of the congestion under low connected and automated vehicles' penetration rate, while the process slowed down or even diminished with more connected and automated vehicles in the traffic network. The travel time, average speed and the emission were applied as the main deterministic indicators of the traffic performance, and the analysis of these three indicators proved the positive effects of the connected and automated vehicles. The congestion brought by the re-organizing traffic flow can be potentially addressed by incorporating connected and automated vehicles, but the results also showed that low penetration rate of the connected and automated vehicles may not be capable of facilitating the high-level cooperative lane-change. On the other hand, when the connected and automated vehicles took the majority of traffic flow, the impacts of the bottlenecks were able to be effectively mitigated. However, the proposed models for the CAV was not able to be calibrated due to a lack of the CAV's field data. Future works would expect the researchers to apply the real-world trajectories to calibrate the parameters in the models. Furthermore, a driving simulator would be expected to validate the collaboration by the heterogenous human drivers in the future. This thesis gave a clear demonstrate of the CAV's benefits, nevertheless, it mainly focused on the freeway where the quantity of entrances and exits is very limited. The authors believe that complex road section would be conducive to highlighting the CAV's benefits, yet more intelligent contents need to be added into the current models. It is obvious that the historical trajectories from a one single driver are able to reflect his/her driving manners; therefore, the trajectories can be applied to assist in predicting the driving maneuvers under various situations. The more trajectories being collected, the more scenarios the prediction model can cover, and therefore, the more accurate the

collaboration will be. The growing of the CAV's market would increase the penetration rate of the CAV, but the traffic would never be deterministic as long as the existence of human drivers on the road. Hence, the interaction among human drivers and intelligent driving systems would still be a popular topic in the future.

Appendices

Appendix A

Investigation on linearization of data driven transport research

1. INTRODUCTION

Transportation engineering, as a practical engineering discipline, relies heavily on the accurate calibration of important parameters from field data, not only for microscopic models at the vehicle (Zhang, Tang & Wang 2019) or bottleneck level, but also for macroscopic models at the planning and network level. When the functional relationships among parameters are linear, linear regression models are usually applied to calibrate the relationships. Sun et al. (2003) applied a local linear method to calibrate the nonlinear time-variant function from a traffic-forecasting model with high computational efficiency. Meng and Qu (2013) applied a linear regression method to calibrate two parameters, passenger boarding time and times of door opening and closing, from a function of dwell time against the number of boarding passengers. Unfortunately, linear equations could not always reflect the relationship between the dependent and independent variables, as a result of the complexity of real-world traffic, and many exhibit notable nonlinearity. As a result, researchers usually either apply nonlinear regression models (Qu, Wang & Zhang 2015; Wang et al. 2011), which require high computational efficiency, or linearize the relationship so that linear regression models can still be applied (Wang & Meng 2012).

Indeed, nonlinear regression has many shortcomings, one of which is that the shape of the regression curve is related to the distribution of the data. Qu et al. (Qu, Wang & Zhang 2015) proposed a theorem stating that the calibration of parameters can be sensitive to collection bias if there exists a nonlinear relation between independent and dependent observations, and put forward a weighted approach to mitigate the impact brought about by the sample selection bias. Other shortcomings include non-convergence or slow convergence, redundant variables and local minima (Motulsky & Ransnas 1987). The nonlinear regression may terminate without convergence when the dataset is either too large or too small, or when the dataset spans with an insufficient range (Motulsky & Ransnas 1987). Furthermore, the choices of

the upper and the lower bound, and the starting value of each parameter also impact the convergence. More specifically, a bad choice of starting value may result in a local minimum, and the tight bound can lead to a sub-optimum with the calibrated parameters lying either on the upper bound or the lower bound. Unfortunately, researchers have to frequently deal with aforementioned situations in transport research where the size and the variance of the dataset is difficult to control, and parameters that are not intuitive (e.g. sensitivity constant) cannot be subjectively regulated. Instead of applying nonlinear regression models, many researchers, for simplicity reasons, linearize the relation by applying a data transformation, and it is found that the transformation of dependent variables has implications for the nature of the residual (Wang & Meng 2012; Motulsky & Ransnas 1987; Nielsen 2007]; however, Motulsky and Ransnas (1987) point out that applying a data transformation may distort the errors.

In this research, the LSM and other extensions of the LSM are adopted as linear/nonlinear regression methods to calibrate linear/nonlinear regression functions. Here, we mainly focus on the calibration of nonlinear regression functions, and the solutions are classified into two groups: applying nonlinear regression methods, such as the nonlinear (weighted) LSM; and using linear regression methods for a linearized nonlinear regression function. The second solution only requires a (weighted) LSM, but it does involve a different objective function, which could be incorrect in some circumstances. Hence, we make a comparison between the linearized LSM with data transformation and the nonlinear LSM using two illustrative examples and analyse the mechanisms of the two different methods in detail.

The remainder of this paper is organized as follows: Section 2 presents the difference between the nonlinear LSM and the LSM for a linearized nonlinear regression function. Section 3 illustrates an example related to the calibration of the fundamental diagram. Both linear regression and nonlinear regression are described in detail. Section 4 presents an example of bunker consumption and sailing speed. Section 5 presents the theoretical investigation and section 6 concludes.

Table A-1 Two-parameter single-regime speed-density models.

Model	Function	Parameter
Greenberg	$v = v_o \ln\left(\frac{k_j}{k}\right)$	v_o , k_j
Underwood	$v = v_f \exp\left(-\frac{k}{k_o}\right)$	v_f, k_o
Northwestern	$v = v_f \exp\left[-\frac{1}{2}\left(\frac{k}{k_o}\right)^2\right]$	v_f, k_o

Notation: v - speed, k - density, v_o - speed at capacity, k_o - density at capacity, v_f - free flow speed, k_j - jam density

2. LINEAR AND NONLINEAR REGRESSION MODEL

2.1 Nonlinear Regression Models

Consider a set of m observations, (x_1, y_1), (x_2, y_2),…, (x_m, y_m), and a nonlinear/linear regression function $\tilde{y_i} = F(x_i)$. Then, the objective of the nonlinear/linear LSM is to minimize the sum of the squared errors, namely,

$$\min S = \min \left(\sum_{i=1}^{m} (y_i - \tilde{y_i})^2\right) \quad \text{(A. 1)}$$

If we consider $\boldsymbol{\beta}$ to be a p -dimensional vector representing the matrix of parameters, $\boldsymbol{Y}$ an $m \times 1$ matrix of dependent observations, $\boldsymbol{X}$ an $m \times p$ matrix of independent observations, and $\boldsymbol{e}$ an $m \times 1$ matrix of residuals, the linear relation can be formatted as

$$\boldsymbol{Y} = \boldsymbol{X\beta} + \boldsymbol{e} \quad \text{(A. 2)}$$

The LSM can easily calibrate the value of β by setting the derivative of the objective function S equal to zero, and $\boldsymbol{\beta} = \arg\min S$ can be directly formulated as a cross product of a matrix, which will be illustrated in detail in the next section. The nonlinear regression model, on the other hand, cannot be written as Eq. (A.2) but must be written as

$$\boldsymbol{Y} = F(\boldsymbol{X}, \boldsymbol{\beta}) + \boldsymbol{e} \quad \text{(A. 3)}$$

In this case, the calibration of $\boldsymbol{\beta}$ requires a high-computational iterative solution; however, linearizing the regression and transforming the observations accordingly can approximate the nonlinear regression model as a linear regression model.

2.2 Linear Regression Model with Linearized Function

After the linearization of the function and data transformation, the nonlinear regression function is transformed into a linear relation between a function of independent variables and a function of dependent variables. Define $g(x_i)$, $i =$

$1, 2, \dots, m$, as the transformation of the independent variables and $f(y_i)$, $i = 1, 2, \dots, m$, as the transformation of the dependent variables. Hence, the observations can be transformed into $g(\boldsymbol{X})$ and $f(\boldsymbol{Y})$. The linearized nonlinear relation can be formatted as

$$f(\boldsymbol{Y}) = F'(g(\boldsymbol{X}), \boldsymbol{\beta'}) + \boldsymbol{e'} = g(\boldsymbol{X})\boldsymbol{\beta'} + \boldsymbol{e'} \quad \text{(A. 4)}$$

where $\boldsymbol{\beta'}$ and $\boldsymbol{e'}$ denote the matrices of parameters and residuals after the data transformation, respectively, and $y = F'(x)$ denotes the linearized function.

As such, the nonlinear regression is transformed into a linear regression. Accordingly, the objective of the LSM is transformed from minimizing the sum of the squared errors between y_i and $\widetilde{y_i}$ to minimizing the sum of the squared errors between $f(y_i)$ and $F'(g(x_i), \boldsymbol{\beta'})$. Substituting $f(y_i)$ and $F'(g(x_i), \boldsymbol{\beta'})$ into the objective function gives

$$\min S' = \min \left(\sum_{i=1}^{m} \left(f(y_i) - F'(g(x_i), \boldsymbol{\beta'})\right)^2\right) \quad \text{(A. 5)}$$

2.3 Discussion

Because a different objective function is being used, there is a high possibility that the calibrated parameters will deviate from the global optimum. Hence, the main goal of this paper is to discuss when the application of a data transformation is feasible and, if it is not feasible, how the regression is impacted.

3. ILLUSTRATIVE EXAMPLE 1: TRAFFIC FLOW FUNDAMENTAL DIAGRAM

The well-known fundamental diagram is the foundation of traffic flow theory, and demonstrates either the speed-density or flow-density relationship (Qu, Zhang Wang 2017). The speed-density relationship often attracts more interest because it presents an intuitive connection with the daily driving experience (Wang & Meng 2012). The calibration of the fundamental diagram has frequently been discussed ever since Greenshields' model (Greenshields, Channing & Miller 1935) was proposed. Many researchers have dedicated themselves to improving the empirical accuracy of the single-regime model, such as Greenberg (1959), Newell (1961), Underwood (2008), Drake et al.(1966), Wang et al. (2012) and Qu et al. (2015). In this study, we select three two-parameter nonlinear single-regime models (demonstrated in Table A-

1) to examine the performance of the nonlinear LSM and the LSM for a linearized regression function.

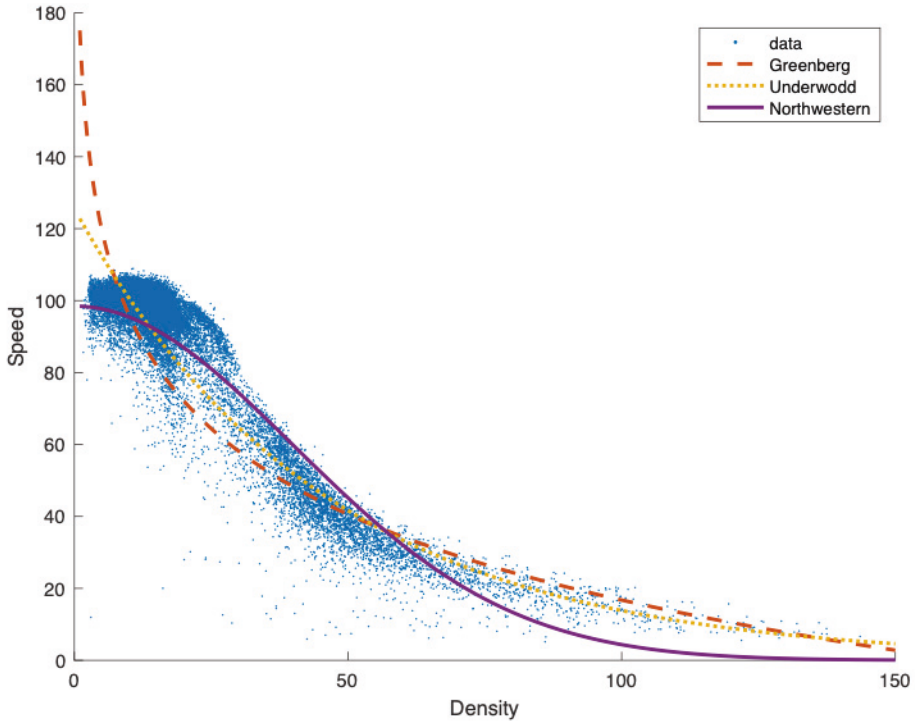

Figure A-1 Single-regime speed-density models and GA400 dataset.

3.1 Data Description

In this paper, we use the Georgia State Route 400 (referred to as the GA400 dataset hereafter) to calibrate the single-regime models. The GA400 dataset contains 47,581 observations that are collected from 76 stations. The one-year continuous observations are aggregated from 20 s to 5 min when they are applied to calibrate the speed-density relation (Sun et al. 2003). In the following context, the observations of the density (observations projected to the abscissa) are denoted as the x-observations and the observations of speed (observations projected to the ordinate) are denoted as the y-observations. Applying a weighted nonlinear LSM (Motulsky & Ransnas 1987), the single-regime models can be calibrated as depicted in Figure A-1.

3.2 Calibration Using Nonlinear Regression Method

Normally, when dealing with linear regression, we would want to minimize the sum of the squared error. Fortunately, that is equivalent to letting the derivative of the

sum of the residuals be equal to zero. Consider a linear relation between densities and velocities $v = F(\beta, k)$, and a set of data points extracted from GA400 dataset (k_1, v_1), (k_2, v_2),…, (k_m, v_m), an m-dimensional vector $\boldsymbol{Y^{m\times 1}} = [v_1, v_2, \dots, v_m]^T$, an $m \times 2$ matrix $\boldsymbol{X^{m\times 2}} = \begin{bmatrix} 1 & k_1 \\ 1 & k_2 \\ \vdots & \vdots \\ 1 & k_m \end{bmatrix}$ and a 2×1 parameter vector $\boldsymbol{\beta^{2\times 1}} = [\beta_1, \beta_2]^T$. Hence, the linear relation between k_i and v_i can be formulated as in Eq. (A.2). Here, $\boldsymbol{e}$ denotes an $m \times 1$ matrix of residuals. Then, the objective function of the LSM can be written as

$$\boldsymbol{S} = (\boldsymbol{Y} - \boldsymbol{X\beta})^T(\boldsymbol{Y} - \boldsymbol{X\beta}) \tag{A.6}$$

The derivative of the squared error can be simplified to

$$\frac{\partial \boldsymbol{S}}{\partial \boldsymbol{\beta}} = -\boldsymbol{X}^T\boldsymbol{Y} + \boldsymbol{X}^T\boldsymbol{X\beta} \tag{A.7}$$

To minimize the squared error, it is necessary to set the derivative of the squared error with respect to $\boldsymbol{\beta}$ to be equal to zero. By letting Eq. (A.7) equal zero, we can solve for an optimal $\boldsymbol{\beta}$; mathematically,

$$\widehat{\boldsymbol{\beta}} = (\boldsymbol{X}^T\boldsymbol{X})^{-1}\boldsymbol{X}^T\boldsymbol{Y} \tag{A.8}$$

Unlike with the LSM, with the nonlinear LSM one cannot calibrate the parameters directly by letting the derivative of the objective function equal zero. Instead, an iterative solution must be adopted, such as Gauss-Newton method and Levenberg-Marquardt method (Levenberg 1944; Marquardt 1963). Nielsen (2007) introduced a nonlinear LSM which is identical to the Gauss-Newton method. Taking Greenberg model (1959) as an example, we approximate the nonlinear regression model by a Taylor expansion at each $\{k_i, v_i\}_{i=1}^m$ and omit the high-order terms (see Eq. (A.9)),

$$v_i = F(\boldsymbol{\beta^t}, X_i) + \sum_{j=1}^{2} \frac{\partial F(\beta_j^t, X_i)}{\partial \beta_j^t}\left(\beta_j^{t+1} - \beta_j^t\right) + e_i \quad i \in \{1,2 \dots, m\} \tag{A.9}$$

where t denotes the iterative index, $\left\{\beta_j^1\right\}_{j=1}^2$ are the initial guesses of the parameters, and X_i denotes the ith row of matrix $\boldsymbol{X^{m\times 2}}$. Consider an $m \times 2$ Jacobian matrix,

Table A-2 Two-parameter single-regime speed-density models with linearization.

Model	Function	Transformation
Greenberg	$v = v_o \ln(k_j) - v_o g(k)$	$g(k) = \ln(k)$
Underwood	$f(v) = \ln(v_f) - \frac{k}{k_o}$	$f(v) = \ln(v)$
Northwestern	$f(v) = \ln(v_f) - \frac{1}{2k_o^2} g(k)$	$f(v) = \ln(v);\ g(k) = k^2$

$$\boldsymbol{J} = \begin{bmatrix} \frac{\partial F(\beta_1^t, k_1)}{\partial \beta_1^t} & \frac{\partial F(\beta_2^t, k_1)}{\partial \beta_2^t} \\ \vdots & \vdots \\ \frac{\partial F(\beta_1^t, k_m)}{\partial \beta_1^t} & \frac{\partial F(\beta_2^t, k_m)}{\partial \beta_2^t} \end{bmatrix} \tag{A.10}$$

Then, we can simplify Eq. (A.9) as

$$\boldsymbol{\varepsilon} = \boldsymbol{J\delta} + \boldsymbol{e} \tag{A.11}$$

where $\varepsilon = v_i - F(\beta_j^t, k_i)$, and $\boldsymbol{\delta}$ is a two-dimensional vector denoting the change of parameters, so mathematically, $\delta = [(\beta_1^{t+1} - \beta_1^t), (\beta_2^{t+1} - \beta_2^t)]^T$. Following the same process as illustrated in Eqs. (A.6)-(A.8) gives

$$\widehat{\boldsymbol{\delta}} = (\boldsymbol{J}^T\boldsymbol{J})^{-1}\boldsymbol{J}^T\boldsymbol{\varepsilon} \tag{A.12}$$

After calculating the optimal change of parameters, we can update the matrix of parameters and start a new iterative step, terminating the iteration when $\widehat{\boldsymbol{\delta}}$ is smaller than a predetermined threshold.

3.3 Calibration Using Simple Linear Regression for Linearized Function

An alternative method consists of linearizing a nonlinear regression function and executing a data transformation of the observations to establish a relation between functions of the independent variables and the corresponding dependent variable. In that way, the aforementioned single-regime models can be linearized, the results of which are shown in Table A-2. Let us take the Greenberg model as an example to demonstrate the process of calibration. The first step is to rearrange the Greenberg model into an $\boldsymbol{f}(\boldsymbol{V}) = \beta_2 \boldsymbol{g}(\boldsymbol{K}) + \beta_1$ format,

$$v = v_o \ln(k_j) - v_o \ln(k) \tag{A.13}$$

where $\boldsymbol{f}(\boldsymbol{V}) = [v_1 \quad v_2 \quad \dots \quad v_m]^T$, $\boldsymbol{g}(\boldsymbol{K}) = [\ln(k_1) \quad \ln(k_2) \quad \dots \quad \ln(k_m)]^T$, $\beta_1 = v_o \ln(k_j)$, and $\beta_2 = v_o$. Let $\boldsymbol{\beta} = \begin{bmatrix} \mathrm{v_o} \ln(\mathrm{k_j}) & \mathrm{v_o} \end{bmatrix}^{\mathrm{T}}$, $\boldsymbol{Y} = \boldsymbol{f}(\boldsymbol{V})$, $\boldsymbol{M}$ be an m-

dimensional vector of ones, $[1 \quad ... \quad 1]^T$, and $\boldsymbol{X} = [M \quad g(K)]$. Solving the linear LSM as we did in Eqs. (A.6)-(A.8) gives Eq. (A.14).

$$[\beta_1 \quad \beta_2]^T = ([\boldsymbol{M} \quad \boldsymbol{g}(\boldsymbol{K})]^T[\boldsymbol{M} \quad \boldsymbol{g}(\boldsymbol{K})])^{-1}[\boldsymbol{M} \quad \boldsymbol{g}(\boldsymbol{K})]^T\boldsymbol{f}(\boldsymbol{V}) \tag{A.14}$$

It should be noted that a new matrix of weights needs to be computed according to $\boldsymbol{g}(\boldsymbol{K})$ when applying the weighted least squares method (WLSM) proposed by Qu et al. (2015).

3.4 Result and Discussion

The root-mean-square error (RMSE) is an efficient way to evaluate the accuracy of predictive models. Therefore, we adopt the RMSE to evaluate the performance of the regression. The RMSE demonstrates the standard deviation between predicted values and field data, and can be formulated as

$$\text{RMSE} = \sqrt{\frac{1}{n}\sum_{i=1}^{n}(v_i - \hat{v}_i)^2} \tag{A.15}$$

In order to give a better demonstration of the regression, the fitting curves and RMSEs are compared simultaneously, and the RMSEs are calculated for each 5 veh/km increment in density. In this section, four calibration methods, the WLSM, WLSM with data transformation (referred to as WLSMT hereafter), OLSM and OLSM with data transformation (referred to as OLSMT hereafter), are illustrated and compared. The curves produced by the four calibration methods are demonstrated in figures, along with their aggregated RMSEs.

By substituting the calibrated β_1 and β_2 (from either the nonlinear LSM or the LSM for the linearized function) into the nonlinear regression function, we can obtain the calibrated Greenberg model as depicted in the sub-figure a of Figure A-2. It is obvious that the linearization and data transformation distort the regression of the WLSM away from the optimum, but do not impact the OLSM, which suggests to us that the weights assigned to the observations make the WLSM vulnerable to the data transformation. With an in-depth investigation into the linearization of the Greenberg model and the corresponding data transformation of the GA400 dataset, it is found that the x-observations are distributed very differently after the logarithm is taken, and the weights are related to the distribution of the x-observations. Therefore, the weights can vary significantly after the transformation.

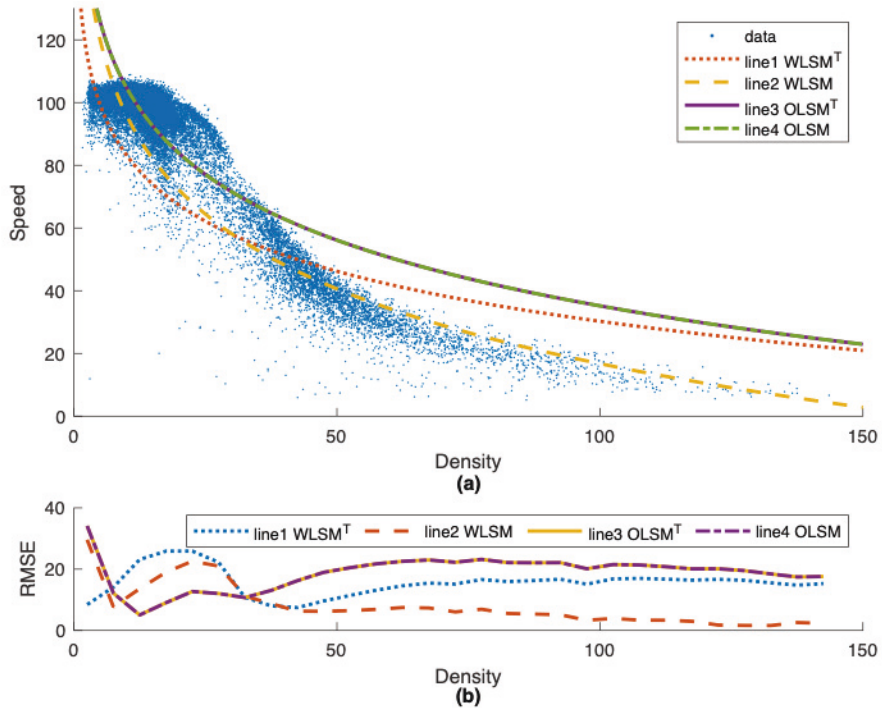

Figure A-2 Performance of Greenberg model with regards to four calibration methods.
a: Result of regressions; b: RMSEs of four methods.

A further investigation into the OLSM shows that the $[\boldsymbol{M} \quad \boldsymbol{g}(\boldsymbol{K})]$ from Eq. (A.14) are the same as the Jacobian Matrix J from Eq. (A.10). If we define $\boldsymbol{V}(\boldsymbol{\beta^t}, \boldsymbol{K})$ as the prediction of speed from the tth iterative solution $\boldsymbol{\beta^t}$ given by the Greenberg model, with parameters $\widehat{\boldsymbol{V}}$ as the velocities, extracted from the GA400 dataset, then Eq. (A.12) can be rewritten as

$$(\boldsymbol{\beta^{t+1}} - \boldsymbol{\beta^t}) = (\boldsymbol{X}^T\boldsymbol{X})^{-1}\boldsymbol{X}^T\left(\widehat{\boldsymbol{V}} - \boldsymbol{V}(\boldsymbol{\beta^t}, \boldsymbol{K})\right) \tag{A.16}$$

Please note that $\boldsymbol{\beta}$ is $[v_0 \ln(k_j) \quad v_0]$ here. If $\boldsymbol{\beta^{t+1}} - \boldsymbol{\beta^t}$ is smaller than a certain threshold, $\boldsymbol{\beta^{t+1}}$ can be regarded as $\widehat{\boldsymbol{\beta}}$, and it is also apparent that $\boldsymbol{\beta^t}$ can be approximated by $\widehat{\boldsymbol{\beta}}$ when $\boldsymbol{V}(\boldsymbol{\beta^t}, \boldsymbol{K})$ approaches $\widehat{\boldsymbol{V}}$. Thus,

$$\boldsymbol{\beta^t} = (\boldsymbol{X}^T\boldsymbol{X})^{-1}\boldsymbol{X}^T\boldsymbol{V}(\boldsymbol{\beta^t}, \boldsymbol{K}) \tag{A.17}$$

Therefore, cancelling out $\boldsymbol{\beta^t}$ and $\boldsymbol{V}(\boldsymbol{\beta^t}, \boldsymbol{K})$ gives

$$\widehat{\boldsymbol{\beta}} = (\boldsymbol{X}^T\boldsymbol{X})^{-1}\boldsymbol{X}^T\widehat{\boldsymbol{V}} \tag{A.18}$$

which is exactly the same matrix of parameters as the one calibrated for the linearized regression function. Hence, the nonlinear LSM and LSM for a linearized function are

essentially the same method when used to calibrate the Greenberg model. More generally, it can be concluded that the LSM for a linearized function will remain mathematically the same mechanism as the nonlinear LSM as long as the regression model only requires a data transformation of independent variables, no matter how those independent variables are transformed. On the other hand, the data transformation and the linearization have a negative impact on the WLSM, especially when there is collection bias. The reason is illustrated in Figure A-3, where the data transformation compels the weight assignment method to put higher weights on originally densely distributed observations. At the same time, the thinly distributed observations receive less weight, preceding to the converging curves depicted by WLSMT and OLSM respectively in Figure A-3. This also corresponds to the converging WLSMT and OLSM curves in Figure A-2. Even though the WLSMT curve diverges from the WLSM curve with an increase in density, WLSMT still outperforms OLSM in terms of RMSE in most circumstances.

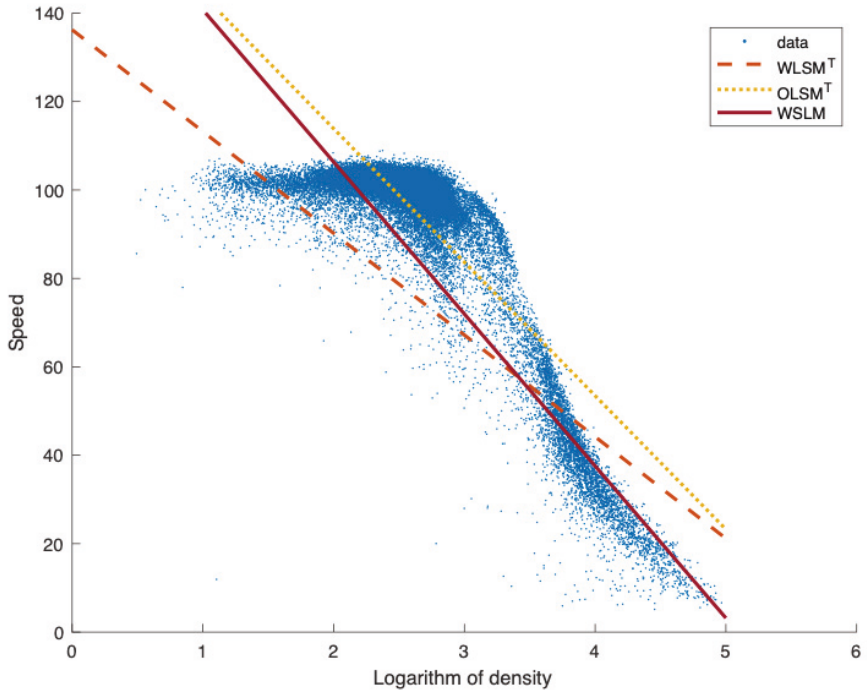

Figure A-3 Greenberg model with data transformation of density.

However, the finding illustrated by Eqs. (A.16)-(A.18) is not applicable to the other two single-regime models. The apparent reason is that either the y-observations (in the Underwood model) or both the x-observations and the y-observations (in the

Northwestern model) are transformed. Nevertheless, the fitting performances of four calibration methods based on the Underwood model are pretty similar to each other as demonstrated in Figure A-4, despite the data transformation. Figure A-5 demonstrates that the data transformation which corresponds to the linearization of the Underwood model delivers the best linear relation of two-dimension observations among the three models. Hence, the linear regressions scarcely vary with the selection of regression method. WLSMT yields similar results to WLSM, as shown in Figure A-4, while WLSM still outperforms WLSMT on the regression of densely distributed observations. Unlike when calibrating the Greenberg model, the weights of the observations are not redistributed because the independent variable is not transformed with the linearization; thus, the impact of the redistributed weights can be eliminated.

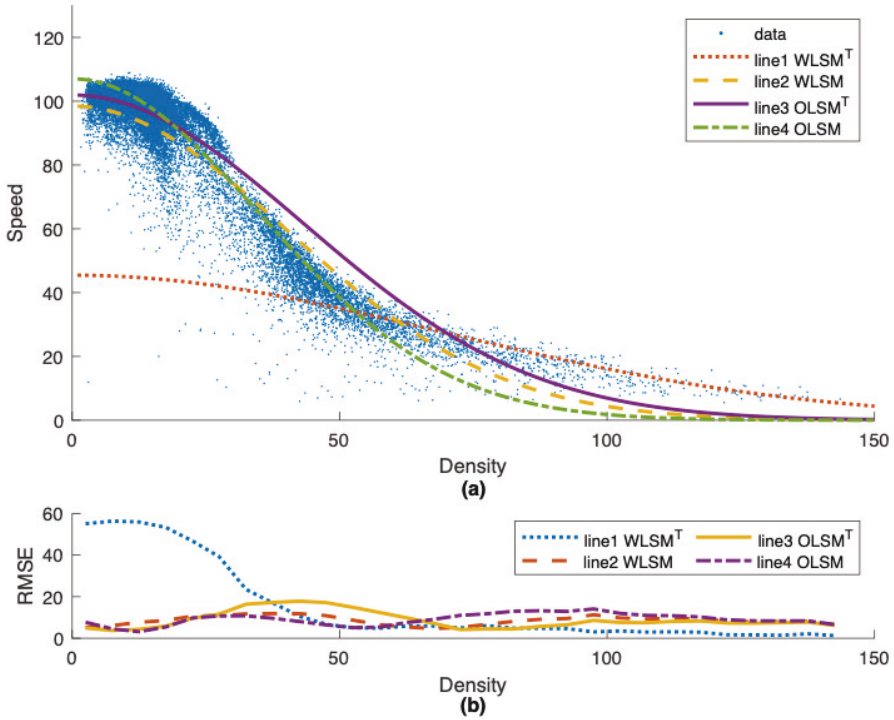

Figure A-4 Performance of Northwestern model with regards to four calibration methods.

a: Result of regressions; b: RMSEs of four methods.

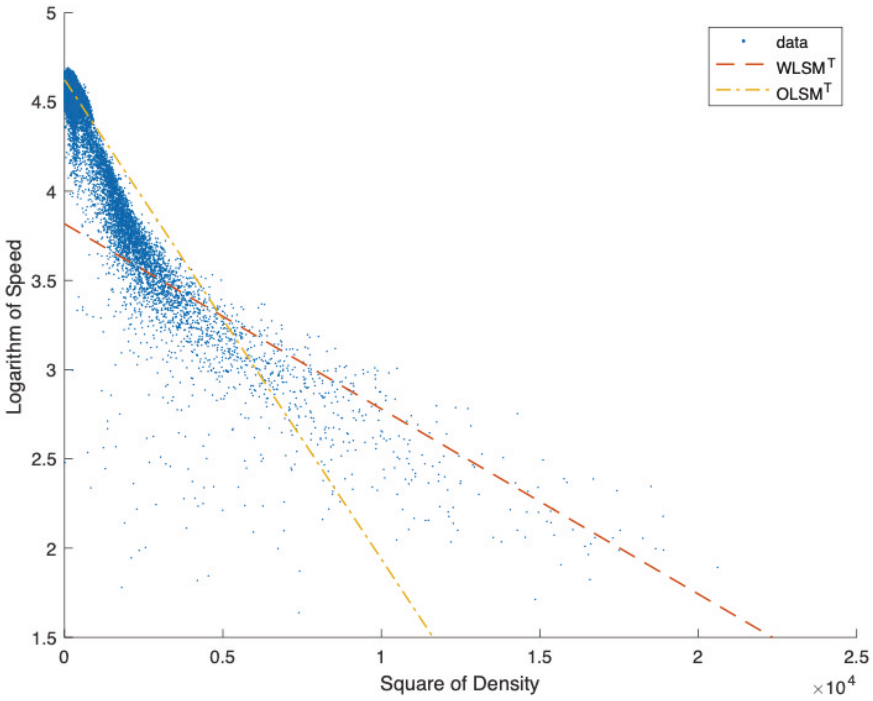

Figure A-5 Northwestern model with data transformation of density.

As for the Northwestern model, the data transformation leads to the worst performance, which can be witnessed in Figure A-6, where there exists a large deviation between the observations and the regression calibrated by WLSMT. One of the reasons (which can be explained based on Figure A-7) is that squaring the x-observations assigns higher weights to the thinly distributed observations, while the densely distributed observations are assigned lower weights; in other words, the importance of previously emphasized observations is overestimated, distorting the regression result away from the densely distributed observations. On the other hand, the performance of the OLSMT is still acceptable, as can be seen in Figure A-6, despite the slight deviation around the density of 50 veh/km.

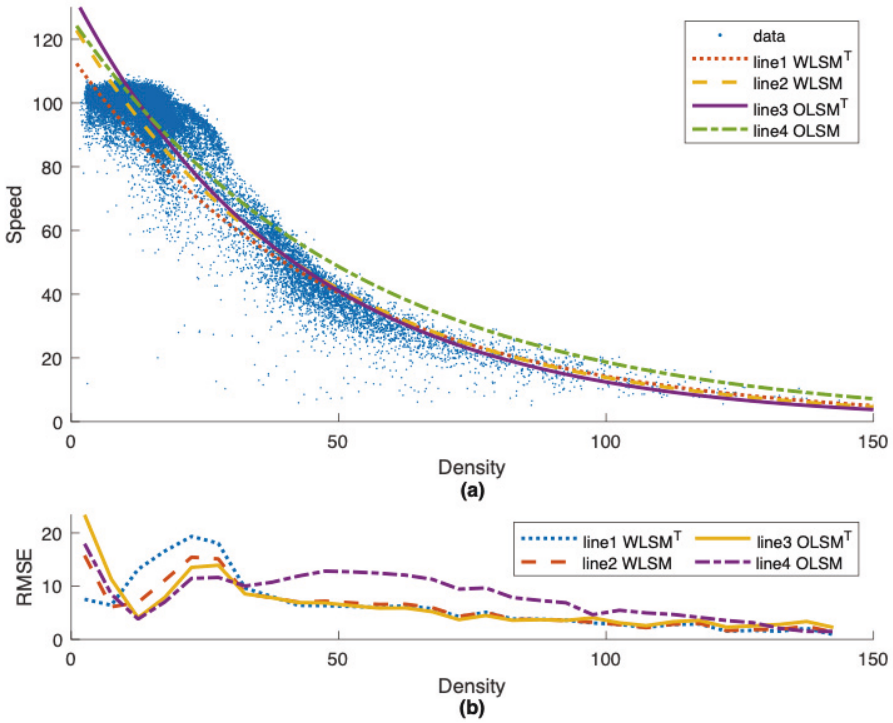

Figure A-6 Performance of Underwood model with regards to four calibration methods.

a: Result of regressions; b: RMSEs of four methods.

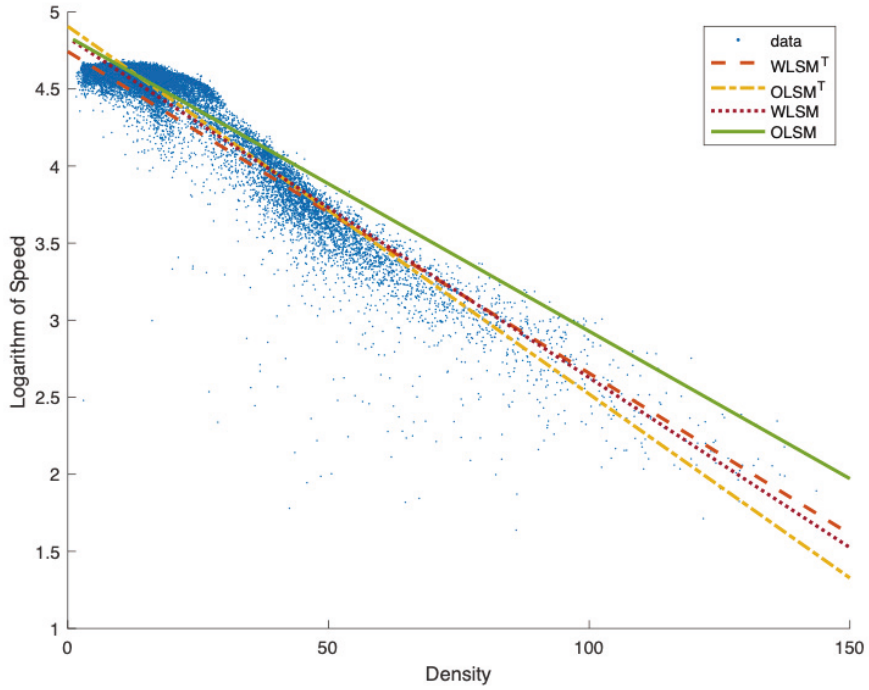

Figure A-7 Underwood model with data transformation of speed.

The deviations could be due to two possible reasons: the mathematical mechanism of each model and (or) the choice of transformed variable. More specifically, the function of each model has its own limitations in the regression of the GA400 dataset; therefore, the result may vary when a different set of observations is adopted for the calibration. Moreover, the transformation of the y-observations gives a different objective function, and the calibration ends up with a sub-optimal matrix of parameters. On the other hand, the transformation of the x-observations gives a different matrix of weights, preceding to a regression that may overfit some observations but underfit others at the same time.

To clarify the cause(s) of the deviations, we rearrange the model to make density a function of speed, as shown in Table A-3, while the functions after the data transformation are demonstrated in Table A-4. The benefits of this rearrangement are two-fold: Firstly, the rearranged Greenberg model takes the same format as the original Underwood model, while the rearranged Underwood model takes the same format as the original Greenberg model. At the same time, the x-observations and y-observations from the GA400 dataset are exchanged so as to make the calibrated parameters physically meaningful. As the objective function changes for the LSM after the transformation, the transformed GA400 dataset is treated as a new dataset. In this way, we are able to compare the performance of similar regression functions when they are calibrated with different datasets. Secondly, although the collection biases of these two datasets are similar, as can be seen in Figure A-8 and Figure A-9, the matrices of weights vary significantly. It is apparent that the observations in the transformed GA400 dataset are more evenly distributed than in the original GA400 dataset. Thus, the impact of the redistributed weights should be mitigated. As can be seen from Figure A-10, the differences between the four LSMs are acceptable and the RMSEs are close to each other, which is also confirmed by Table A-5, where the corresponding calibrated parameters are very close to each other. This finding is consistent with the performance of the original Underwood model, and both methods avoid the impact of a varying weight distribution.

Table A-3 Rearranged single-regime models.

Model	Function	Parameter
Greenberg	$k = k_j \exp\left(-\frac{v}{v_o}\right)$	v_o , k_j
Underwood	$k = k_o \ln\left(\frac{v_f}{v}\right)$	v_f, k_o
Northwestern	$k = k_o\sqrt{2\ln\left(\frac{v_f}{v}\right)}$	v_f, k_o

Notation: $\boldsymbol{v}$ - speed, $\boldsymbol{k}$ - density, $\boldsymbol{v_o}$ - speed at capacity, $\boldsymbol{k_o}$ - density at capacity, $\boldsymbol{v_f}$ - free flow speed, $\boldsymbol{k_j}$ - jam density

Table A-4 Rearranged single-regime models with linearization.

Model	Function	Transformation
Greenberg	$g(k) = \ln(k_j) - \frac{v}{v_o}$	$g(k) = \ln(k)$
Underwood	$k = k_o \ln(v_f) - k_o f(v)$	$f(v) = \ln(v)$
Northwestern	$g(k) = 2k_o^2(\ln(v_f) - f(v))$	$g(k) = k^2; f(v) = \ln(v)$

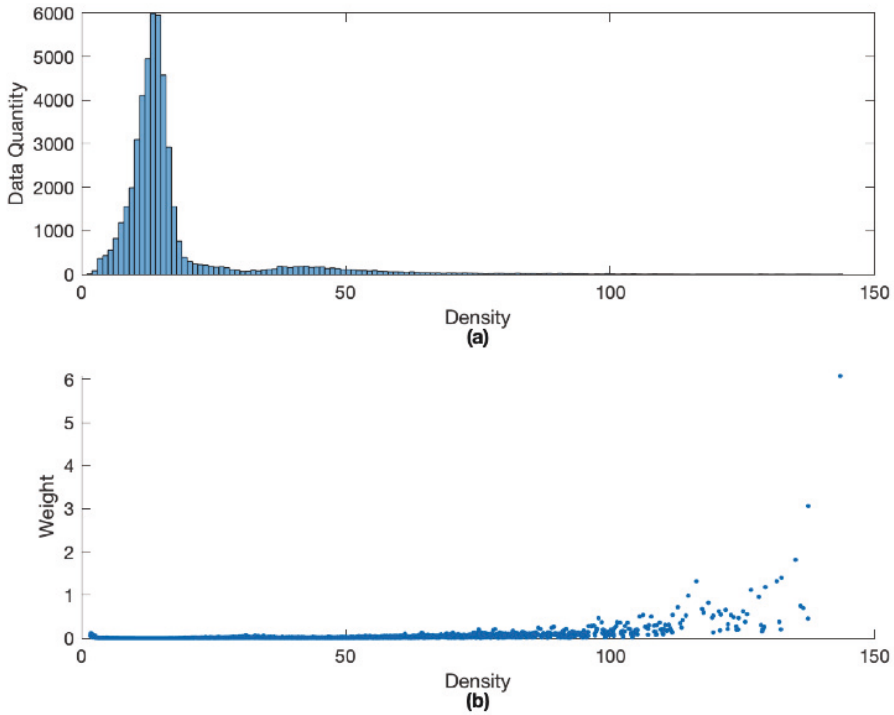

Figure A-8 GA400 dataset distributions of densities and assigned weights.

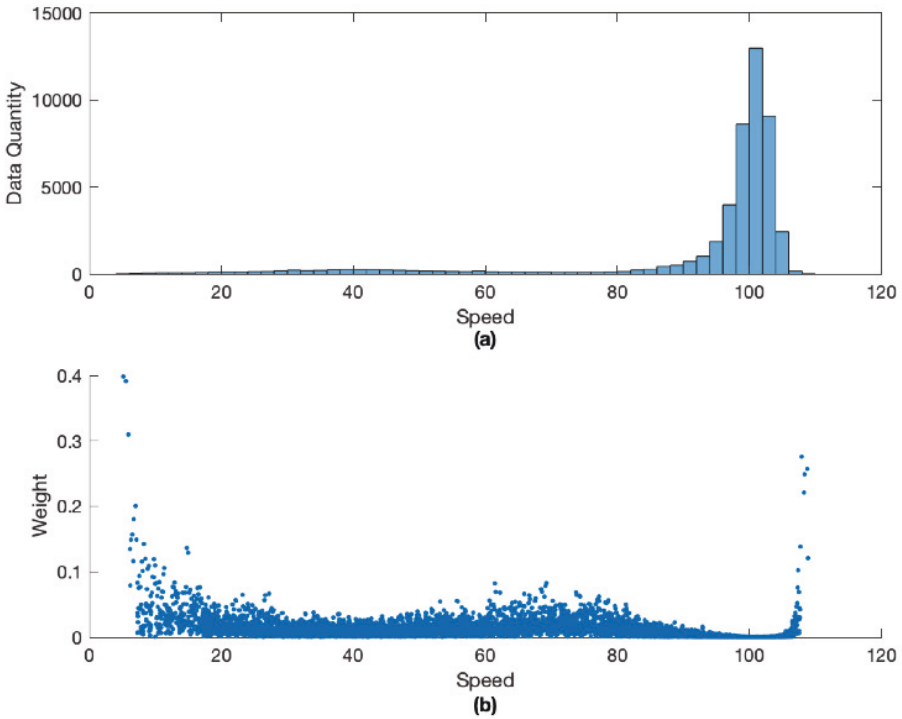

Figure A-9 GA400 dataset distributions of speeds and assigned weights.

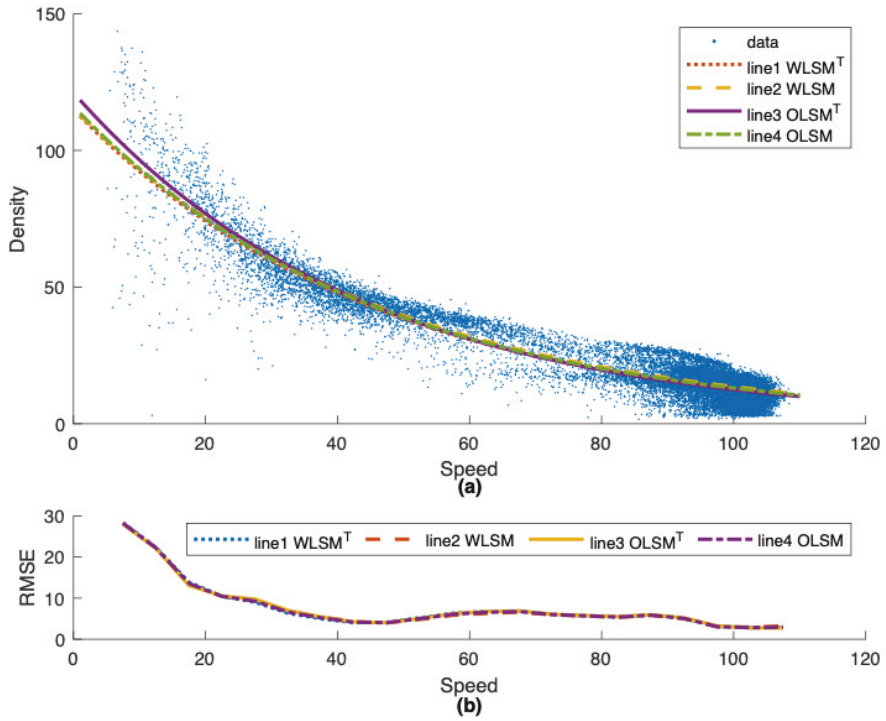

Figure A-10 Performance of rearranged Greenberg model with regards to the four calibration methods.

Table A-5 Calibrated parameters in single-regime models.

	Speed-density[1]		Density-speed[2]	
Greenberg	v_o	k_j	v_o	k_j
WLSM	34.39	162.77	46.68	115.43
WLSM^T	23.01	372.34	45.59	115.01
OLSM	30.21	320.42	45.76	116.13
OLSM^T	30.21	320.42	44.01	121.14
Underwood	v_f	k_o	v_f	k_o
WLSM	125.54	45.34	150.87	35.29
WLSM^T	114.77	47.91	185.68	31.07
OLSM	126.63	52.27	141.15	37.80
OLSM^T	135.11	41.91	141.15	37.80
Northwestern	v_f	k_o	v_f	k_o
WLSM	98.46	40.05	109.00 (LB)	37.04
WLSM^T	45.45	69.43	84.82	45.33
OLSM	107.01	34.96	109.00 (LB)	33.73
OLSM^T	101.94	43.15	104.72	39.01

Notation: [1]: v_o, k_j calibrated by taking density as x-coordinate, speed as y-coordinate; [2]: v_o, k_j calibrated by taking speed as x-coordinate, density as y-coordinate; [3]: LB denotes lower bound applied in LSM

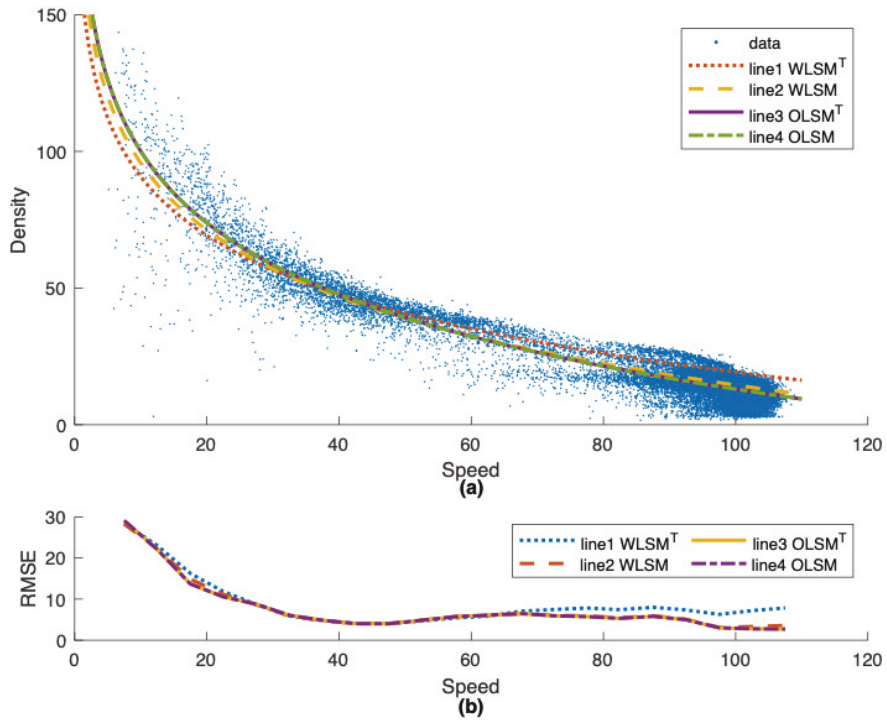

Figure A-11 Performance of rearranged Underwood model with regards to the four calibration methods.

In Figure A-11, the calibrations of OLSM and OLSMT deliver the same result, which is consistent with the finding illustrated by Eqs. (A.16)-(A.18). The fitted curve calibrated by WLSMT still shows a slight deviation when compared to the other methods; however, the deviation is much smaller than that shown in Figure A-2, as the weights are more evenly distributed. Thus, the collection bias will not distort the fitted curve dramatically. To summarize, the mechanism of the function does not impact on the regressions, while the choice of observations to transform does have an impact. Discussion of the rearranged Northwestern model is omitted because the rearranged function requires the speed-related parameter to be greater than the maximum observation of speed, otherwise imaginary values will be given. In such circumstances, the linearizing of the nonlinear regression model will produce a loose bound on the LSM. In Table A-5, all of the parameters of the speed-density and density-speed relations are shown. The sum of the squared errors for the curves calibrated by the four methods are also calculated, for a better comparison, and provided in Table A-6. It is found that the linear regression for the linearized function cannot deliver the optimal choices of parameters, except in the case where only the independent variables are transformed, as illustrated by Eqs. (A.16)-(A.18); however, the accuracy of the WLSM is more vulnerable to the data transformation of the independent variables.

Table A-6 Sum of squared errors of the four calibration methods

	Greenberg	Underwood	Northwestern
$WLSM$	1.0432×10^7	3.5114×10^6	3.0921×10^6
$WLSM^T$	2.2709×10^7	8.1354×10^6	1.3068×10^8
$OLSM$	5.1363×10^6	2.3962×10^6	1.2340×10^6
$OLSM^T$	5.1363×10^6	2.8289×10^6	2.1089×10^6

Table A-7 Statistical analysis of nonlinear and linear regressions.

	Nonlinear regression		Linear regression	
Voyage legs	a	b	a	b
Singapore-Jakarta	0.0137	2.8918	0.0095	3.0218
Singapore-Kaohsiung	0.0104	3.0019	0.0067	3.1494
Hong Kong-Singapore	0.0043	3.3143	0.0058	3.2138
Yantian-Los Angeles	0.0112	3.1177	0.0094	3.1759
Tokyo-Xiamen	0.0372	2.7092	0.0296	2.7881

Table A-8 Squared errors from predicted values.

	S	S of linearized model	S'
Singapore-Jakarta	31.1213	32.8969	0.0158
Singapore-Kaohsiung	121.0043	127.2445	0.0171
Hong Kong-Singapore	66.8693	69.2825	0.0155
Yantian-Los Angeles	82.8022	89.1935	0.0062
Tokyo-Xiamen	60.0832	68.2390	0.0077

4. ILLUSTRATIVE EXAMPLE 2: DAILY BUNKER CONSUMPTION

Bunker consumption, which impacts the profits of liner shipping companies, is introduced as another example. Research has shown that daily bunker consumption has a positive relation with sailing speed, and more specifically a particular power relation (Wang & Meng 2012; Levenberg 1944; Marquardt1963; Ronen 1982, 2011; Corbett, Wang & Winebrake 2009; Meng & Weng 2010, 2011). Wang and Meng (2012) proposed a more general model (referred to as the Bunker-Speed model for short), as shown in Eq. (5.19), as an alternative to the third power function of sailing speed:

$$Q = a \times v^b \tag{A.19}$$

4.1 Data Description

Data are collected on the basis of three types of ship, from a global liner company, with 20 observations recorded on each voyage leg, to demonstrate the relation between daily bunker consumption and average sailing speed (Wang & Meng 2012). The quantity of observations is much smaller than in the GA400 dataset and the observations are well-distributed along the abscissa, which reduces concerns about sample selection bias.

4.2 Calibration Using Nonlinear Regression Method

As described in illustrative example 1, the nonlinear LSM starts with an approximation of the Taylor expansion (see Eq. (A.20)), where i indexes the data, t denotes the number of iterations, and Q and V represent daily bunker consumption (in tons) and sailing velocity (in knots), respectively. Let $\boldsymbol{\varepsilon} = \begin{bmatrix} Q_1 - a^t V_1^{b^t} \\ \vdots \\ Q_{20} - a^t V_{20}^{b^t} \end{bmatrix}$, Jacobian

matrix $\boldsymbol{J} = \begin{bmatrix} V_1^{b^t} & a^t V_1^{b^t} \ln(V_1) \\ \vdots & \vdots \\ V_{20}^{b^t} & a^t V_{20}^{b^t} \ln(V_{20}) \end{bmatrix}$, and iterative step $\boldsymbol{\delta} = [a^{t+1} - a^t \quad b^{t+1} - b^t]^T$.

Then, the optimal parameters can be calculated at a specific iteration when $\boldsymbol{\delta}$ is smaller than a predetermined threshold. In Table A-7, the calibrated parameters are shown in the second and third columns.

4.3 Using Simple Linear Regression for Linearized Function

By taking the logarithm of both sides of Eq. (A.19), the relation can be simplified to a linear relation between $\ln Q$ and $\ln v$, mathematically,

$$\ln Q = \ln a + b \times \ln v \tag{A.21}$$

Thus, the nonlinear regression is transformed into a simple linear regression of transformed observations. Wang and Meng (2012) apply the LSM to calibrate Eq. (A.21). Here, we can directly substitute the relevant parameters and transformed observations into Eq. (A.8), namely,

$$[\ln a \quad b]^T = ([\boldsymbol{M} \quad \ln v]^T [\boldsymbol{M} \quad \ln v])^{-1} [\boldsymbol{M} \quad \ln v]^T \ln Q \tag{A.22}$$

where $\boldsymbol{M}$ denotes a 20×1 matrix of ones. For comparison, the calibrated parameters are shown in the fourth and fifth columns of Table A-7.

4.4 Result and Discussion

Compared to the GA400 dataset, the bunker consumption and sailing speed dataset contains much fewer observations (specifically, 20 compared to 47,581) for each voyage leg and the observations of sailing speed span a much smaller range than the densities do. Despite that, deviations between the nonlinear regression method and the linear regression for the linearized function can still be observed in Figures A-12 to A-16. Table A-7 shows the calibrated parameters of the nonlinear regression and the linear regression of the linearized model. Some of the variances are acceptable, but others, such as parameter a for the Singapore-Kaohsiung voyage leg, are relatively huge compared to the magnitudes of the parameters. Nevertheless, 213 demonstrates that the error between the two regressions does not explode because the sailing speed is limited to a small range.

Table A-7 Statistical analysis of nonlinear and linear regressions.

	Nonlinear regression		Linear regression	
Voyage legs	a	b	a	b
Singapore-Jakarta	0.0137	2.8918	0.0095	3.0218
Singapore-Kaohsiung	0.0104	3.0019	0.0067	3.1494
Hong Kong-Singapore	0.0043	3.3143	0.0058	3.2138
Yantian-Los Angeles	0.0112	3.1177	0.0094	3.1759
Tokyo-Xiamen	0.0372	2.7092	0.0296	2.7881

compares the two methods based on the sum of squared errors. As the objectives of the two regression methods are to minimize the squared errors, we believe that the value of the squared error can assist in comparing the fit performance of the two regression methods. In Table A-8, S represents the sum of the squared deviations between the predictions from the nonlinear regression (based on Eq. (A.19)) and the observations of bunker consumption. On the other hand, S' represents the sum of the squared deviations between the predictions from the linear regression (based on Eq. (A.21)) and the logarithm of bunker consumption. Even though both methods aim at minimizing the sum of squared errors, the optimization processes rely on different objective functions, as illustrated in Eqs. (A.1) and (A.5) respectively; therefore, we cannot conclude from S' being less than S that the linear regression method for the linearized function outperforms the nonlinear regression method. To standardize the deviations, we substitute the parameters from the linear regression into Eq. (A.19) and recalculate the squared deviations between the predictions and observations. The results are given by the column named S from the linearized model from Table A-8. It is found that S from the linearized model is greater than S for every voyage leg, which means that the calibration of the linear regression does not deliver the optimal choices of parameters, even though the regression achieves the optimal solution in the linear regression. Thus, the linear regression for the linearized function can predict with acceptable deviations when the sailing speed is within a given range.

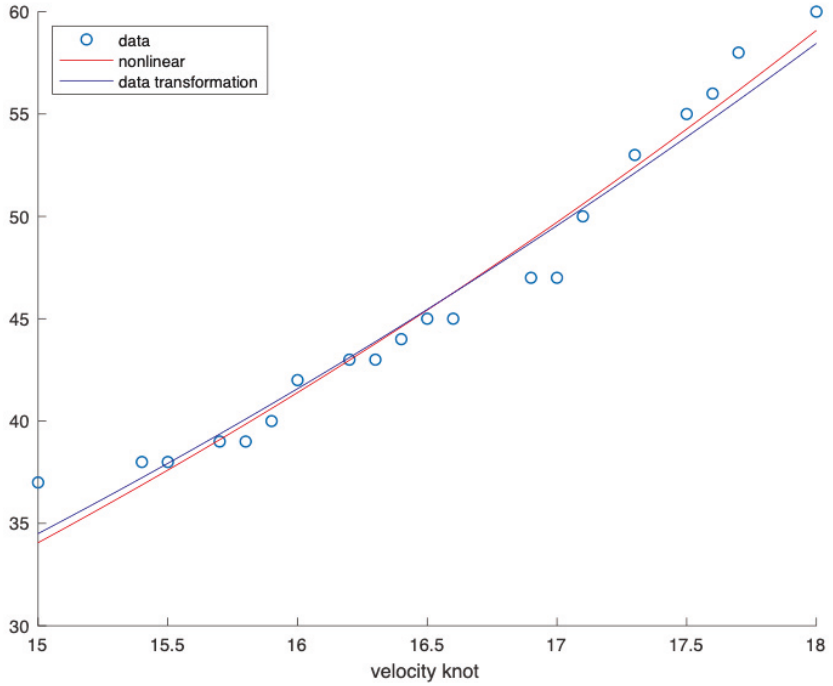

Figure A-12 Relation between bunker consumption and sailing speed of SG-JK given by nonlinear regression and linear regression.

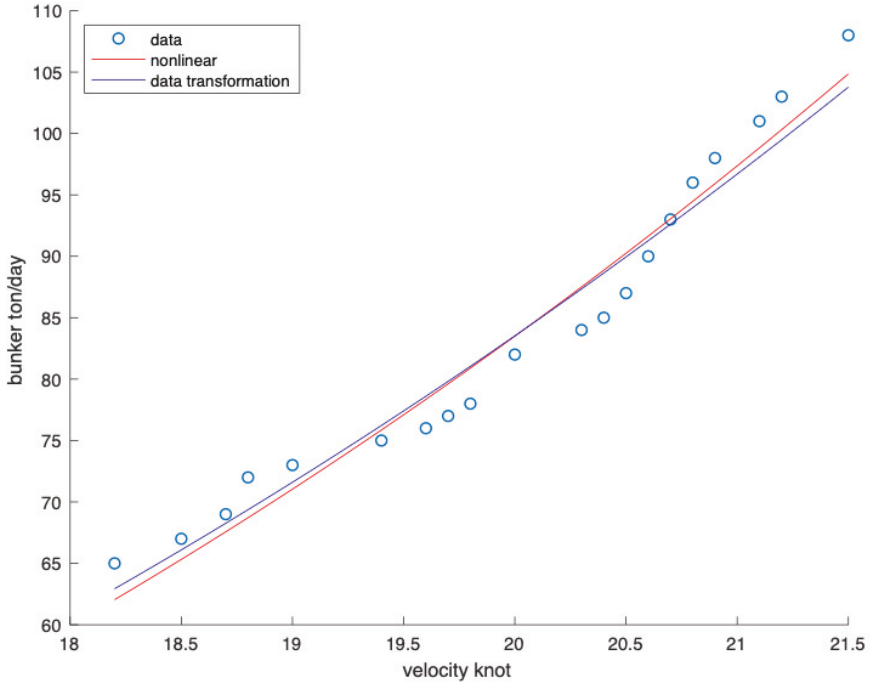

Figure A-13 Relation between bunker consumption and sailing speed of SG-KS given by nonlinear regression and linear regression.

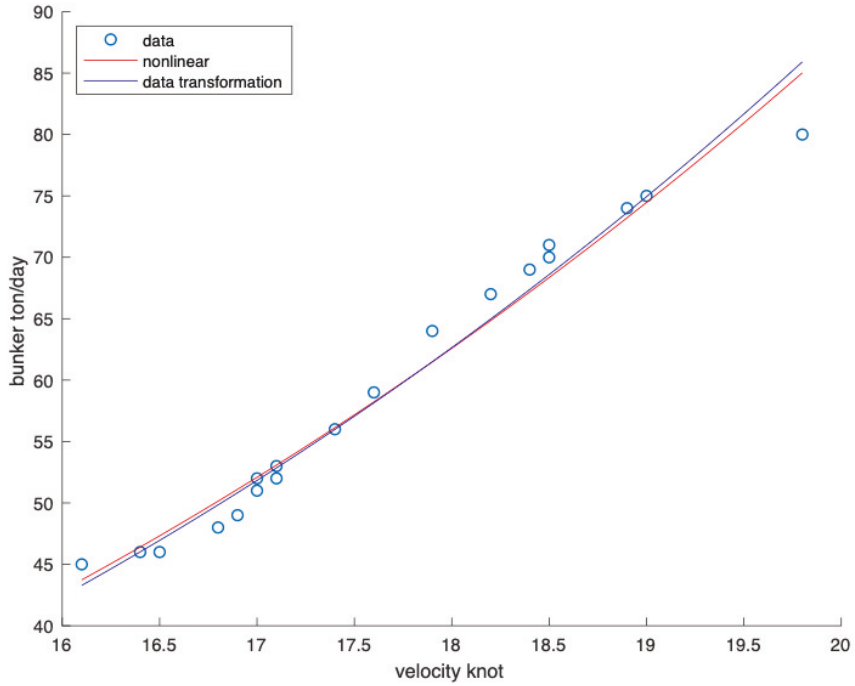

Figure A-14 Relation between bunker consumption and sailing speed of HK-SG given by nonlinear regression and linear regression.

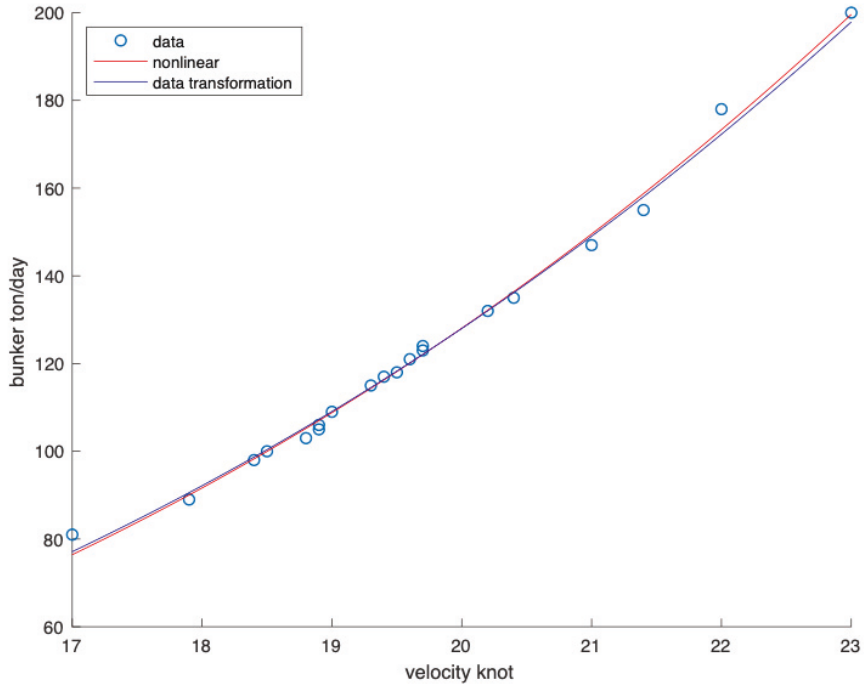

Figure A-15 Relation between bunker consumption and sailing speed of YT-LA given by nonlinear regression and linear regression.

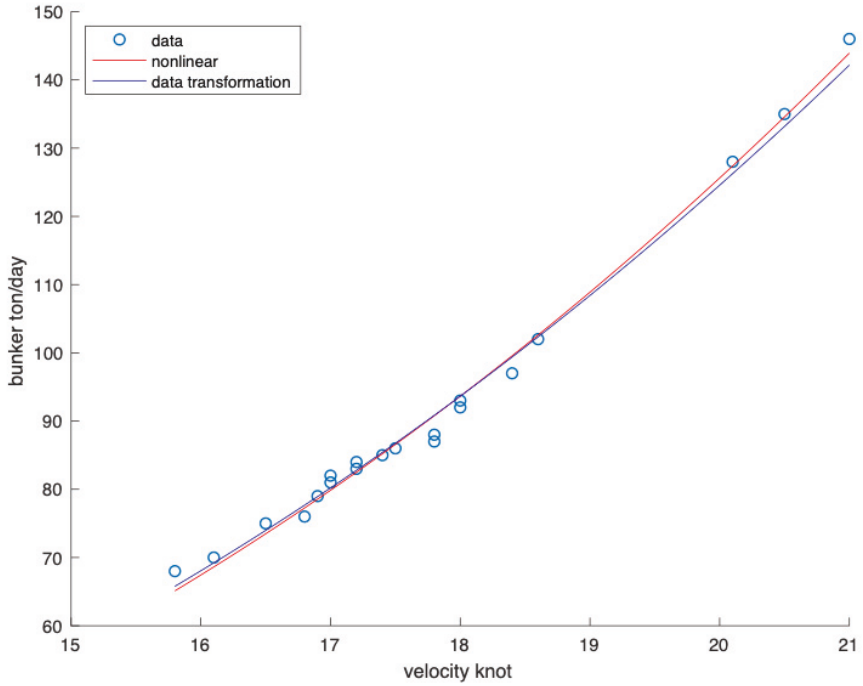

Figure A-16 Relation between bunker consumption and sailing speed of TK-XM given by nonlinear regression and linear regression.

5. SUMMARY

In this research, we creatively analyse the feasibility of linear regression for a linearized model and compare it to the nonlinear LSM. After the linearization, the nonlinear regression models are transformed into linear relations between functions of independent or dependent variables, and data transformations of the observations are also executed, accordingly.

Two illustrative examples are provided to intuitively investigate the reason for the deviations. In the calibration of the fundamental diagram with the GA400 dataset, the WLSM is adopted to overcome the drawbacks of selection bias; however, it is found to be extremely vulnerable to redistributed weights after the data transformation of the independent variables. We also rearrange the regression model to calibrate the density-speed relation, in order to see whether the deviation is caused by the regression models' mathematical mechanism or by the selection of observations to transform. After a comparison of the corresponding regressions, it is found that the difference between the objective functions of the nonlinear regression method and the linear regression method for the linearized function is the main reason for the sub-optimal

matrix of parameters, while the redistributed weights contribute more to the deviations of WLSMT.

The subsequent illustrative example uses the relation between bunker consumption and sailing speed. Due to the limited quantity and span of observations, the OLSM is applied to calibrate the two related parameters. The transformation applied to the bunker-speed model also changes the objective function from Eq. (A.1) to Eq. (A.5). A deviation is witnessed; however, it does not explode due to the narrow span of the x-observations. The calibration of the bunker-speed model shows that linearization can be applied to calibrating a high-order polynomial, but further investigations, using a large dataset to calibrate the bunker-speed model, will need to be carried out.

All in all, a suggestion is given that linearization of nonlinear regression needs to be conditionally applied when dealing with nonlinear regression. More specifically, the WLSMT need to be avoided when the linearization changes the distribution of the x-observations, but OLSMT can produce a same regression as long as the y-observations and the dependent variable are not transformed during the linearization. Once the dependent variable is transformed, the regression will apply a different objective function, which means that the calibration will adopt a sub-optimal solution; however, when the span of x-observation is narrow, linear regression of linearized function can be approximate into the nonlinear regression of its original function, through which the nonconvergence due to the narrow span can be also avoided.

Appendix B

Figures of velocities with regards to the location in a work zone

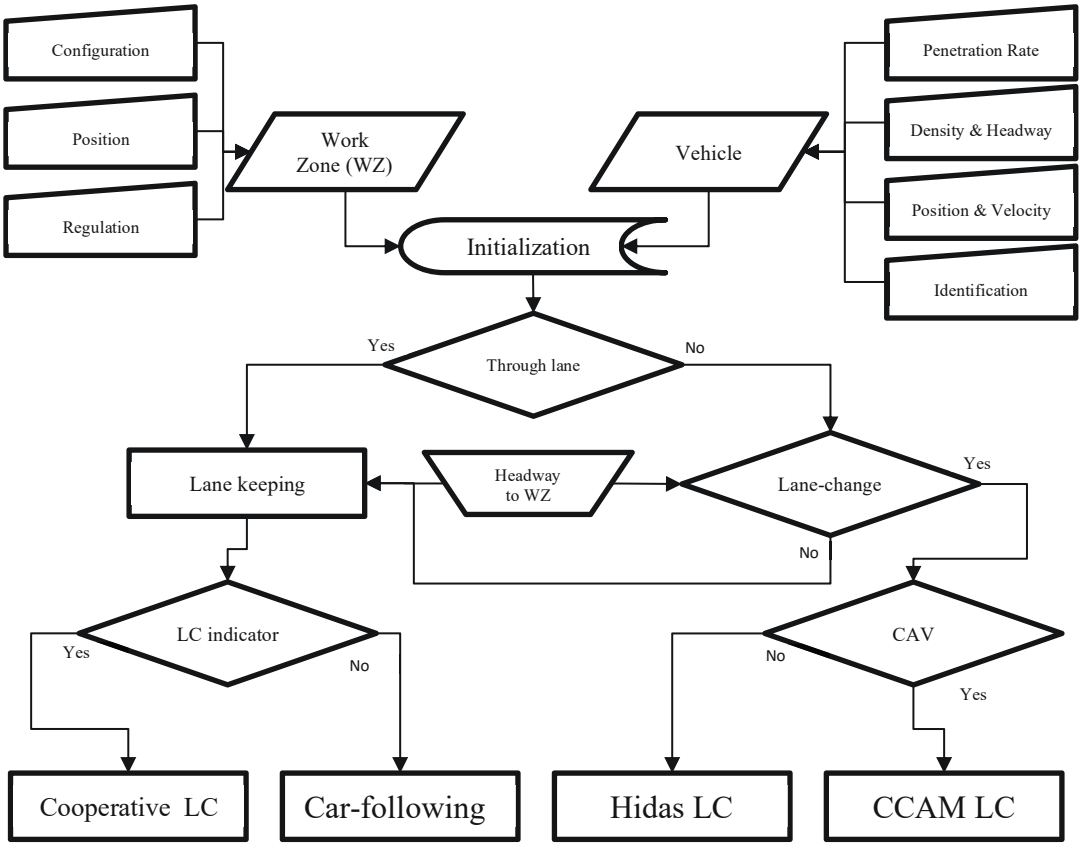

Figure B-1 Model demonstrate of the CCAM.

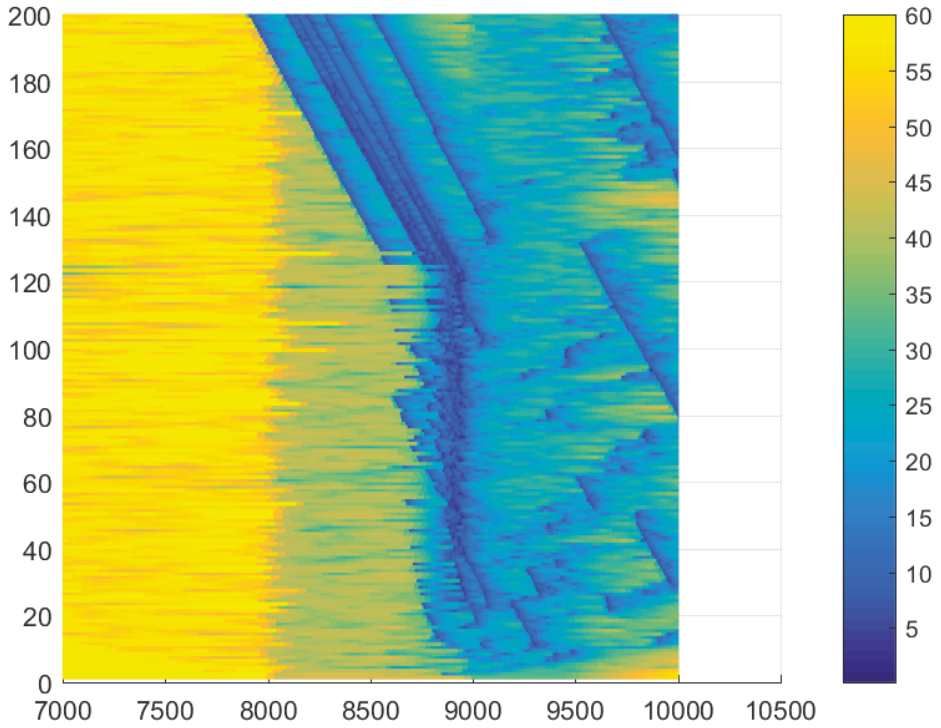

Figure B-2 Velocities over longitudinal positions with 0 % penetration.

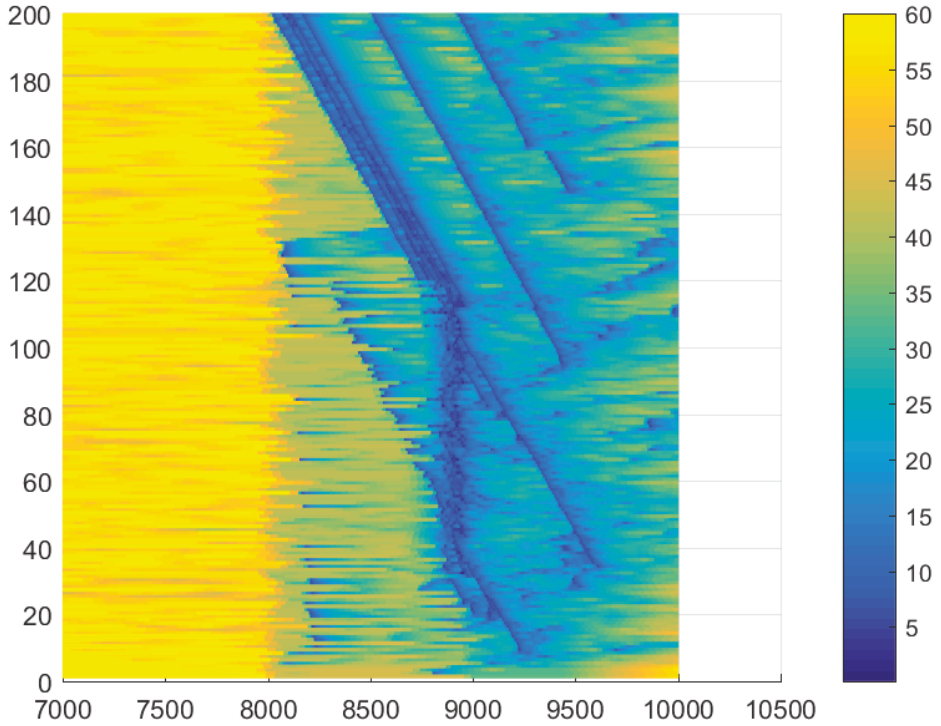

Figure B-3 Velocities over longitudinal positions with 10 % penetration.

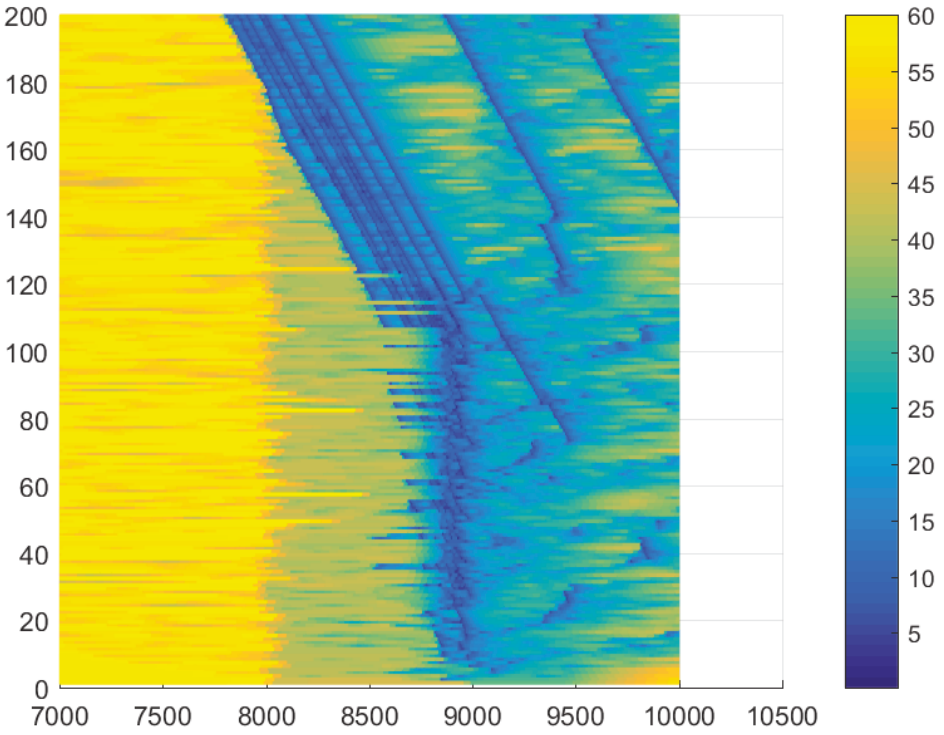

Figure B-4 Velocities over longitudinal positions with 20 % penetration.

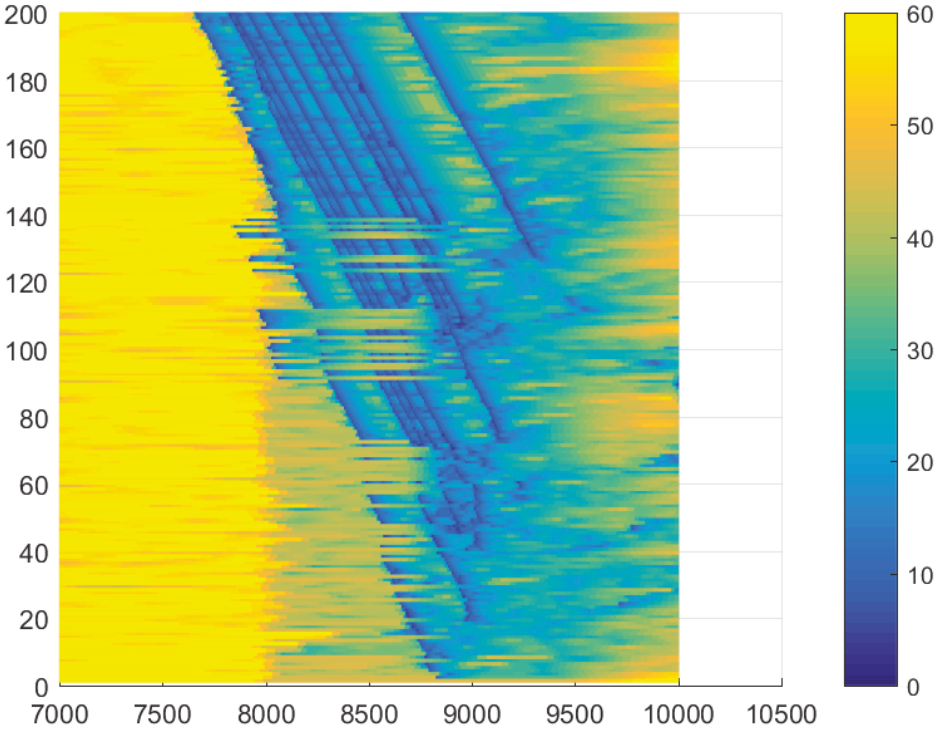

Figure B-5 Velocities over longitudinal positions with 40 % penetration.

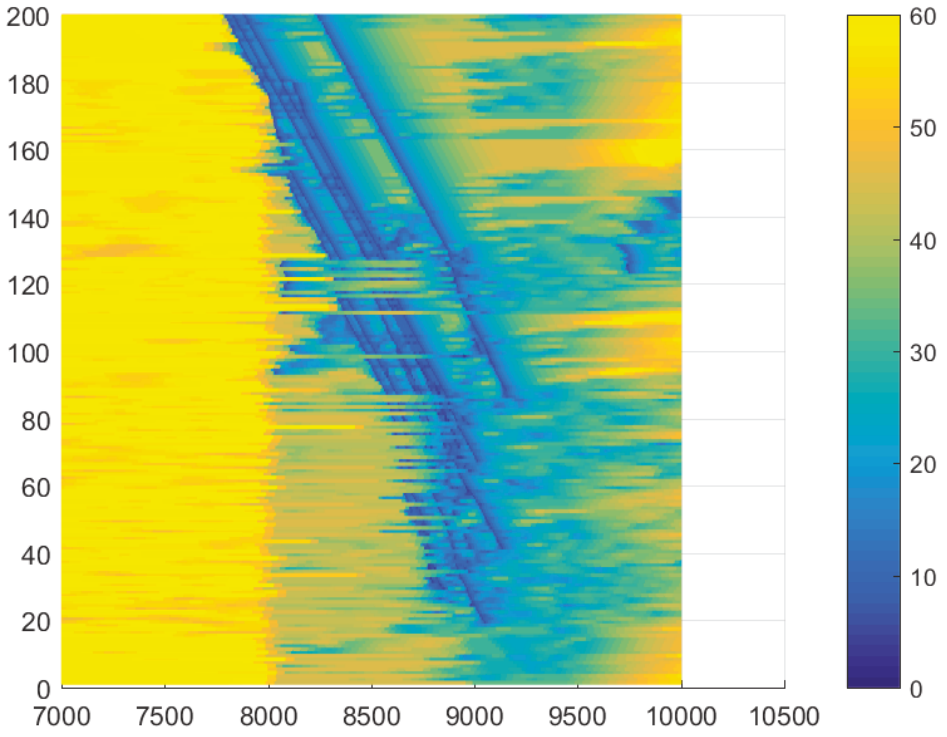

Figure B-6 Velocities over longitudinal positions with 50 % penetration.

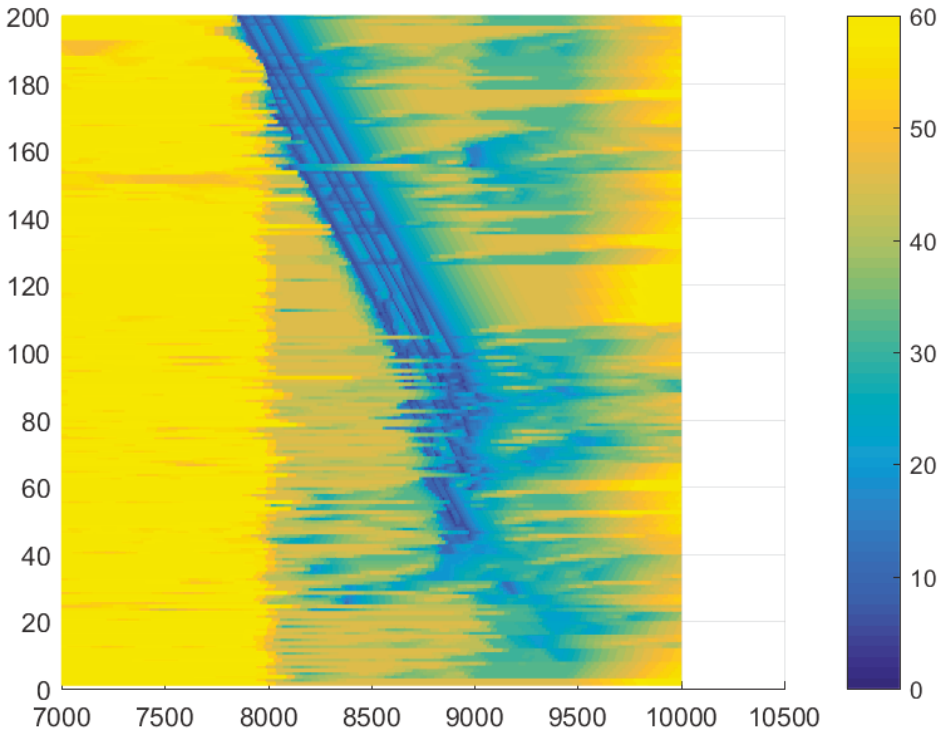

Figure B-7 Velocities over longitudinal positions with 70 % penetration.

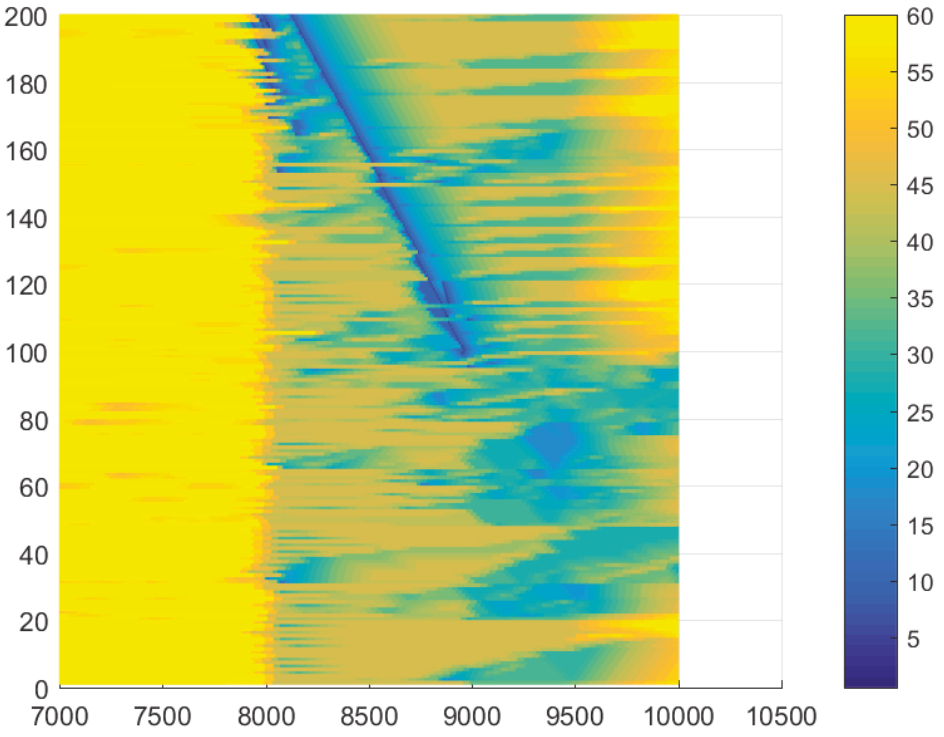

Figure B-8 Velocities over longitudinal positions with 80 % penetration.

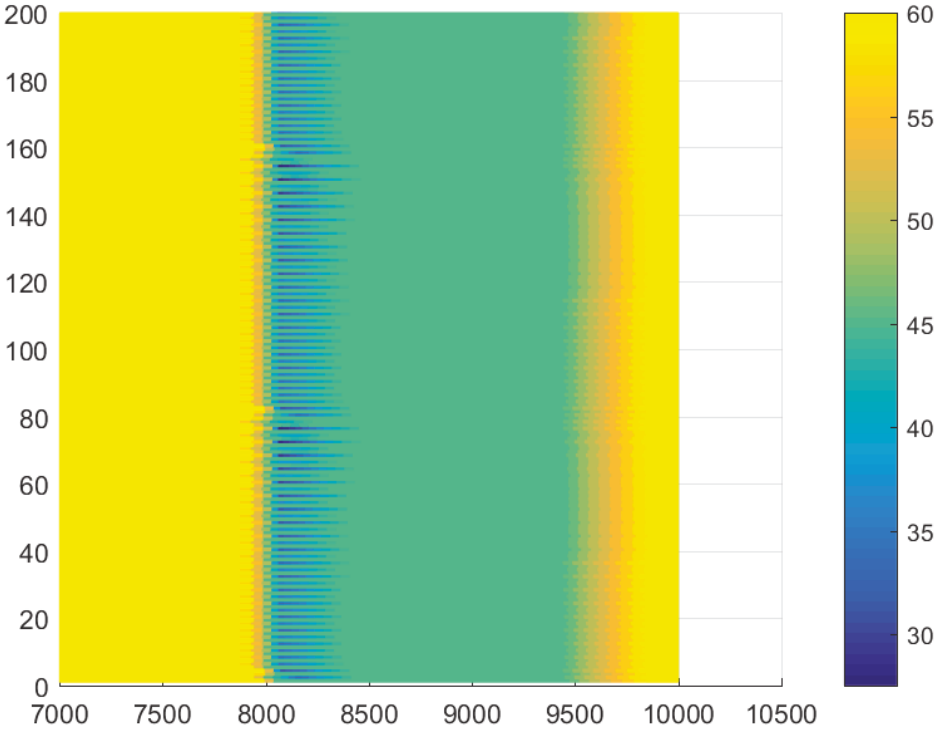

Figure B-9 Velocities over longitudinal positions with 100 % penetration.

Appendix C

Figures of trajectories for work zone traffic regulation

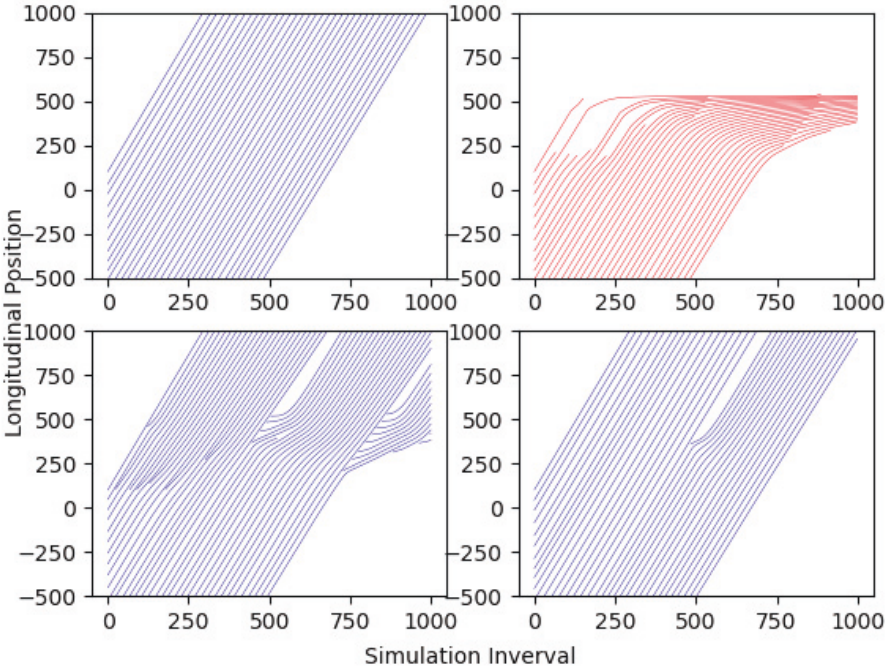

Figure C-1 Longitudinal position with 10 % CAV penetration rate.

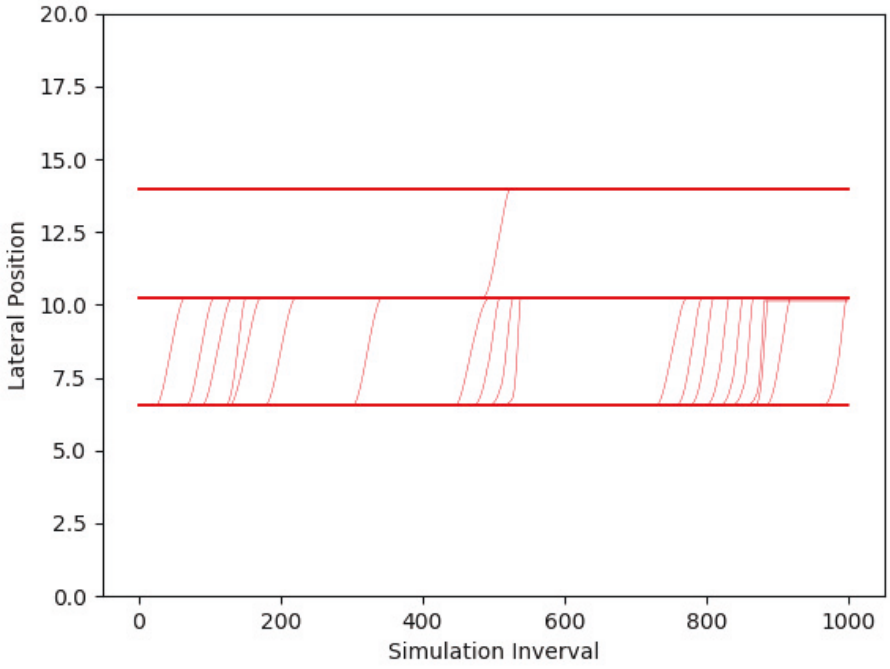

Figure C-2 Lateral position with 10 % CAV penetration rate.

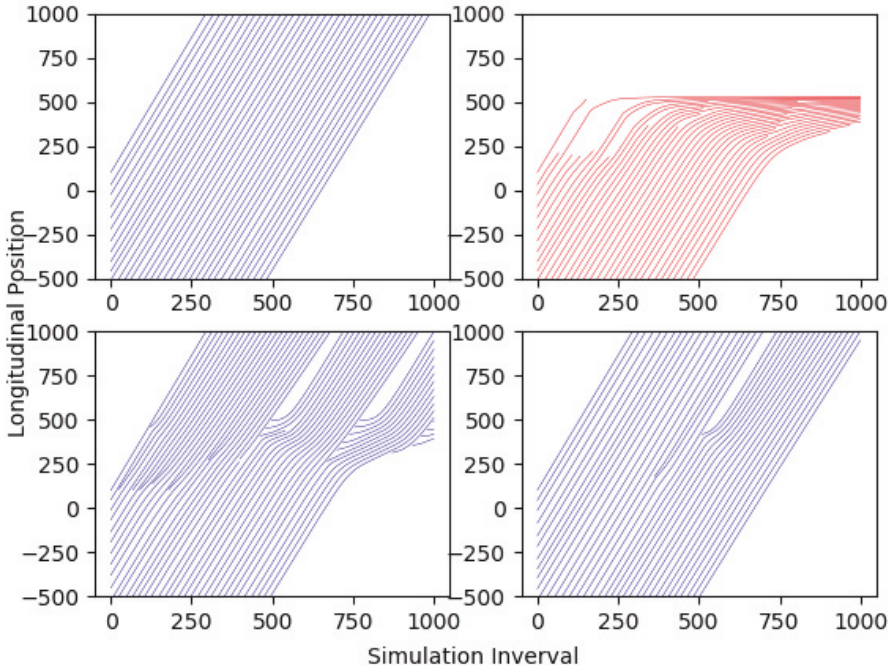

Figure C-3 Longitudinal position with 20 % CAV penetration rate.

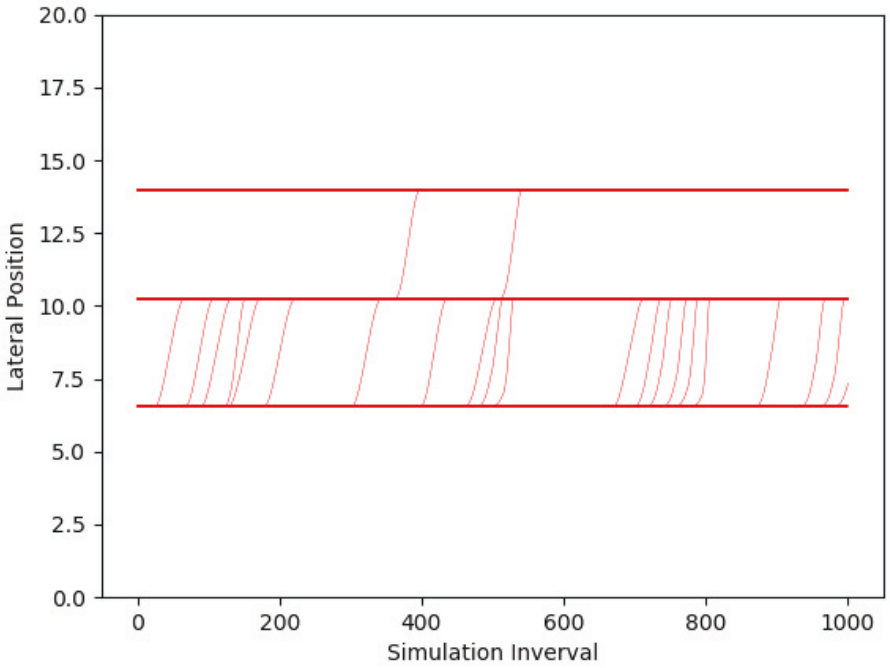

Figure C-4 Lateral position with 20 % CAV penetration rate.

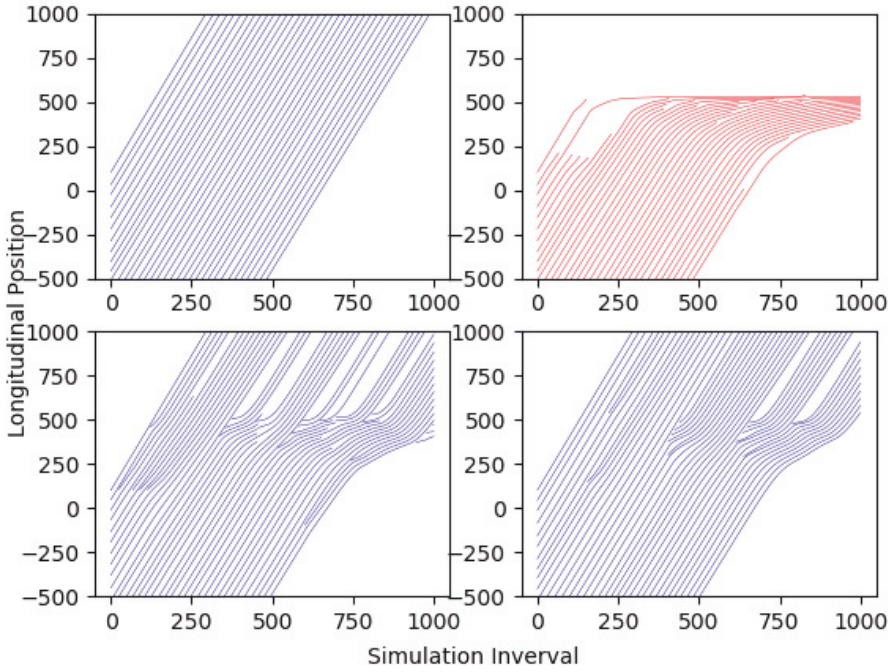

Figure C-5 Longitudinal position with 40 % CAV penetration rate.

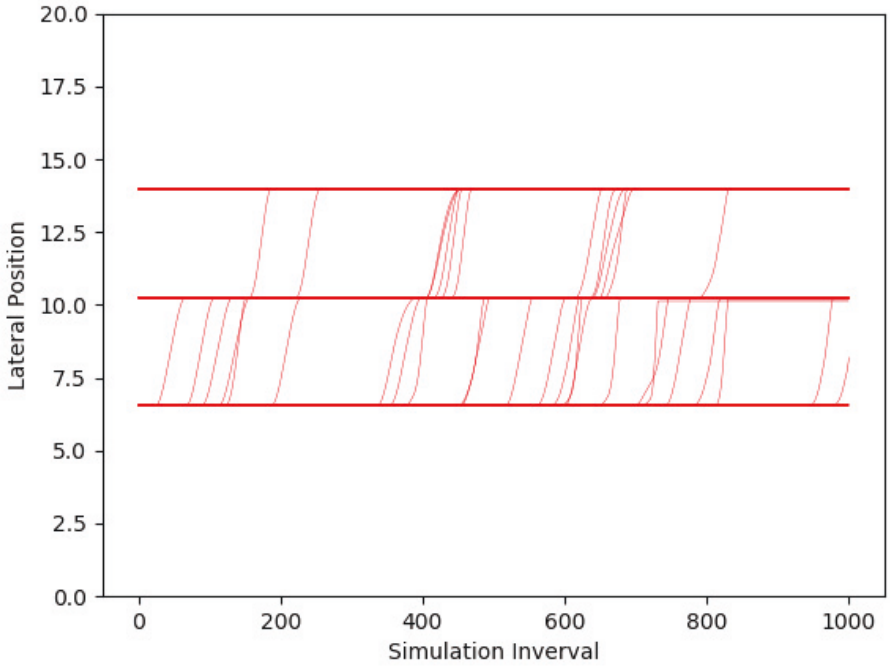

Figure C-6 Lateral position with 40 % CAV penetration rate.

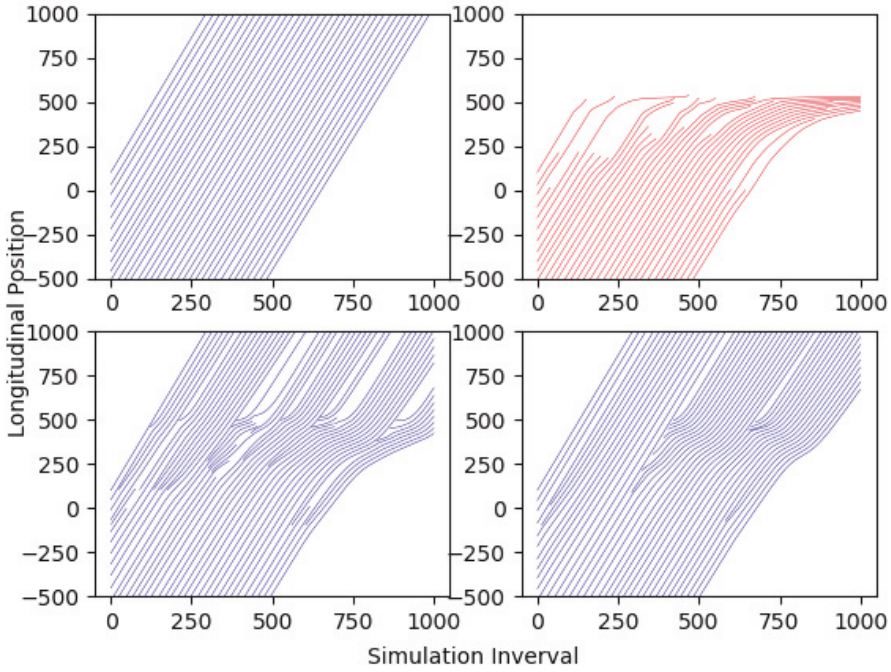

Figure C-7 Longitudinal position with 50 % CAV penetration rate.

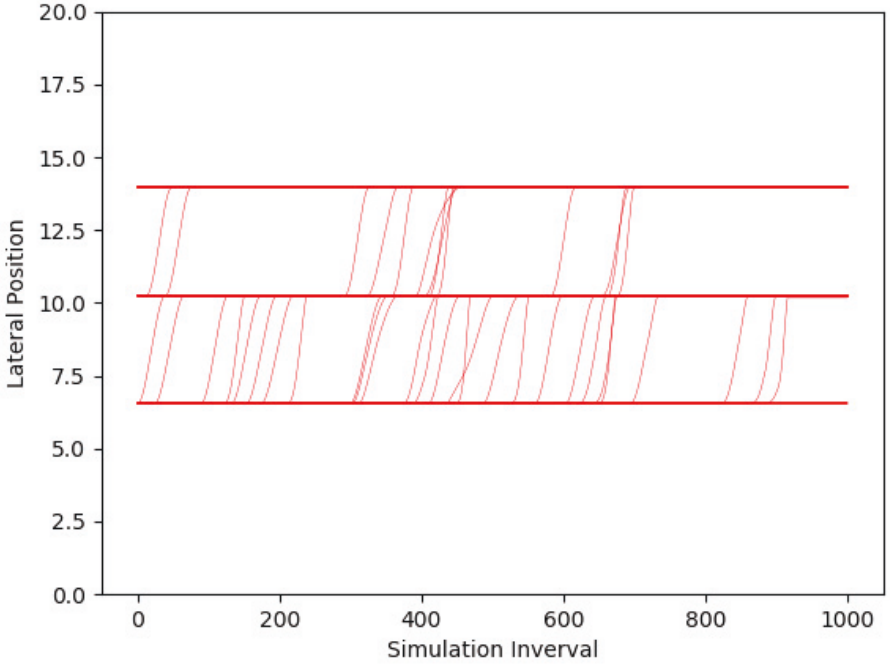

Figure C-8 Lateral position with 50 % CAV penetration rate.

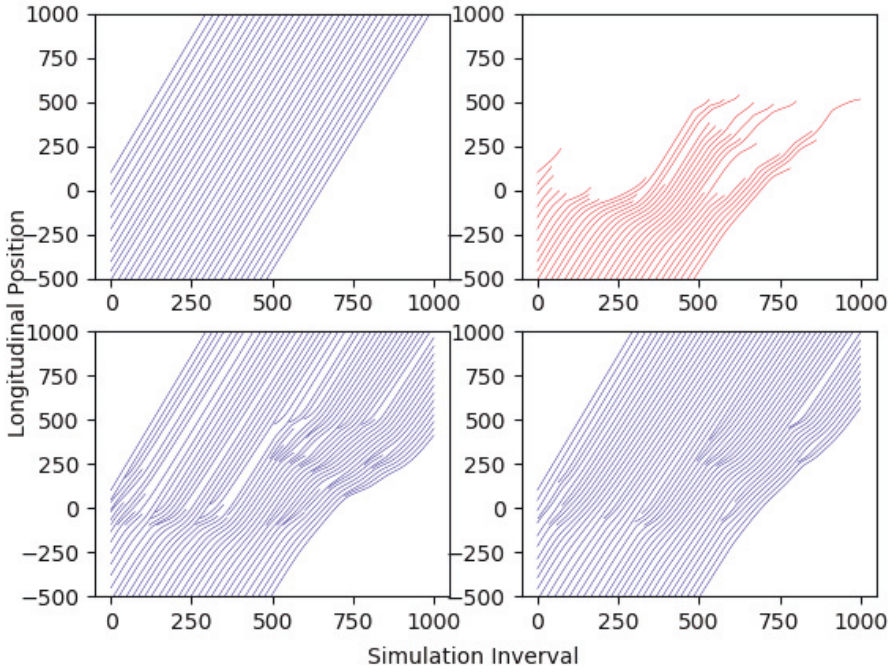

Figure C-9 Longitudinal position with 70 % CAV penetration rate.

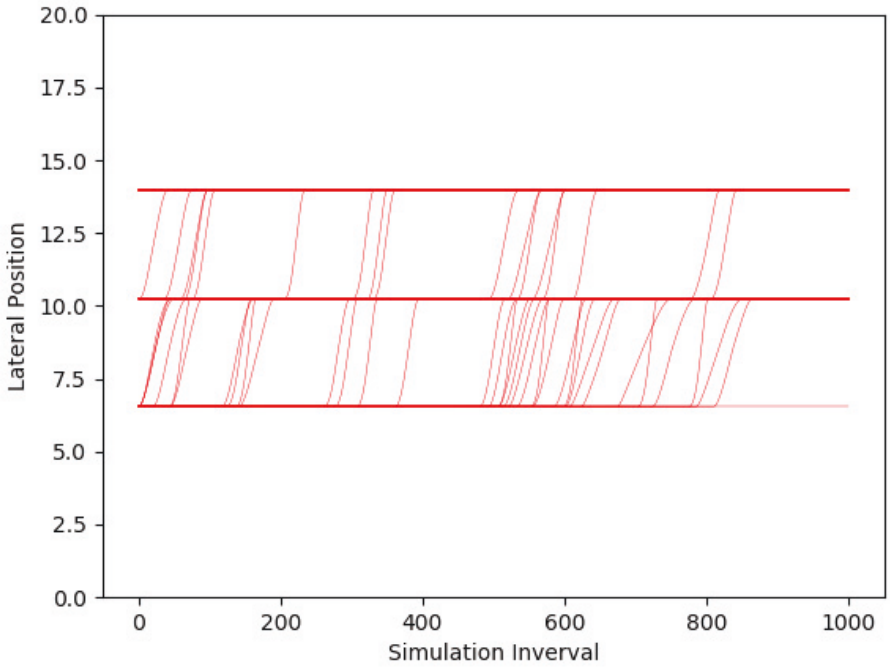

Figure C-10 Lateral position with 70 % CAV penetration rate.

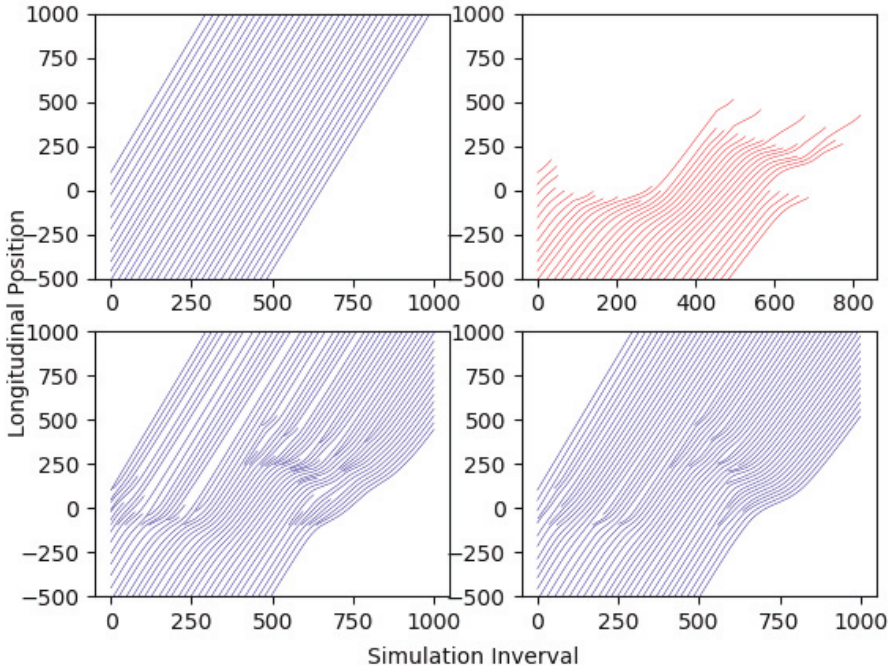

Figure C-11 Longitudinal position with 80 % CAV penetration rate.

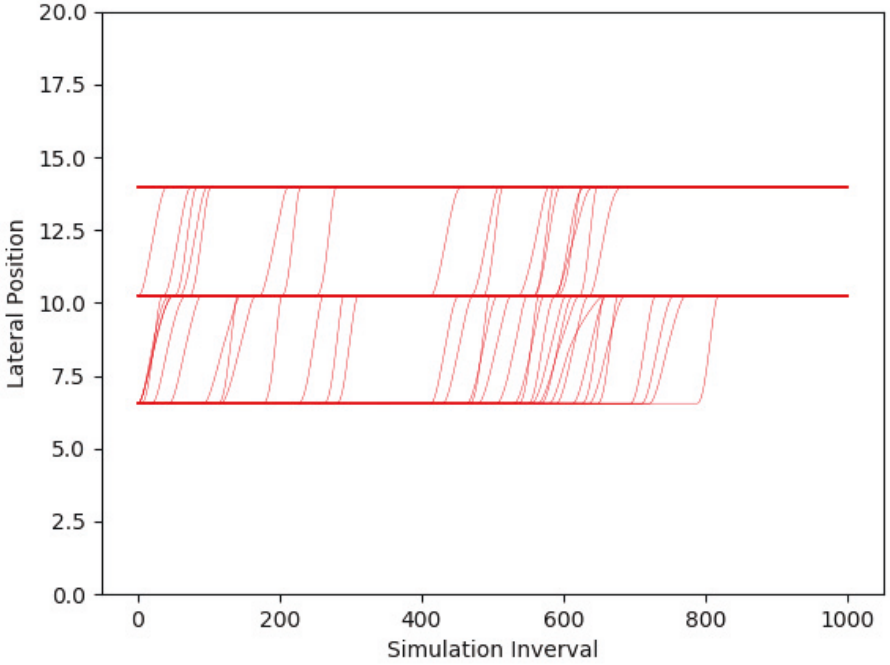

Figure C-12 Lateral position with 80 % CAV penetration rate.

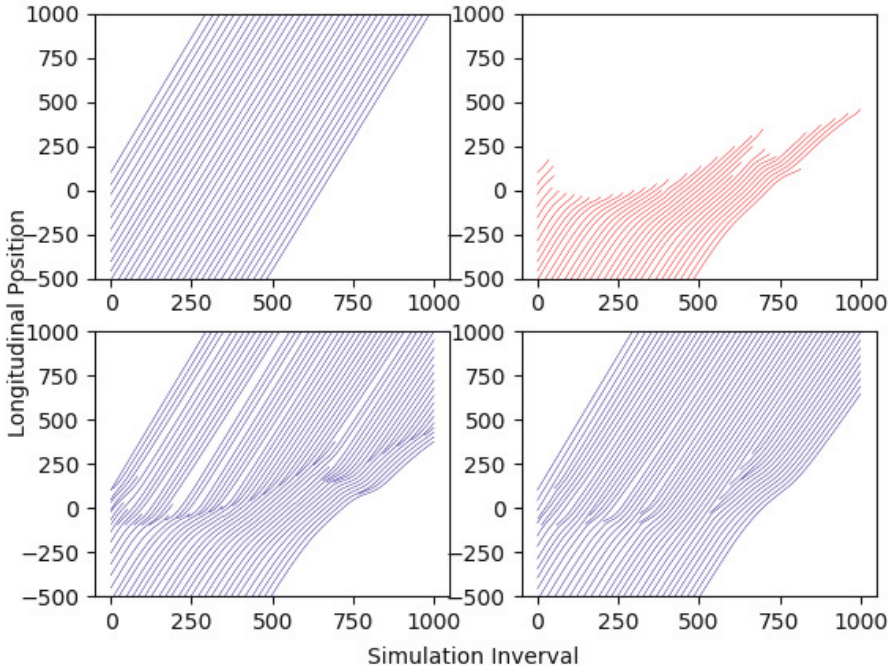

Figure C-13 Longitudinal position with 100 % CAV penetration rate.

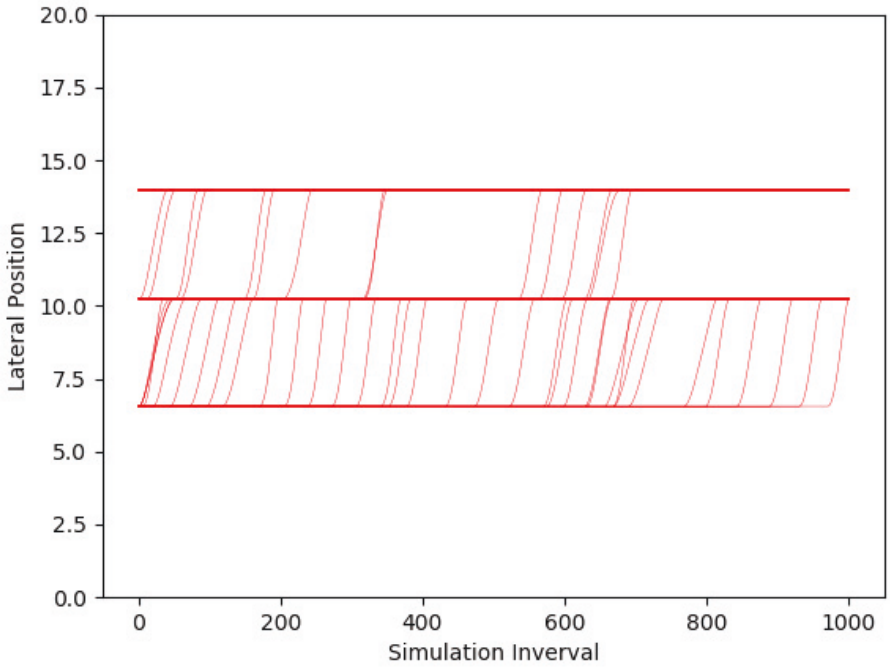

Figure C-14 Lateral position with 100 % CAV penetration rate.

Appendix D

Figures of trajectories for incident-affected traffic regulation

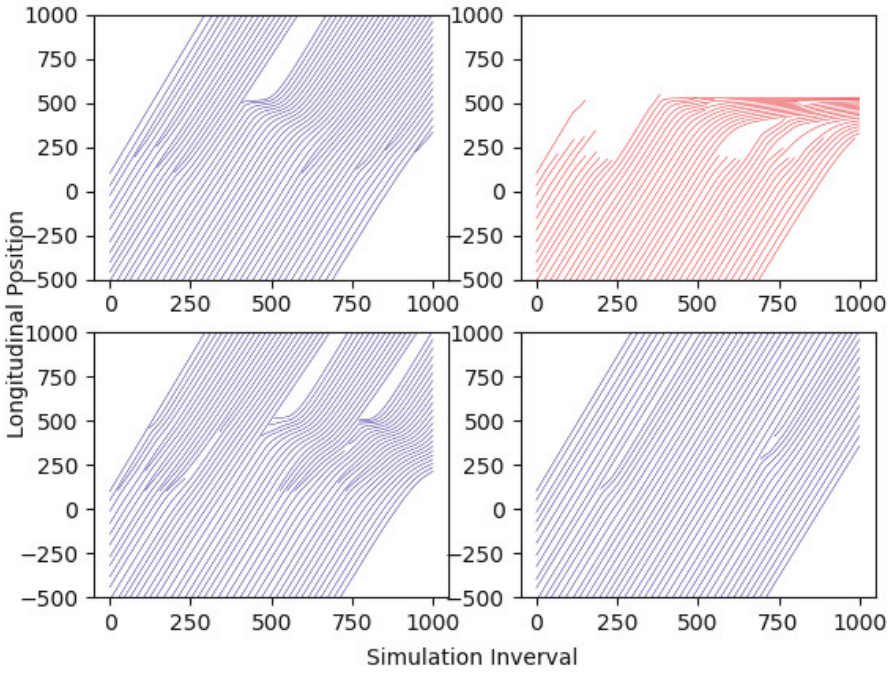

Figure D-1 Longitudinal position with 10 % CAV penetration rate.

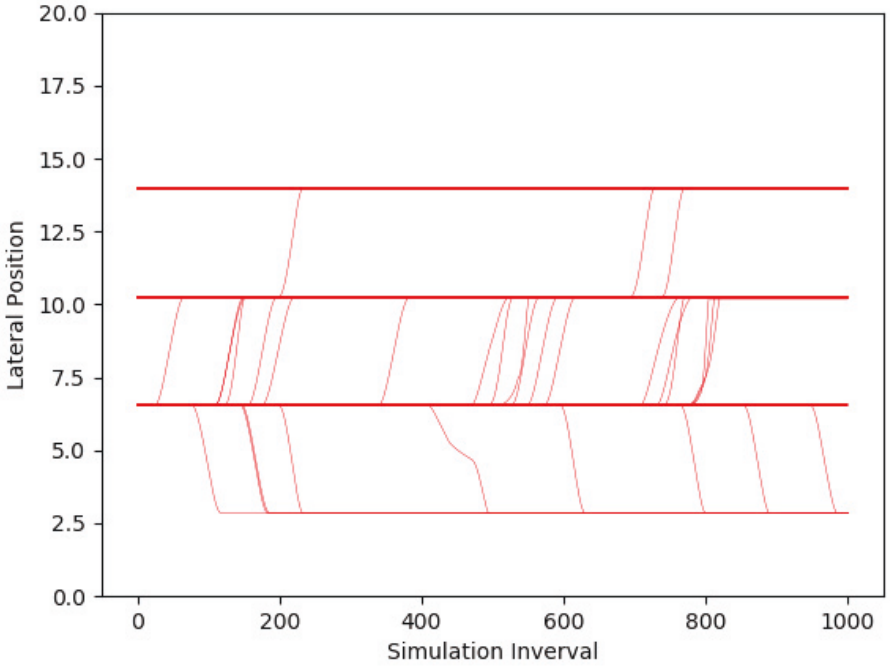

Figure D-2 Lateral position with 10 % CAV penetration rate.

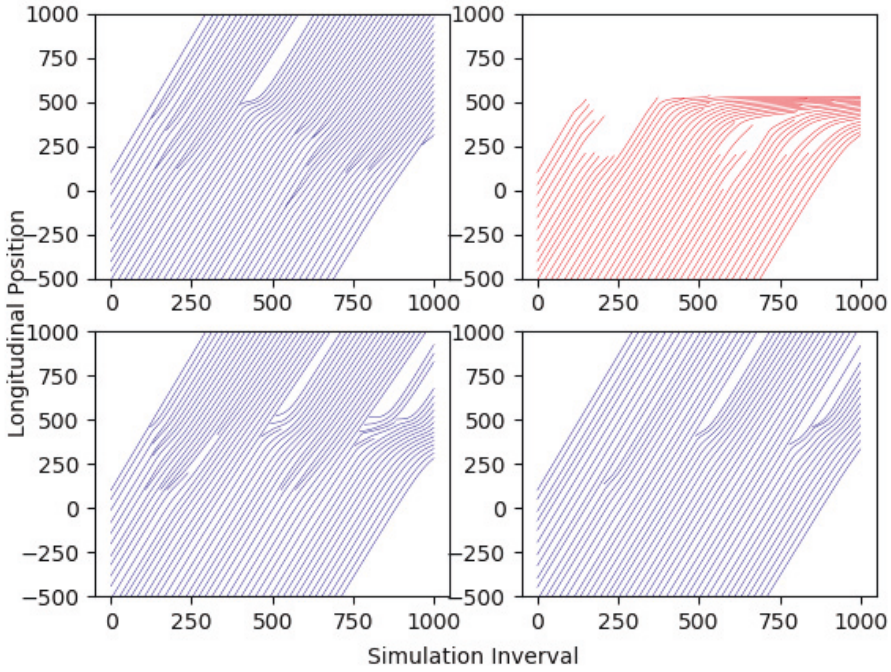

Figure D-3 Longitudinal position with 20 % CAV penetration rate.

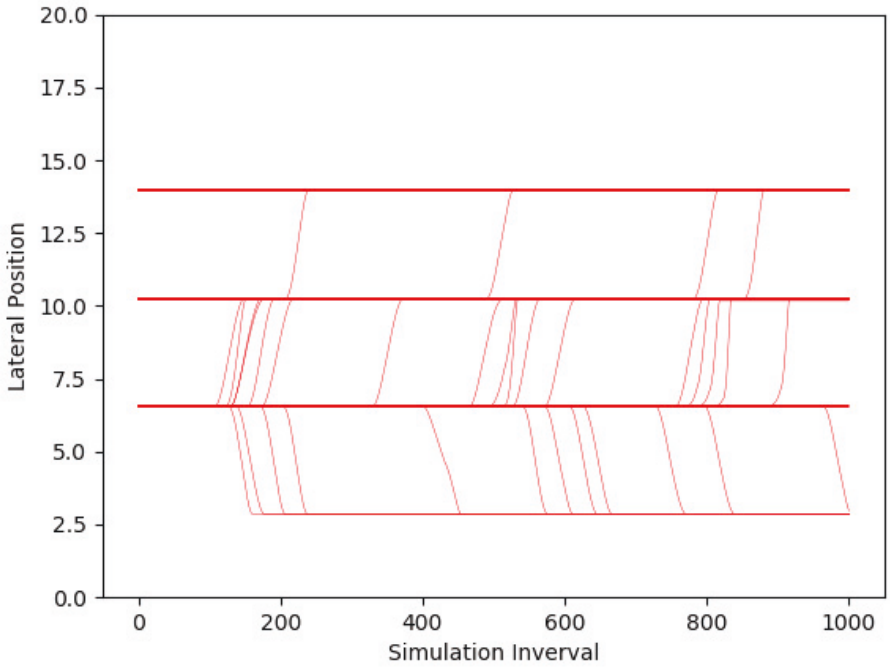

Figure D-4 Lateral position with 20 % CAV penetration rate.

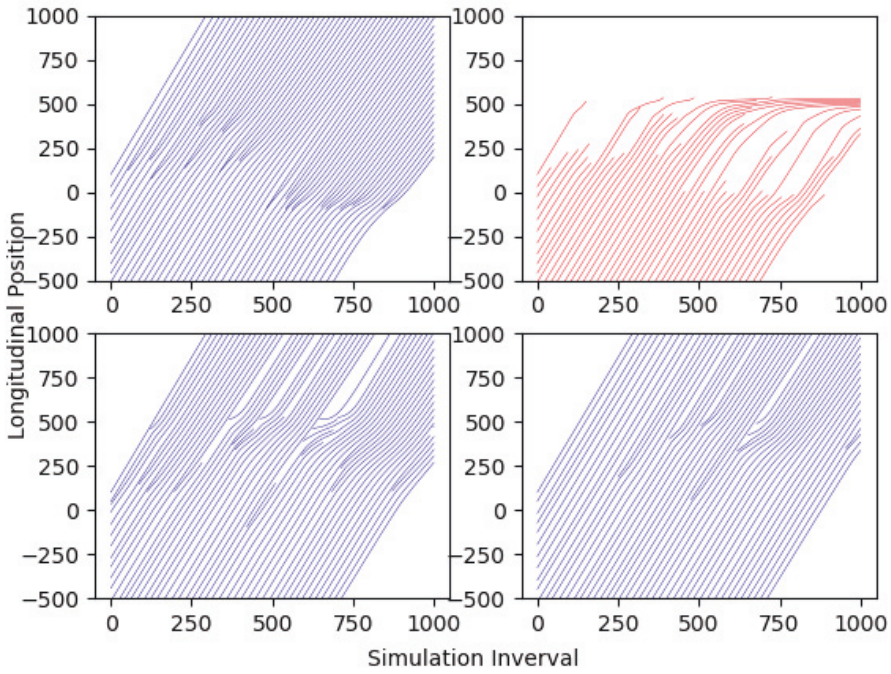

Figure D-5 Longitudinal position with 40 % CAV penetration rate.

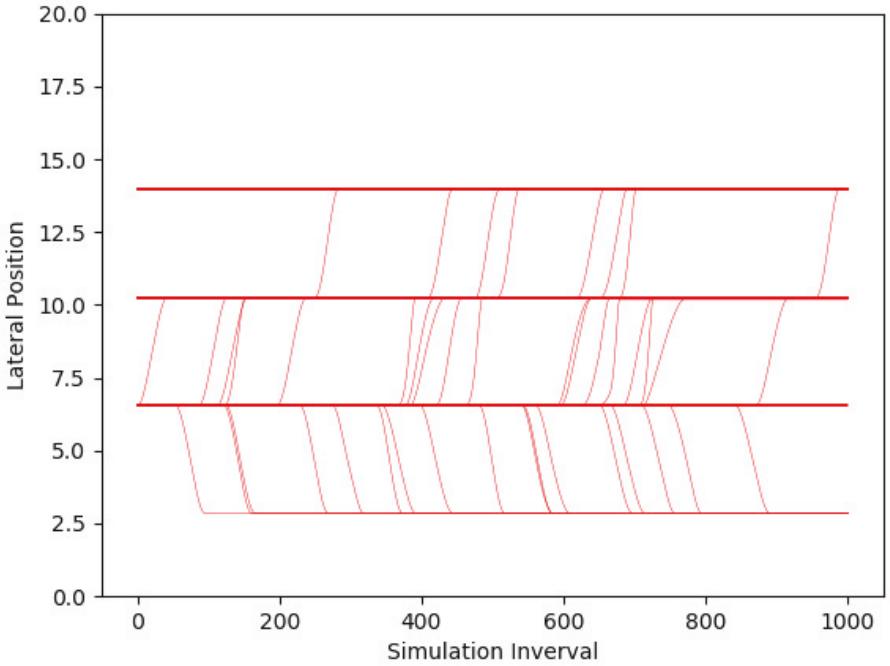

Figure D-6 Lateral position with 40 % CAV penetration rate.

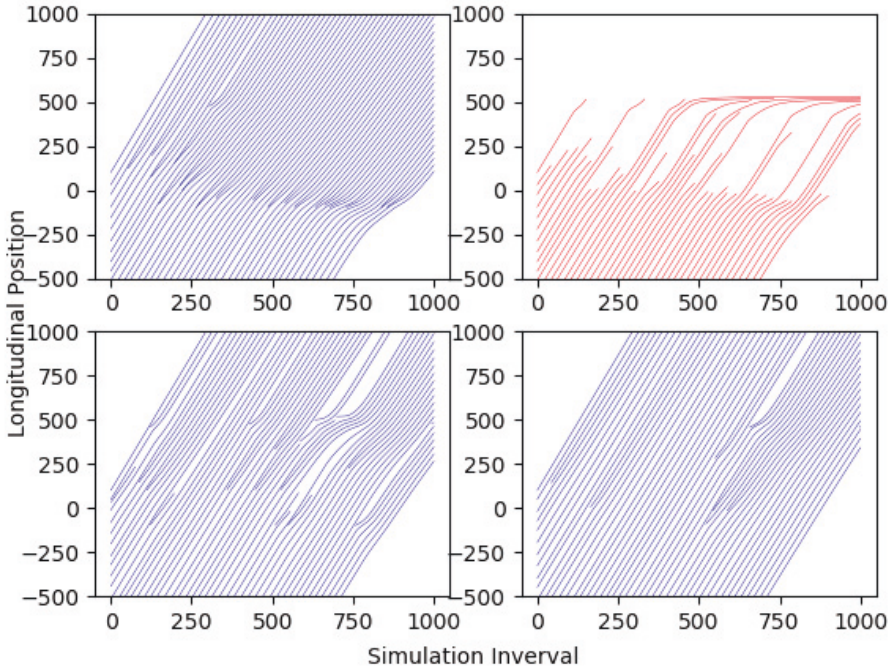

Figure D-7 Longitudinal position with 50 % CAV penetration rate.

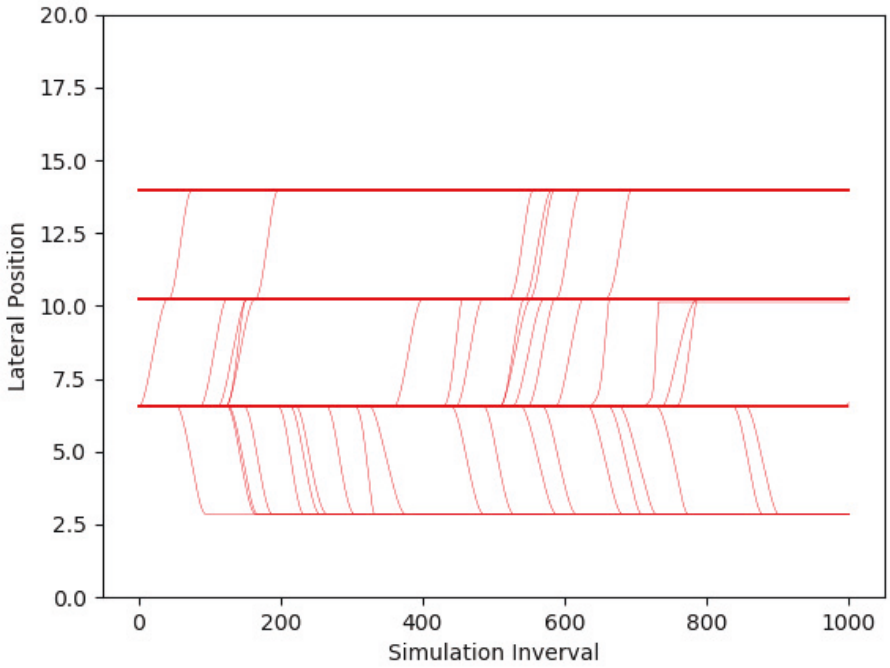

Figure D-8 Lateral position with 50 % CAV penetration rate.

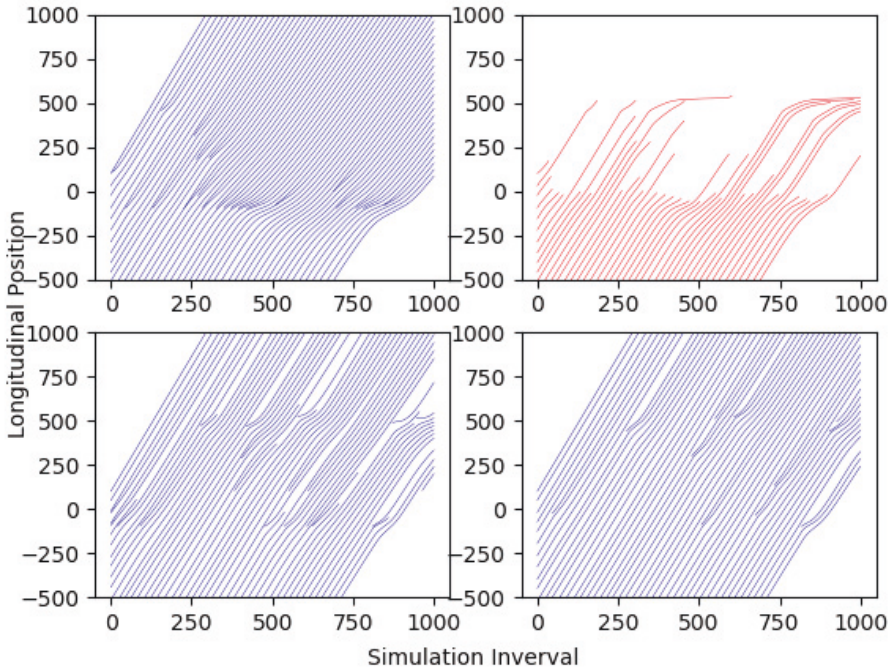

Figure D-9 Longitudinal position with 60 % CAV penetration rate.

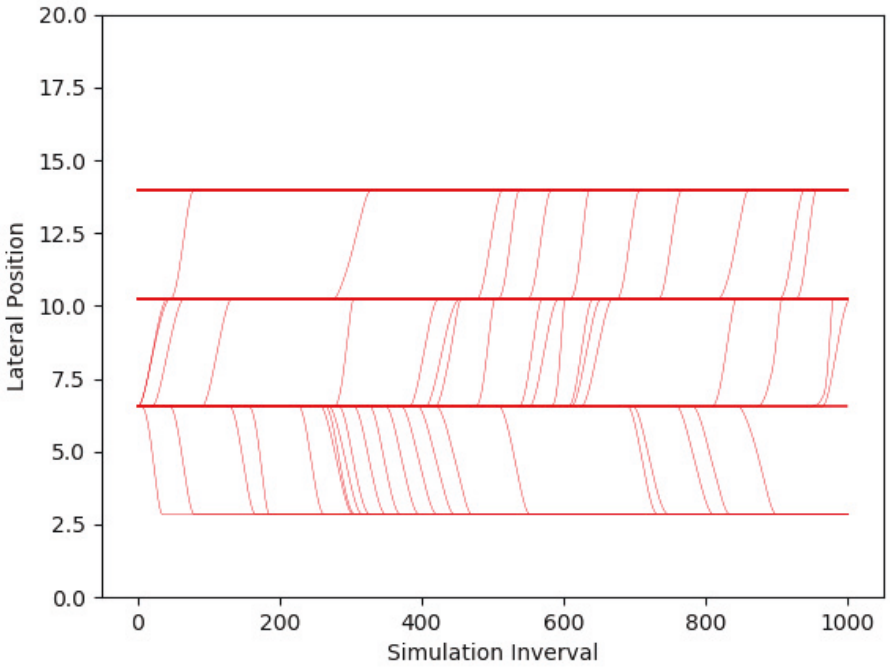

Figure D-10 Lateral position with 60 % CAV penetration rate.

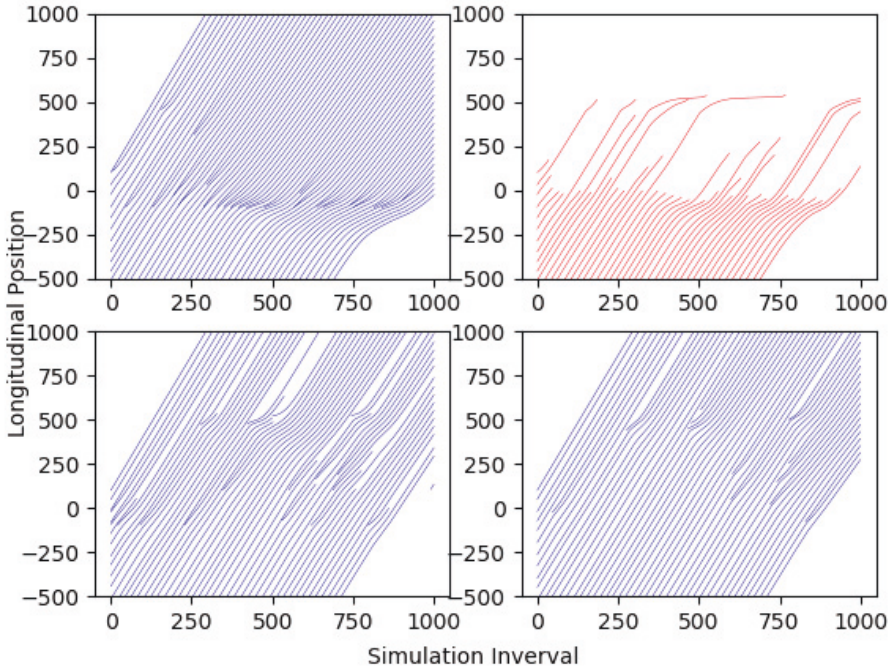

Figure D-11 Longitudinal position with 70 % CAV penetration rate.

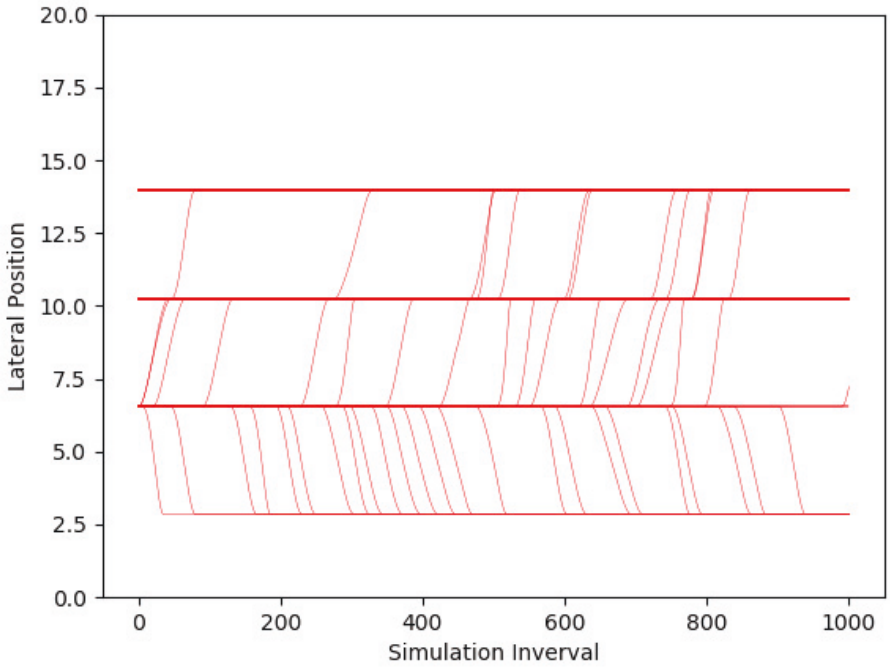

Figure D-12 Lateral position with 70 % CAV penetration rate.

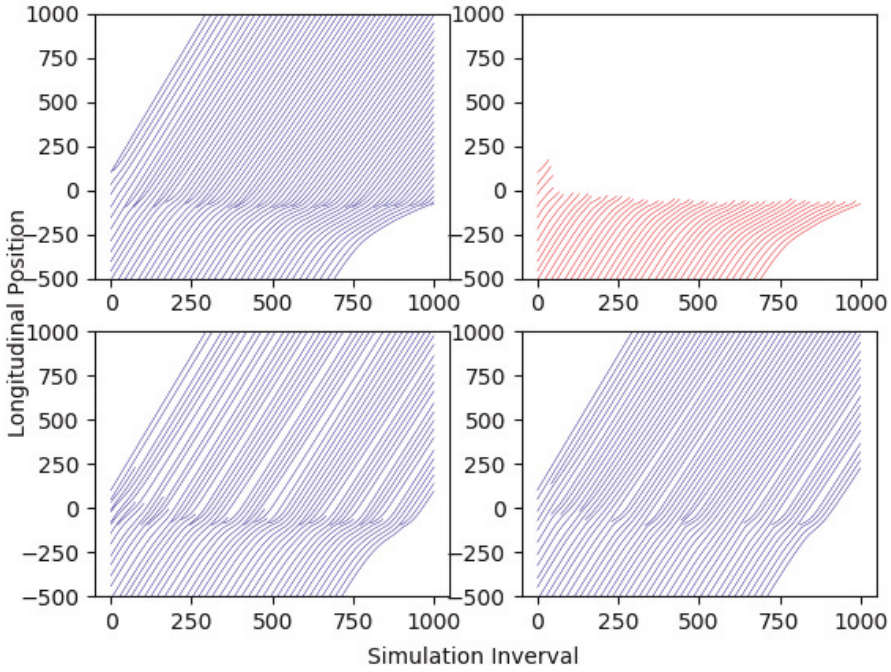

Figure D-13 Longitudinal position with 100 % CAV penetration rate.

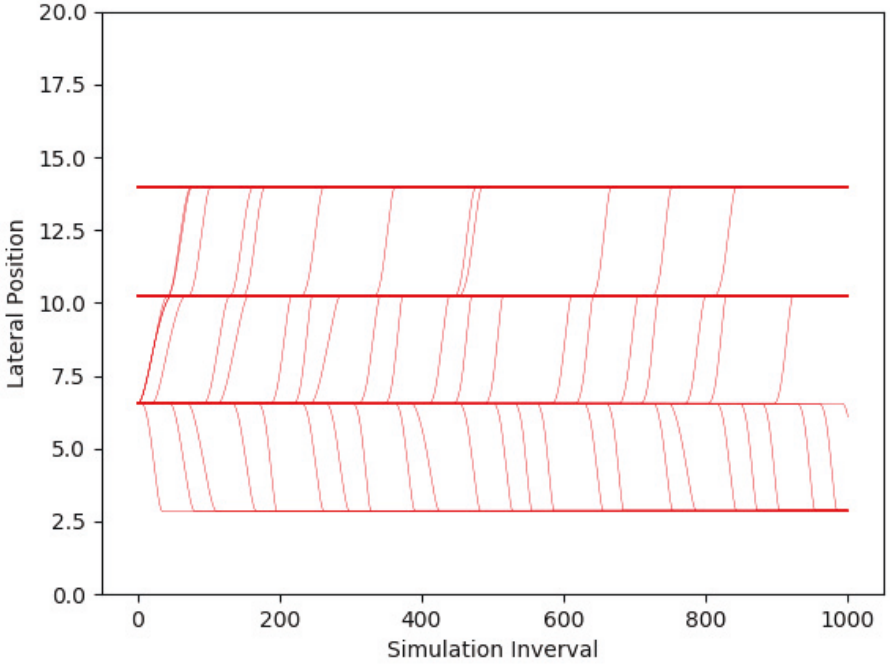

Figure D-14 Lateral position with 100 % CAV penetration rate.

Bibliography

Adeli, H., & Jiang, X. (2003). Neuro-fuzzy logic model for freeway work zone capacity estimation. Journal of Transportation Engineering, 129(5), 484-493.

Ahn, K., Rakha, H., Trani, A., & Van Aerde, M. (2002). Estimating vehicle fuel consumption and emissions based on instantaneous speed and acceleration levels. Journal of transportation engineering, 128(2), 182-190.

American Association of State Highway and Transportation Officials (AASHTO) (2004), A Policy on Geometric Design of Highways and Street. Retrived from http://redlightrobber.com/red/links_pdf/AASHTO_Perception-Times-Studies.pdf.

Balal, E., Cheu, R. L., Gyan-Sarkodie, T., & Miramontes, J. (2014). Analysis of discretionary lane changing parameters on freeways. International Journal of Transportation Science and Technology, 3(3), 277-296.

Bando, M., Hasebe, K., Nakayama, A., Shibata, A., & Sugiyama, Y. (1995). Dynamical model of traffic congestion and numerical simulation. Physical review E, 51(2), 1035.

Bento, L. C., Parafita, R., & Nunes, U. (2012, September). Intelligent traffic management at intersections supported by V2V and V2I communications. In 2012 15th International IEEE Conference on Intelligent Transportation Systems (pp. 1495-1502). Piscataway, NJ: IEEE.

Buturović, L. J. (1993). Improving k-nearest neighbor density and error estimates. Pattern Recognition, 26(4), 611-616.

Cambridge Systematics (December 2005). NGSIM I-80 Data Analysis. Oaklane California: Federal Highway Administration.

Cambridge Systematics (December 2005). NGSIM U.S. 101 Data Analysis. Oaklane California: Federal Highway Administration.

Chung, Y., Walubita, L. F., & Choi, K. (2010). Modeling accident duration and its mitigation strategies on South Korean freeway systems. Transportation research record, 2178(1), 49-57.

Corbett, J. J., Wang, H., & Winebrake, J. J. (2009). The effectiveness and costs of speed reductions on emissions from international shipping. Transportation Research Part D: Transport and Environment, 14(8), 593-598.

Dey, K. C., Rayamajhi, A., Chowdhury, M., Bhavsar, P., & Martin, J. (2016). Vehicle-to-vehicle (V2V) and vehicle-to-infrastructure (V2I) communication in a heterogeneous wireless network–Performance evaluation. Transportation Research Part C: Emerging Technologies, 68, 168-184.

Diels, C., & Bos, J. E. (2016). Self-driving carsickness. Applied Ergonomics, 53, 374-382.

Ding, C., Wang, W., Wang, X., & Baumann, M. (2013). A neural network model for driver's lane-changing trajectory prediction in urban traffic flow. Mathematical Problems in Engineering, 2013.

Domeniconi, C., Gunopulos, D., & Peng, J. (2005). Large margin nearest neighbor classifiers. IEEE transactions on neural networks, 16(4), 899-909.

Dou, Y., Yan, F., & Feng, D. (2016, July). Lane changing prediction at highway lane drops using support vector machine and artificial neural network classifiers. In 2016 IEEE International Conference on Advanced Intelligent Mechatronics (AIM) (pp. 901-906). Piscataway, NJ: IEEE.

Drake, J. L., & Schofer, J. L. (1966). A statistical analysis of speed-density hypotheses. Highway Research Record 154, 53-87.

Duret, A., Buisson, C., & Chiabaut, N. (2008). Estimating individual speed-spacing relationship and assessing ability of Newell's car-following model to reproduce trajectories. Transportation research record, 2088(1), 188-197.

Federal Highway Administration (1998). Our nation's highways: Selected facts and figures (Tech. Rep. No. FHWA- PL-00-014). Washington, DC: U.S. Dept. of Transportation.

Gackstatter, C., Heinemann, P., Thomas, S., Rosenhahn, B., & Klinker, G. (2010, September). Fusion of clothoid segments for a more accurate and updated prediction of the road geometry. In 13th International IEEE Conference on Intelligent Transportation Systems (pp. 1691-1696). Piscataway, NJ: IEEE.

Garber, N. J., & Zhao, M. (2002). Distribution and characteristics of crashes at different work zone locations in Virginia. Transportation Research Record, 1794(1), 19-25.

Gipps, P. G. (1986). A model for the structure of lane-changing decisions. Transportation Research Part B: Methodological, 20(5), 403-414.

Greenberg, H. (1959). An analysis of traffic flow. Operations research, 7(1), 79-85.

Greenshields, B. D., Channing, W., & Miller, H. (1935). A study of traffic capacity. In Highway research board proceedings(Vol. 1935). National Research Council (USA), Highway Research Board.

Haghani, A., Tian, Q., & Hu, H. (2004). Simulation model for real-time emergency vehicle dispatching and routing. Transportation Research Record, 1882(1), 176-183.

Hecht, J. (2018). Lidar for self-driving cars. Optics and Photonics News, 29(1), 26-33.

Helbing, D., & Tilch, B. (1998). Generalized force model of traffic dynamics. Physical review E, 58(1), 133.

Hidas, P. (2002). Modelling lane changing and merging in microscopic traffic simulation. Transportation Research Part C: Emerging Technologies, 10(5-6), 351-371.

Hidas, P. (2005). Modelling vehicle interactions in microscopic simulation of merging and weaving. Transportation Research Part C: Emerging Technologies, 13(1), 37-62.

Hou, Y., Edara, P., & Sun, C. (2013). Modeling mandatory lane changing using Bayes classifier and decision trees. IEEE Transactions on Intelligent Transportation Systems, 15(2), 647-655.

Hou, Y., Edara, P., & Sun, C. (2015). Situation assessment and decision making for lane change assistance using ensemble learning methods. Expert Systems with Applications, 42(8), 3875-3882.

Hunt, J. G., & Lyons, G. D. (1994). Modelling dual carriageway lane changing using neural networks. Transportation Research Part C: Emerging Technologies, 2(4), 231-245.

Jiang, R., & Wu, Q. S. (2002). Cellular automata models for synchronized traffic flow. Journal of Physics A: Mathematical and General, 36(2), 381.

Jiang, R., Wu, Q., & Zhu, Z. (2001). Full velocity difference model for a car-following theory. Physical Review E, 64(1), 017101.

Jiang, X., & Adeli, H. (2004). Clustering-neural network models for freeway work zone capacity estimation. International Journal of Neural Systems, 14(03), 147-163

Jiang, X., & Adeli, H. (2004). Object‐oriented model for freeway work zone capacity and queue delay estimation. Computer‐Aided Civil and Infrastructure Engineering, 19(2), 144-156.

Kang, K. P., & Chang, G. L. (2009). Lane-based dynamic merge control strategy based on optimal thresholds for highway work zone operations. Journal of transportation engineering, 135(6), 359-370.

Kasper, D., Weidl, G., Dang, T., Breuel, G., Tamke, A., Wedel, A., & Rosenstiel, W. (2012). Object-oriented Bayesian networks for detection of lane change maneuvers. IEEE Intelligent Transportation Systems Magazine, 4(3), 19-31.

Kesting, A., & Treiber, M. (2008). Calibrating car-following models by using trajectory data: Methodological study. Transportation Research Record, 2088(1), 148-156.

Kesting, A., Treiber, M., & Helbing, D. (2007). General lane-changing model MOBIL for car-following models. Transportation Research Record, 1999(1), 86-94.

Khattak, A. J., Khattak, A. J., & Council, F. M. (2002). Effects of work zone presence on injury and non-injury crashes. Accident Analysis & Prevention, 34(1), 19-29.

Kiefer, R. J., LeBlanc, D., Palmer, M. D., Salinger, J., Deering, R. K., & Shulman, M. (1999). Development and validation of functional definitions and evaluation procedures for collision warning/avoidance systems (No. DOT-HS-808-964). United States. Department of Transportation. National Highway Traffic Safety Administration.

Kuang, Y., Qu, X., & Wang, S. (2015). A tree-structured crash surrogate measure for freeways. Accident Analysis & Prevention, 77, 137-148.

Lárraga, M. E., Del Rio, J. A., & Alvarez-Lcaza, L. (2005). Cellular automata for one-lane traffic flow modeling. Transportation Research Part C: Emerging Technologies, 13(1), 63-74.

Laval, J. A., & Daganzo, C. F. (2006). Lane-changing in traffic streams. Transportation Research Part B: Methodological, 40(3), 251-264.

Lee, J., & Park, B. (2012). Development and evaluation of a cooperative vehicle intersection control algorithm under the connected vehicles environment. IEEE Transactions on Intelligent Transportation Systems, 13(1), 81-90.

Lee, S. E., Olsen, E. C., & Wierwille, W. W. (2004). A comprehensive examination of naturalistic lane-changes (No. FHWA-JPO-04-092). United States. National Highway Traffic Safety Administration.

Levenberg, K. (1944). A method for the solution of certain non-linear problems in least squares. Quarterly of applied mathematics, 2(2), 164-168.

Li, L., Zhang, M., & Liu, R. (2015, November). The application of Bayesian filter and neural networks in lane changing prediction. In 5th International Conference on Civil Engineering and Transportation. Guangzhou, China: Atlantis Press.

Li, X., Ghiasi, A., Xu, Z., & Qu, X. (2018). A piecewise trajectory optimization model for connected automated vehicles: Exact optimization algorithm and queue propagation analysis. Transportation Research Part B: Methodological, 118, 429-456.

Li, X., Medal, H., & Qu, X. (2019). Connected infrastructure location design under additive service utilities. Transportation Research Part B: Methodological, 120, 99-124.

Luo, Y., Xiang, Y., Cao, K., & Li, K. (2016). A dynamic automated lane change maneuver based on vehicle-to-vehicle communication. Transportation Research Part C: Emerging Technologies, 62, 87-102.

Lv, W., Song, W. G., & Fang, Z. M. (2011). Three-lane changing behaviour simulation using a modified optimal velocity model. Physica A: Statistical Mechanics and its Applications, 390(12), 2303-2314.

Macadam, C. C. (2003). Understanding and modeling the human driver. Vehicle system dynamics, 40(1-3), 101-134.

Mandalia, H. M., & Salvucci, M. D. D. (2005, September). Using support vector machines for lane-change detection. In Proceedings of the human factors and ergonomics society annual meeting (Vol. 49, No. 22, pp. 1965-1969). Sage CA: Los Angeles, CA: SAGE Publications.

Marquardt, D. W. (1963). An algorithm for least-squares estimation of nonlinear parameters. Journal of the society for Industrial and Applied Mathematics, 11(2), 431-441.

Meng, Q., & Qu, X. (2013). Bus dwell time estimation at bus bays: A probabilistic approach. Transportation Research Part C: Emerging Technologies, 36, 61-71.

Meng, Q., & Wang, S. (2011). Optimal operating strategy for a long-haul liner service route. European Journal of Operational Research, 215(1), 105-114.

Meng, Q., & Wang, T. (2010). A chance constrained programming model for short-term liner ship fleet planning problems. Marit. Pol. Mgmt., 37(4), 329-346.

Meng, Q., & Weng, J. (2010). Cellular automata model for work zone traffic. Transportation Research Record, 2188(1), 131-139.

Meng, Q., & Weng, J. (2011). A genetic algorithm approach to assessing work zone casualty risk. Safety science, 49(8-9), 1283-1288.

Meng, Q., & Weng, J. (2011). An improved cellular automata model for heterogeneous work zone traffic. Transportation research part C: emerging technologies, 19(6), 1263-1275.

Meng, Q., & Weng, J. (2011). Impact analysis of work zone configuration, traffic flow and heavy vehicle percentage on traffic delay at work zones. In Proceedings of the Eastern Asia Society for Transportation Studies Vol. 8 (The 9th International Conference of Eastern Asia Society for Transportation Studies, 2011) (pp. 289-289). Tokyo, Japan: Eastern Asia Society for Transportation Studies.

Milanés, V., Llorca, D. F., Villagrá, J., Pérez, J., Fernández, C., Parra, I., ... & Sotelo, M. A. (2012). Intelligent automatic overtaking system using vision for vehicle detection. Expert Systems with Applications, 39(3), 3362-3373.

Miller, J. (2008, June). Vehicle-to-vehicle-to-infrastructure (V2V2I) intelligent transportation system architecture. In 2008 IEEE intelligent vehicles symposium (pp. 715-720). Piscataway, NJ: IEEE.

Motulsky, H. J., & Ransnas, L. A. (1987). Fitting curves to data using nonlinear regression: a practical and nonmathematical review. The FASEB journal, 1(5), 365-374.

Nagel, K., & Schreckenberg, M. (1992). A cellular automaton model for freeway traffic. Journal de physique I, 2(12), 2221-2229.

Nagel, K., Wolf, D. E., Wagner, P., & Simon, P. (1998). Two-lane traffic rules for cellular automata: A systematic approach. Physical Review E, 58(2), 1425.

Newell, G. F. (1961). Nonlinear effects in the dynamics of car following. Operations research, 9(2), 209-229.

Nielsen, A. A. (2007). Least squares adjustment: Linear and nonlinear weighted regression analysis. Danish National Space Center/Informatics and mathematical modelling, Technical Univ. of Denmark.

Ntousakis, I. A., Nikolos, I. K., & Papageorgiou, M. (2016). Optimal vehicle trajectory planning in the context of cooperative merging on highways. Transportation research part C: emerging technologies, 71, 464-488.

Ossen, S., & Hoogendoorn, S. P. (2008). Validity of trajectory-based calibration approach of car-following models in presence of measurement errors. Transportation Research Record, 2088(1), 117-125.

Papageorgiou, M., Papamichail, I., Spiliopoulou, A. D., & Lentzakis, A. F. (2008). Real-time merging traffic control with applications to toll plaza and work zone management. Transportation Research Part C: Emerging Technologies, 16(5), 535-553.

Peden, M., Scurfield, R., Sleet, D., Mohan, D., Hyder, A. A., Jarawan, E. & Mathers, C. (2004). World report on road traffic injury prevention. Gevena: World Health Organization.

Punzo, V., Borzacchiello, M. T., & Ciuffo, B. (2009, January). Estimation of vehicle trajectories from observed discrete positions and next-generation simulation program (NGSIM) data. In TRB 88 annual meeting (pp. 11-15). Washington DC, USA. Retrived from https://trid.trb.org/view/882483.

Qu, X., & Wang, S. (2015). Long‐distance‐commuter (LDC) lane: A new concept for freeway traffic management. Computer‐Aided Civil and Infrastructure Engineering, 30(10), 815-823.

Qu, X., Wang, S., & Zhang, J. (2015). On the fundamental diagram for freeway traffic: A novel calibration approach for single-regime models. Transportation Research Part B: Methodological, 73, 91-102.

Qu, X., Yu, Y., Zhou, M., Lin, C. T., & Wang, X. (2020). Jointly dampening traffic oscillations and improving energy consumption with electric, connected and automated vehicles: A reinforcement learning based approach. Applied Energy, 257, 114030.

Qu, X., Zhang, J., & Wang, S. (2017). On the stochastic fundamental diagram for freeway traffic: model development, analytical properties, validation, and extensive applications. Transportation research part B: methodological, 104, 256-271.

Ronen, D. (1982). The effect of oil price on the optimal speed of ships. Journal of the Operational Research Society, 33(11), 1035-1040.

Ronen, D. (2011). The effect of oil price on containership speed and fleet size. Journal of the Operational Research Society, 62(1), 211-216.

Rouphail, N. M., Yang, Z. S., & Fazio, J. (1988). Comparative study of short-and long-term urban freeway work zones. Transportation Research Record, 1163, 4-14.

SAE On-Road Automated Vehicle Standards Committee. (2014). Taxonomy and definitions for terms related to on-road motor vehicle automated driving systems. SAE Standard J, 3016, 1-16.

SHILLER, Z., & SUNDAR, S. (1998). Emergency lane-change maneuvers of autonomous vehicles. Journal of dynamic systems, measurement, and control, 120(1), 37-44.

Skabardonis, A., Varaiya, P., & Petty, K. F. (2003). Measuring recurrent and nonrecurrent traffic congestion. Transportation Research Record, 1856(1), 118-124.

Sledge, N. H., & Marshek, K. M. (1998). Development and validation of an optimized emergency lane-change trajectory(No. 980231). SAE Technical Paper.

Smith, B. L., Qin, L., & Venkatanarayana, R. (2003). Characterization of freeway capacity reduction resulting from traffic accidents. Journal of Transportation Engineering, 129(4), 362-368.

Su, Y., Yan, X., Xue, S., Weng, J., & Chen, D. (2016). Comparative Study on Beijing and Singapore's Work Zone Rear-End Crash Risks. In CICTP 2016 (pp. 1284-1296).

Sun, H., Liu, H. X., Xiao, H., He, R. R., & Ran, B. (2003). Use of local linear regression model for short-term traffic forecasting. Transportation Research Record, 1836(1), 143-150.

Tang, J., Liu, F., Zhang, W., Ke, R., & Zou, Y. (2018). Lane-changes prediction based on adaptive fuzzy neural network. Expert Systems with Applications, 91, 452-463.

Tang, T., Shi, W., Shang, H., & Wang, Y. (2014). A new car-following model with consideration of inter-vehicle communication. Nonlinear dynamics, 76(4), 2017-2023.

Tarko, A. P., Shamo, D., & Wasson, J. (1999). Indiana lane merge system for work zones on rural freeways. Journal of transportation engineering, 125(5), 415-420.

Thiemann, C., Treiber, M., & Kesting, A. (2008). Estimating acceleration and lane-changing dynamics from next generation simulation trajectory data. Transportation Research Record, 2088(1), 90-101.

Tomar, R. S., & Verma, S. (2012). Safety of Lane Change Maneuver Through A Priori Prediction of Trajectory Using Neural Networks. Network Protocols & Algorithms, 4(1), 4-21.

Tomar, R. S., Verma, S., & Tomar, G. S. (2010, November). Prediction of lane change trajectories through neural network. In 2010 International Conference on Computational Intelligence and Communication Networks (pp. 249-253). Piscataway, NJ: IEEE.

Underwood, R. T. (2008). Speed, volume, and density relationship: Quality and theory of traffic flow, yale bureau of highway traffic (1961) 141–188. New Haven, Connecticut.

USDOT. (2015). Connected Vehicle Reference Implementation Architecture. <http://www.iteris.com/cvria/html/applications/applications.html>. Accessed on July 27, 2015.

Wang, H., Li, J., Chen, Q. Y., & Ni, D. (2011). Logistic modeling of the equilibrium speed–density relationship. Transportation research part A: policy and practice, 45(6), 554-566.

Wang, J. Q., Chai, R., & Cao, N. (2014). Modeling highway lane changing using Bayesian networks. In Applied Mechanics and Materials (Vol. 505, pp. 1143-1147). Trans Tech Publications Ltd.

Wang, J., Hughes, W. E., Council, F. M., & Paniati, J. F. (1996). Investigation of highway work zone crashes: What we know and what we don't know. Transportation Research Record, 1529(1), 54-62.

Wang, S., & Meng, Q. (2012). Sailing speed optimization for container ships in a liner shipping network. Transportation Research Part E: Logistics and Transportation Review, 48(3), 701-714.

Wei, H., & Pavithran, M. (2006). Concept of dynamic merge metering approach for work zone traffic control. IFAC Proceedings Volumes, 39(12), 374-379.

Weng, J. (2011). Collision avoidance analysis for transition taper length. Transportation planning and technology, 34(8), 811-822.

Weng, J., & Meng, Q. (2014). Rear‐end crash potential estimation in the work zone merging areas. Journal of Advanced Transportation, 48(3), 238-249.

Weng, J., & Yan, X. (2016). Probability distribution‐based model for work zone capacity prediction. Journal of Advanced Transportation, 50(2), 165-179.

Xue, S., & Weng, J. (2014). Analysis of Uncertainty Associated with Response Time in Work Zone Traffic Accidents. In CICTP 2014: Safe, Smart, and Sustainable Multimodal Transportation Systems (pp. 3710-3722).

Yang, N., Chang, G. L., & Kang, K. P. (2009). Simulation-based study on a lane-based signal system for merge control at freeway work zones. Journal of Transportation Engineering, 135(1), 9-17.

Yang, Q., & Koutsopoulos, H. N. (1996). A microscopic traffic simulator for evaluation of dynamic traffic management systems. Transportation Research Part C: Emerging Technologies, 4(3), 113-129.

Yi, D., Su, J., Liu, C., & Chen, W. H. (2016, November). Data-driven situation awareness algorithm for vehicle lane change. In 2016 IEEE 19th International Conference on Intelligent Transportation Systems (ITSC) (pp. 998-1003). Piscataway, NJ: IEEE.

Yoo, J. B., Kim, J., & Park, C. Y. (2010, June). Road reservation for fast and safe emergency vehicle response using ubiquitous sensor network. In 2010 IEEE International Conference on Sensor Networks, Ubiquitous, and Trustworthy Computing (pp. 353-358). Piscataway, NJ: IEEE.

Yu, Y., Jiang, R., & Qu, X. (2019). A Modified Full Velocity Difference Model with Acceleration and Deceleration Confinement: Calibrations, Validations, and Scenario Analyses. IEEE Intelligent Transportation Systems Magazine.

Pei, Y., & Dai, L. (2007). Study on intelligent lane merge control system for freeway work zones. In 2007 IEEE Intelligent Transportation Systems Conference (pp. 586-591). Piscataway, NJ: IEEE.

Zhang, J., Qu, X., & Wang, S. (2018). Reproducible generation of experimental data sample for calibrating traffic flow fundamental diagram. Transportation Research Part A: Policy and Practice, 111, 41-52.

Zhang, J., Tang, T. Q., & Wang, T. (2019). Some features of car-following behaviour in the vicinity of signalised intersection and how to model them. IET Intelligent Transport Systems, 13(11), 1686-1693.

Zheng, J., Suzuki, K., & Fujita, M. (2014). Predicting driver's lane-changing decisions using a neural network model. Simulation Modelling Practice and Theory, 42, 73-83.

Zheng, Z. (2014). Recent developments and research needs in modeling lane changing. Transportation research part B: methodological, 60, 16-32.

Zhou, M., Qu, X., & Jin, S. (2016). On the impact of cooperative autonomous vehicles in improving freeway merging: a modified intelligent driver model-based approach. IEEE Transactions on Intelligent Transportation Systems, 18(6), 1422-1428.

Zhou, M., Qu, X., & Li, X. (2017). A recurrent neural network based microscopic car following model to predict traffic oscillation. Transportation research part C: emerging technologies, 84, 245-264.

Zhou, M., Yu, Y., & Qu, X. (2019). Development of an efficient driving strategy for connected and automated vehicles at signalized intersections: A reinforcement learning approach. IEEE Transactions on Intelligent Transportation Systems.

Zohdy, I. H., & Rakha, H. A. (2016). Intersection management via vehicle connectivity: The intersection cooperative adaptive cruise control system concept. Journal of Intelligent Transportation Systems, 20(1), 17-32.

Zou, Y., & Qu, X. (2018). On the impact of connected automated vehicles in freeway work zones: a cooperative cellular automata model based approach. Journal of Intelligent and Connected Vehicles, 1(1), 1-14.